Dissertation zur Erlangung des Doktorgrades
der Fakultät für Chemie und Pharmazie

der Ludwig-Maximilians-Universität München

Optimized CRISPR/Cas9 Delivery System for Enhanced Gene Editing and Correction

Xianjin Luo

aus

Suining, Sichuan, China

2025

Erklärung

Diese Dissertation wurde im Sinne von § 7 der Promotionsordnung vom 28. November 2011 von Herrn Prof. Dr. Ernst Wagner betreut.

Eidesstattliche Versicherung

Diese Dissertation wurde eigenständig und ohne unerlaubte Hilfe erarbeitet.

München, 22.05.2025

…….....

Xianjin Luo

Dissertation eingereicht am: 06.08.2025

1. Gutachter: Prof. Dr. Ernst Wagner

2. Gutachter: Prof. Dr. Wolfgang Friess

Mündliche Prüfung am: 31.07.2025

To my family

致家人

天行健，君子以自强不惜

——《周易》

Table of contents

1 Introduction

This chapter is intended to give a brief introduction into the research field and to put the experimental data of the following chapters into a broader context. It is not considered to be a complete review of the whole scientific area.

1.1 The evolution of CRISPR-Cas9 technology

Pioneering studies in the early 1990s using homing endonucleases like I-SceI demonstrated that targeted double-strand breaks (DSBs) in mammalian cells stimulated homologous recombination [1]. Building on this concept, zinc-finger nucleases (ZFNs) were introduced in the early 2000s for genome editing, and later transcription activator-like effector nucleases (TALENs) in 2010–2011 [2, 3], but their complex design limited their use. The discovery and advancement of the clustered regularly interspaced short palindromic repeat (CRISPR) -Cas nucleases, with their simplicity, specificity, and versatility, revolutionized genome editing.

By 2007, studies had confirmed that CRISPR-Cas systems in prokaryotes function as adaptive immune mechanisms, enabling the identification and elimination of foreign genetic material from viruses (phages) and mobile genetic elements [4]. Within these systems, invading DNA fragments are captured and integrated into repetitive genomic sequences, which, upon transcription and processing, produce CRISPR RNAs (crRNAs). These crRNAs guide protein complexes containing Cas enzymes to recognize and degrade foreign nucleic acids [5].

In 2011, Emmanuelle Charpentier’s research team discovered a crucial molecule involved in crRNA processing, later named tracrRNA (trans-activating CRISPR RNA), which plays a key role in activating nuclease activity [6]. Further investigations revealed its function in DNA cleavage mechanisms, a discovery that ultimately earned a Nobel Prize. It was also proposed that crRNA and tracrRNA could be fused into a single chimeric molecule, known as single-guide RNA (sgRNA), which significantly facilitated the practical application of the CRISPR-Cas9 system.

Following the identification of the essential components required for CRISPR-Cas9 activity, researchers rapidly sought to apply this technology to genome editing in human and animal cells. In January 2013, nearly simultaneously, five independent research

groups published studies demonstrating that the expression of Cas9 and its corresponding sgRNA in eukaryotic cells led to precise genetic modifications at targeted genome loci [7]. Among these, two papers from George Church's lab [8] at Harvard University and Feng Zhang's team [9] at the Broad Institute, both published in Science, presented some of the most effective strategies for CRISPR-based genome engineering. Subsequently, CRISPR technology continued to evolve, leading to the development of more refined and efficient genome-editing tools with broader applications across various fields, including medicine, agriculture, and biotechnology.

1.2 Beyond CRISPR-Cas9: Derivative technologies and the rise of RNA editing

1.2.1 Mechanism and application of CRISPR-Cas9

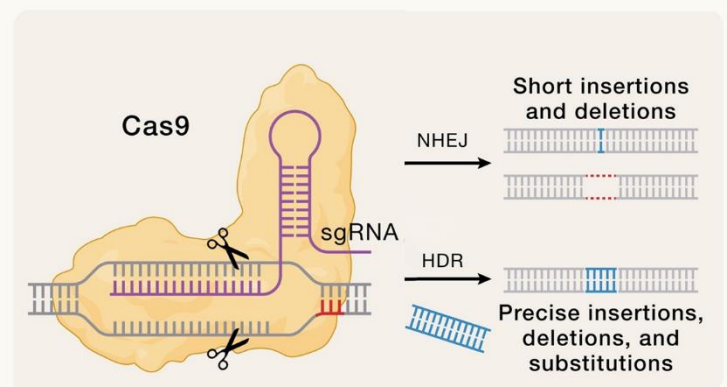

Figure 1. Molecular principles of CRISPR/Cas9 genome editing.

The past decade has witnessed the remarkable success of CRISPR/Cas9-induced gene editing, which has transformed both basic and translational research while demonstrating immense potential in agriculture and therapeutic development. The Cas9-mediated gene editing pathway primarily involves two mechanisms (**Fig.1**): non-homologous end joining (NHEJ) [10] and the more precise homology-directed repair (HDR) [11]. NHEJ involves the direct re-ligation of cleaved DNA strands without the use of a homologous DNA template. This error-prone mechanism can lead to random insertions and deletions (indels) at the cleavage site, often resulting in frameshift mutations and target gene knockout. In the presence of a homologous DNA template, HDR facilitates accurate repair and enables the precise insertion of a defined DNA sequence between the homology arms at the cleavage site.

For safe and effective genome editing *in vitro* and *in vivo*, genome editing systems must be accurate, efficient, and capable of being delivered to the desired cells or tissues. Cas9

and sgRNA can be introduced into target cells in various forms, including plasmid DNA (Cas9 and sgRNA encoding plasmids), mRNA/sgRNA, or Cas9 protein/sgRNA ribonucleoprotein (RNP), each with its own advantages and limitations. For gene editing using Cas9 plasmids, Liang et al. developed an LC09 (OS cell-specific aptamer)-functionalized PEG-PEI-Cholesterol (PPC) lipopolymer encapsulating CRISPR/Cas9 plasmids encoding VEGFA gRNA and Cas9 [12]. This delivery system enabled selective distribution of CRISPR/Cas9 in both orthotopic OS and lung metastases via LC09, leading to effective VEGFA genome editing in tumors, reduced VEGFA expression and secretion, inhibition of orthotopic OS malignancy and lung metastases, as well as decreased angiogenesis and bone lesions, with no detectable toxicity. Similarly, Deng et al. designed an AMP (1-(3-aminopropyl)-4-methylpiperazine)-modified PBAE (aPBAE) for delivering the CRISPR/Cas9 plasmid to malignant tissues, successfully knocking out cyclin-dependent kinase 5 (Cdk5) to downregulate PD-L1 expression on tumor cells *in vivo* [13]. For gene editing using Cas9 mRNA/sgRNA, Kataoka et al. employed PEGylated polyplex micelles (PMs) to deliver Cas9 mRNA/sgRNA, marking the first report of genome editing in brain parenchymal cells [14]. The study also demonstrated that co-delivery of Cas9 mRNA/sgRNA via PMs was superior to loading Cas9 mRNA and sgRNA separately, improving sgRNA stability against enzymatic degradation and enhancing gene editing efficiency. Additionally, Morrissey et al. developed a lipid nanoparticle (LNP)-mediated delivery system for Cas9 mRNA/sgRNA that, with a single administration, achieved significant editing of the mouse transthyretin (Ttr) gene in the liver, resulting in a >97% reduction in serum protein levels that persisted for at least 12 months [15]. For gene editing using the Cas9 RNP format, Siegwart et al. reported using a SORT LNP-based Cas9 RNP delivery system to restore dystrophin expression in DMD mice and significantly reduce serum PCSK9 levels in C57BL/6 mice, demonstrating strong therapeutic potential [16]. Additionally, Paul B et al. designed peptide-based delivery agents by fusing the endosomolytic peptide CM18 and the cell-penetrating peptide (CPP) PTD4 with six-histidine tags at one or both ends (CM18-PTD4), enabling efficient Cas9 RNP delivery to hard-to-transduce human natural killer (NK) cells [17]. Furthermore, the instillation of shuttle peptides combined with SpCas9 or AsCas12a RNP successfully facilitated the editing of loxP sites in the airway epithelia of ROSAmT/mG mice.

As above shown, CRISPR cas9 -based gene editing has progressed at an extraordinary speed. Early genome-editing tools, which depend on DSBs and are built on Cas9, have undergone continuous refinement. These innovations have not only broadened their applications but also improved precision while reducing unintended modifications. However, safety remains a major concern, as both off-target effects and the potential genotoxicity of DSBs—such as p53 activation—pose risks [18]. To minimize unwanted edits, researchers have developed various methods for precise spatial and temporal regulation of CRISPR activity [19, 20], including the use of natural anti-CRISPR proteins to restrict editing to specific tissues [21]. Moreover, concerns about DSB-associated

genotoxicity and the inefficiency of HDR have spurred the development of “second-generation” CRISPR technologies, such as base editors (BEs) and prime editors (PEs) in **Fig.2**, which enable genome modifications without requiring DSBs or HDR.

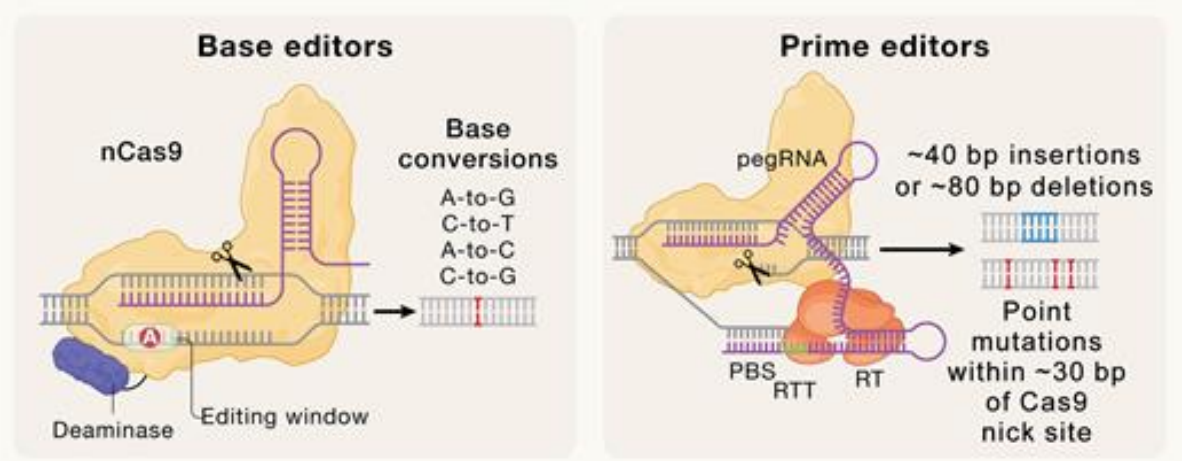

Figure 2. “Second-generation” CRISPR editing technologies: base editors (BEs) and prime editors (PEs).

1.2.2 Base editor

CRISPR-based base editors (BEs) have emerged as a powerful tool for introducing precise point mutations without requiring double-strand breaks (DSBs) or homology-directed repair templates. This makes them particularly useful for editing cells that lack efficient HDR pathways [22]. Structurally, BEs (**Fig. 2**, left) consist of a catalytically modified Cas9 nickase fused to a nucleotide deaminase enzyme [23]. Initially, two main types were introduced: cytosine base editors (CBEs) and adenine base editors (ABEs). CBEs, incorporating catalytic domains from cytidine deaminases such as APOBEC1 along with an uracil glycosylase inhibitor (UGI), facilitate the conversion of C- to –T [24]. In contrast, ABEs enable A-to-G changes through a TadA-derived adenosine deaminase, which has been evolutionarily engineered to function on single-stranded DNA [22].

Once the Cas9 module binds to its target, the base editor modifies cytosine or adenine within a defined "editing window" in the non-target strand’s PAM-distal region, converting cytosine to uracil or adenine to inosine. These changes are recognized during DNA replication as thymine and guanine, respectively, leading to transition mutations. Since

their initial development, both CBEs and ABEs have undergone multiple refinements to enhance efficiency and minimize off-target activity [25-27]. To address these limitations, researchers have turned to well-established non-viral delivery methods, such as LNP, especially for delivering base editor mRNA. A notable example is Verve Therapeutics, which launched a clinical trial in August 2022 using intravenously administered LNP to transport ABE mRNA along with a guide RNA targeting the PCSK9 gene in patients with familial hypercholesterolemia [28]. Looking ahead, Verve's investigational therapy, VERVE-102, is expected to advance into a Phase 1 clinical trial in the first half of 2024, employing a more precisely targeted LNP delivery system. Another significant advancement in CRISPR base editing comes from Beam Therapeutics, which has received FDA approval to conduct clinical trials for BEAM-101, a base editor-based treatment for sickle cell disease [29]. BEAM-101 is an autologous, patient-specific blood stem cell therapy designed as a potential one-time cure for both sickle cell disease and beta-thalassemia. This approach leverages specific point mutations linked to sustained fetal hemoglobin production—an established strategy, but one that, for the first time, integrates a base editor. Notably, Sun and colleagues demonstrated that optimized lung-targeting LNP can achieve high-efficiency genome editing in stem cells, leading to long-lasting therapeutic effects. In the context of cystic fibrosis (CF), NG-ABE8e mRNA–sgR553X LNP achieved over 95% correction of CFTR DNA, successfully restoring CFTR function in primary bronchial epithelial cells derived from patients. The restoration was comparable to the effects of Trikafta in treating the F508del mutation. Additionally, this approach corrected intestinal organoids and repaired R553X nonsense mutations in 50% of lung stem cells in a CF mouse model [30].

1.2.3 Prime editor

Although highly efficient, base editors are restricted to introducing specific point mutations and cannot facilitate deletions or insertions. This limitation led to the development of prime editors (PEs) (**Fig.2**, right), which enable precise insertions and deletions with minimal unintended modifications and virtually no off-target effects. Similar to base editors, PEs operate without inducing DSBs, thereby minimizing the risk of chromosomal abnormalities and cellular toxicity—key factors in ensuring the safety of gene editing [31]. PEs function by combining a nickase Cas9 (nCas9) with prime editing guide RNA (pegRNA).

The pegRNA consists of two key components: a spacer sequence that identifies and binds to the target site, and an additional sequence that serves as a template for reverse transcription, including a primer-binding site (PBS) and an RT template sequence. Once the PE complex binds to the target site and pairs with the guide RNA, nCas9 nicks one DNA strand, creating an R-loop. This exposes a short single-stranded DNA (ssDNA)

segment on the non-complementary strand, with a free 3′ end where new bases can be incorporated. Unlike homology-directed repair, prime editing does not require external repair machinery or donor templates; instead, the molecular complex itself directly inserts the edited DNA sequence into the genome [32]. PEs, when combined with sgRNA, exceed 7 kb in size, posing challenges for delivery via a single viral vector. To overcome this limitation, Davis et al. recently developed a dual AAV system (v1em and v3em PE-AAV), enabling therapeutically relevant prime editing in various mouse tissues, achieving efficiencies of up to 42% in the cortex, 46% in the liver, and 11% in the heart. This system was applied *in vivo* to introduce protective mutations associated with Alzheimer's disease in astrocytes and coronary artery disease in hepatocytes. Notably, *in vivo* prime editing using v3em PE-AAV showed no detectable off-target effects or significant alterations in liver enzyme levels or tissue histology [33]. Similarly, due to the relatively large size of the prime editor complex, direct delivery as a ribonucleoprotein poses challenges for non-viral delivery systems. As a result, current non-viral delivery strategies for PE primarily rely on non-viral vectors to transport either plasmid DNA (pDNA) or messenger RNA (mRNA).

Among these approaches, mRNA delivery offers distinct advantages over DNA-based methods, including more rapid onset of action, transient expression, reduced off-target effects, and a lower risk of insertional mutagenesis [34]. For example, Barrera et al. developed a novel reporter cell line to facilitate the rapid identification of LNPs optimized for prime editing. Using enhanced LNPs (eLNPs) incorporating the cholesterol analog β-sitosterol at optimal RNA cargo ratios, they achieved a prime editing efficiency of 54% [35]. Additionally, Prime Medicine Inc. reported at the European Society of Gene and Cell Therapy (ESGCT) meeting that their targeted LNPs enabled precise editing of p L348 in non-human primates (NHPs), reaching efficiencies of up to 50% in the whole liver and 83% in hepatocytes by day 14. Importantly, intravenous administration of these LNPs resulted in no significant unintended edits or safety concerns [36].

Moreover, novel approaches and methodologies are continuously being developed and refined to overcome limitations and enhance the efficacy and versatility of CRISPR-based genome editing. This has led to the emergence of third-generation tools and technologies, including epigenome editors, RNA editors, and other advanced systems.

1.2.4 Epigenome editors

Permanent genetic modifications come with significant risks, including off-target mutations and ethical concerns, particularly regarding germline genome editing. As an alternative, CRISPR-based epigenome editing offers a way to regulate gene expression without altering the DNA sequence itself. This approach enables targeted epigenetic modifications that can persist across multiple cell divisions while avoiding direct changes to the genome

[37]. By coupling nuclease-dead Cas9 (dCas9) with enzymes that modify DNA or histones, researchers can manipulate chromatin structure at specific genomic sites to either activate or repress gene expression. One notable advancement, CRISPRoff, utilizes DNA methyltransferases like Dnmt3A or Dnmt3L along with KRAB transcriptional repressor domains to induce stable gene silencing over multiple generations of proliferating cells [38]. Conversely, gene expression can be restored using CRISPRon, which combines dCas9 with TET1 demethylase and transcriptional activation domains to reverse the epigenetic modifications.

Histone acetylation is another method of epigenetic regulation, where histone acetyltransferases (HATs) promote gene activation, while histone deacetylases (HDACs) suppress expression by altering chromatin accessibility [39, 40]. Despite its potential, epigenome editing still faces challenges. Cas9's ability to bind unintended sites based on partial guide RNA complementarity raises concerns about off-target effects [41, 42]. Furthermore, the durability and potential long-term consequences of these epigenetic modifications require further study, especially in the context of treating complex diseases.

1.2.5 RNA editor

Similar to epigenome editing, modifying RNA instead of DNA provides a potentially safer alternative for gene regulation, as mRNA has a transient presence in cells [43]. This limits the risk of permanent genetic changes while still allowing for precise intervention. RNA editing technologies have advanced significantly, offering greater control and specificity in modifying transcripts. One major breakthrough is the discovery of the Cas7-11 system, a single-protein CRISPR-Cas effector capable of targeting and cleaving RNA using guide RNAs [[44]. Unlike Cas13a-based approaches, Cas7-11 has been optimized to knock down transcripts with high specificity, minimal off-target effects, and no detectable collateral cleavage activity in mammalian cells RNAs [45]. Another innovative RNA-editing strategy involves CRISPR-mediated trans-splicing, which enables the targeted replacement or insertion of long RNA segments. This method leverages RNA-targeting Cas13 enzymes in combination with trans-splicing RNAs, allowing precise modifications of mammalian transcripts. These emerging RNA-editing technologies hold great promise for therapeutic applications, particularly for genetic disorders where temporary gene correction is beneficial [46]. By enabling reversible and highly targeted interventions, RNA editing expands the possibilities for genomic medicine and the development of novel treatment strategies.

Here, we provide an overview of the key features of various genome editors and compare them in detail, as illustrated in **Fig. 3**.

Feature	Cas9	Prime Editor (PE)	Base Editor (BE)	Epigenome Editing	RNA Editor
Primary Function	Generates double-strand breaks (DSBs) for gene knockout or insertion	Enables precise insertions, deletions, or base substitutions	Enables single-base changes (e.g., C→T or A→G)	Regulates gene expression without altering DNA sequence	Edits RNA to regulate gene expression or correct RNA errors
DNA Cleavage	Generates DSBs	No DSBs, may introduce single-strand nicks (nicking)	No DSBs, introduces single-strand nicks (nicking)	No DNA cleavage	No DNA cleavage
PAM Requirement	Yes (e.g., SpCas9 requires NGG)	Yes (e.g., SpCas9 requires NGG)	Yes (e.g., SpCas9 requires NGG)	Yes (if using dCas9)	No PAM requirement
Editing Scope	Large insertions, deletions, or replacements	Precise insertions, deletions, or base substitutions	Single-base changes (C→T or A→G)	Gene expression regulation (activation or repression)	RNA base editing (e.g., A→I)
DSBs Required	Yes	No	No	No	No
Single-Strand Nicking	No	Optional (when using nCas9)	Yes (uses nCas9)	No	No
Off-Target Effects	High (DSBs can cause unintended mutations)	Low (no DSBs)	Low (but risks DNA and RNA off-targets)	Low (but may affect non-target gene expression)	Low (RNA editing is often reversible)
Applications	Gene knockout, large insertions	Precise gene editing, point mutation repair	Single-base editing, point mutation repair	Gene expression regulation, epigenetic research	RNA repair, gene expression regulation
Example Tools	SpCas9, SaCas9	PE2, PE3	ABE (A→G), CBE (C→T)	dCas9-DNMT, dCas9-TET1	ADAR, Cas13
Alters DNA Sequence	Yes	Yes	Yes	No	No
Alters RNA Sequence	No	No	No	No	Yes
Persistence	Permanent DNA change	Permanent DNA change	Permanent DNA change	Reversible (epigenetic marks can be erased)	Reversible (RNA editing does not alter DNA)
Delivery Difficulty	Moderate (Cas9 is large)	High (PE system is large)	Moderate (BE system is large)	Moderate (dCas9 fusion proteins are large)	Low (RNA editors are smaller)

Figure 3. Comparison of CRISPR-Cas9, its derivatives, and RNA editing.

1.3 The clinical applications of CRISPR Cas9 based gene therapy

1.3.1 Cancer treatments

Cancer is a multifaceted disease driven by both genetic and epigenetic alterations in oncogenes and tumor suppressor genes. CRISPR–Cas9 has emerged as a powerful tool in cancer research. Notably, CRISPR has been applied in the treatment of hematological malignancies, such as leukemia and lymphoma, and has also been tested in solid tumor trials [47]. Epigenetic regulators are frequently mutated in myeloid malignancies. CRISPR-Cas9 technology has been used to correct mutations in the additional sex combs-like 1 (ASXL1) gene, successfully restoring ASXL1 protein expression and significantly inhibiting leukemia cell proliferation in mouse xenograft models [48]. Similarly, CRISPR-Cas9 was utilized to disrupt the myeloid cell leukemia-1 (MCL-1) gene, a member of the emerging B-cell lymphoma 2 (BCL2) family, in human Burkitt lymphoma (BL) cells. This deletion induced apoptosis in BL cells, indicating that MCL-1 may serve as a promising target for cancer therapy due to its role in cell differentiation, proliferation, and tumor development [49].

In 2016, a lung cancer patient received an infusion of PD-1-modified T cells, demonstrating early clinical application of CRISPR technology. Similarly, a CRISPR-based cancer immunotherapy trial in the United States has been completed, with several others currently underway [50]. One prominent study conducted at Sichuan University's West China Hospital involved 12 patients with non-small-cell lung cancer who were treated with PD-1-edited T cells. Unlike CAR-T therapy, which is not yet applicable to lung cancer, this approach aimed to evaluate safety, tolerability, and therapeutic response [51]. Another completed trial in China assessed the safety of PD-1 knockout T cells in patients with advanced esophageal cancer. Additionally, ongoing clinical trials are exploring CRISPR-based treatments for various solid tumors, including gastric, nasopharyngeal, and hepatocellular carcinomas, as well as renal cell carcinoma, B-cell leukemia, and lymphoma [52].

One of the major challenges in cancer chemotherapy is drug resistance. The multidrug resistance-1 (MDR1) gene encodes P-glycoprotein, a membrane efflux pump responsible for expelling anticancer drugs from cells, thereby reducing their efficacy. Targeted knockdown of MDR1 using CRISPR-Cas9 in osteosarcoma cell lines successfully restored drug sensitivity [53]. Similarly, overcoming acquired drug resistance caused by secondary mutations, such as the T790M mutation in exon 20 of the epidermal growth factor receptor (EGFR), represents a potential strategy for improving lung cancer treatment outcomes [54].

Apart from cancer treatment, infectious diseases also represent a significant area for CRISPR-Cas9 applications.

1.3.2 Infectious diseases

HIV/AIDS remains a life-threatening disease, affecting approximately 39 million people globally [55]. HIV was also the first infectious disease to be targeted in a gene therapy clinical trial. Research has demonstrated that individuals with CCR5-null blood cells exhibit resistance to HIV-1 infection, suggesting that CRISPR/Cas-mediated CCR5 knockout could serve as a potential strategy for eliminating the HIV provirus from infected cells [56]. In a 2017 clinical trial (NCT03164135), CRISPR/Cas9 was applied via a non-viral delivery system to introduce insertions and deletions (indels) in the CCR5 gene of donor-derived hematopoietic stem and progenitor cells (HSPCs, $CD34^+$ cells). While a follow-up over 19 months indicated a CCR5 knockout efficiency of only 5.2–8.28% in the bone marrow, no detectable off-target effects were reported [57].

Human papillomavirus (HPV) is a major driver of cervical intraepithelial neoplasia (CIN) and cervical cancer [58]. In 2014, Yu et al. pioneered the use of CRISPR/Cas9 to target HPV16 E6. Subsequently, a Phase 1 clinical trial (NCT03057912) was launched in 2017 at the First Affiliated Hospital of Sun Yat-Sen University to evaluate the safety and efficacy of CRISPR/Cas9 in treating cervical neoplasms and persistent HPV infection [59]. This trial aimed to disrupt the E6 and E7 oncogenes within the HPV genome. However, as of now, no public data has been released regarding the trial's outcomes.

For COVID-19, research has shown that disease severity can be influenced by immune system modulation [60, 61]. Scientists have investigated autologous T-cell therapies as a potential treatment, leveraging CRISPR/Cas technology to engineer immune cells such as CAR-T and CAR-NK. One notable strategy involves knocking out PD-1 to counteract immune suppression [62]. In this approach, virus-specific exhausted $CD8^+$ memory T cells are isolated from patients, and CRISPR/Cas9 is used to delete PD-1 and/or ACE2 genes. This modification enhances immune response, potentially providing long-term immunity against COVID-19 and other viral infections.

1.3.3 Inherited diseases

1.3.3.1 Sickle cell disease and transfusion-dependent β-thalassemia

Genetic disorders often arise due to gene mutations that alter protein function. Among them, sickle cell disease (SCD) and transfusion-dependent β-thalassemia (TDT) are considered the most severe monogenic conditions, characterized by serious and potentially life-threatening symptoms. Both SCD and TDT result from mutations in the human hemoglobin β subunit (HBB) gene [63, 64]. In TDT, mutations in the HBB gene disrupt β-globin production, leading to ineffective erythropoiesis and causing the disorder

in affected children [63]. On the other hand, SCD occurs due to a specific point mutation in HBB, where valine replaces glutamic acid at a particular amino acid position [63]. A recent study reported the development of a CRISPR/Cas9 system designed to target the erythroid-specific enhancer of BCL11A [64]. The findings revealed that approximately 80% of alleles were successfully edited at this locus without detectable off-target effects. Following myeloablation, two patients—one with TDT and the other with SCD—received autologous $CD34^+$ cells genetically modified using CRISPR/Cas9 to target the same BCL11A enhancer. In 2023, the FDA approved Casgevy, a cell-based gene therapy for SCD and TDT, for patients aged 12 and older. Casgevy is the first therapy to utilize CRISPR/Cas9 technology for SCD treatment and has been authorized by the FDA to prevent severe vaso-occlusive crises (VOCs). In an ongoing clinical trial involving 44 SCD patients, Casgevy demonstrated significant efficacy, with 93.5% of evaluable participants achieving at least 12 consecutive months without severe VOC episodes [64, 65].

1.3.3.2 Atherosclerosis and phenylketonuria

Hypercholesterolemia (HC) is a condition marked by excessively high levels of low-density lipoprotein (LDL) cholesterol in the blood. Research has shown that using CRISPR/Cas9 in combination with AAV to treat the mutant LdlrE208X strain resulted in a partial restoration of LDLR gene expression and a noticeable reduction in the risk of atherosclerosis [66]. Phenylketonuria (PKU), a metabolic disorder caused by a recessive mutation in the phenylalanine hydroxylase (PAH) gene, is one of the most common neonatal inborn errors of metabolism (IEMs). A study by Richards et al. (2020) demonstrated that CRISPR/Cas9 technology successfully corrected the Pahenu2 allele in a portion of liver cells in PKU-affected mice. This intervention led to a significant decrease in blood phenylalanine levels, partial restoration of liver PAH activity, and prevention of maternal PKU complications during pregnancy [67].

1.3.3.3 Muscular dystrophy

Muscular dystrophy (MD) is a progressive disorder characterized by the degeneration of skeletal muscles due to genetic or spontaneously inherited mutations. The presence of human dystrophin was detected *in vivo* after genetically modified patient cells were transplanted into immune-deficient mice. Notably, the advanced multiplex genome-editing capabilities of the CRISPR/Cas9 platform enable the deletion of specific genetic sequences, effectively correcting up to 62% of DMD mutations [68]. Building on this, Bengtsson et al. (2017) developed various genomic editing strategies to correct mutations in dystrophic mdx4cv mice using single and dual AAV vectors for Cas9 delivery, combined

with a sgRNA cassette to precisely repair the dystrophin gene. Studies have shown that muscle-restricted expression of Cas9 facilitates highly accurate gene editing, allowing for targeted mutation correction, multi-exon deletion, or full gene restoration using HDR in myogenic cells [69]. In line with this, Zhang et al. (2020) reported that efficient *in vivo* genome editing requires high doses of AAV, with Cas9 nuclease packaged in single-stranded AAV (ssAAV) and sgRNA in self-complementary AAV (scAAV). Their dual AAV strategy demonstrated that the scAAV dosage required for effective gene editing was at least 20 times lower than that of ssAAV. Furthermore, systemic therapy in mice led to the restoration of dystrophin expression and improved muscle contractility [70].

1.3.3.4 Hereditary hearing loss

Hereditary hearing loss (HHL) is a neurosensory disorder caused by monogenic or polygenic mutations, affecting approximately 1 in 500 infants worldwide and nearly one-third of individuals over the age of 65 [71]. Previous research on hearing loss suggests that *in vivo* gene correction in the inner ear via HDR has shown only limited success, primarily due to the low efficiency of HDR (<1%) compared to NHEJ (>85%) [72]. In a study involving inherited C57BL/6NTac mice, CRISPR/Cas9-mediated HDR was applied through microinjection at the zygote stage. Specifically, the Cas9 (D10A) nickase enzyme, combined with a single-stranded oligonucleotide donor and guide RNA (gRNA), was used to effectively correct defective alleles. This approach successfully repaired the faulty gene at the genotype level, leading to the phenotypic restoration of auditory function [73].

CRISPR/Cas9 technology has emerged as a powerful tool for treating genetic disorders by enabling precise gene editing. It has been successfully applied to various conditions, including sickle cell disease, β-thalassemia, muscular dystrophy, hereditary hearing loss, and metabolic disorders like phenylketonuria and hypercholesterolemia. Additionally, diseases such as Primary Hyperoxaluria Type 1 and Dystrophic Epidermolysis Bullosa have also been targeted using CRISPR/Cas9. This technology holds great promise for correcting genetic mutations, restoring normal gene function, and advancing the development of gene therapies.

1.4 Peptide-based delivery systems for Cas9: Development and application in AK Wagner

Building on previous studies, this thesis further advanced the development of artificial peptide-based Cas9 delivery systems. Our former colleague, Jasmin Kuhn, was the first to design and develop T-shaped peptides for the delivery of Cas9 RNP complexes. These lipid-containing oligoaminoamides (lipo-OAAs) incorporated synthetic amino acid Stp, cysteine residues (C), hydrophobic motifs such as a tyrosine (Y) tripeptide, and the unsaturated C18 fatty acid oleic acid (OleA). In parallel, other variants were synthesized using saturated stearic acid, bis-unsaturated linoleic acid (LinA), 8-nonanamidooctanoic acid (NonOcA), and hydroxystearic acid (OHSteA). Among these, the OHSteA-based lipo-OAAs formed smaller and more uniform nanoparticles when complexed with Cas9/sgRNA RNP. These particles exhibited enhanced cellular uptake and more efficient endosomal escape, leading to increased nuclear localization and the highest observed levels of gene knockout [74]. Furthermore, Yi Lin et al. designed (FolA)-PEG to conjugates OHSteA-based lipo-OAAs for enhancing receptor-mediated uptake and gene editing efficiency in tumor cells. Subsequently, FolA-modified Cas9 RNP nanocarriers were applied for cancer treatment by targeting the knockout of immune checkpoints PD-L1 and PVR. In *in vivo* experiments, these FolA-modified nanocarriers achieved significantly higher gene editing efficiency, including simultaneous disruption of both PD-L1 and PVR genes, following injection into CT26 tumors. In a syngeneic mouse model, dual knockout of PD-L1 and PVR resulted in enhanced recruitment of $CD8^+$ T cells and pronounced inhibition of CT26 tumor growth, outperforming the effects of individual gene knockouts [75].

To further explore novel oligomers for Cas9 RNP delivery efficiency, Yi Lin et al. designed various backbones, and modulated their hydrophobic properties by changing with various Stp analogues to optimize Cas9 delivery. The optimized amphiphilic carriers, based on a novel Xenopeptide structure, enabled approximately 88% eGFP knockout at a Cas9 RNP dose of only 1 nM, and achieved up to 40% HDR in eGFP/BFP switchable reporter cells through co-delivery with an ssDNA template [76]. Interestingly, Anna-Lina Lessl et al. employed the new Xenopeptide to conjugate with phosphorodiamidate morpholino oligomers (PMOs) for DMD gene therapy applications. The resulting PMO–XP conjugate formulation exhibited highly potent exon skipping *in vitro* and altered PMO biodistribution across multiple organs *in vivo* [77].

Concurrently, Sophie Thalmayr et al. developed novel lipoamino fatty acids (LAFs) and incorporated Stp residues to construct various topologies—such as block, bundle, T-shape, and U-shape—based dual pH-responsive Xenopeptides (XP), which demonstrated high potential for the delivery of pDNA, mRNA, and siRNA. In *in vivo* studies, the dual pH-responsive Xenopeptide-based mRNA formulation showed strong expression, particularly in the spleen, tumor, lungs, and liver, following intravenous administration of

1–3 µg of luciferase-encoding mRNA in mice [78]. Subsequently, Janin Germer et al. applied these dual pH-responsive Xenopeptides to deliver Cas9 mRNA for gene editing and correction. Genome editing efficacy of the top Xenopeptide (XP)-based carriers was observed at sub-nanomolar EC_{50} concentrations (0.1 nM sgRNA), even after incubation in ≥90% serum. Co-delivery of Cas9 mRNA and sgRNA with a single-stranded DNA template via LAF-XP-based polyplexes achieved up to 38% conversion of eGFP to BFP in reporter cells. In *in vivo* experiments, XP-LNPs mediated efficient gene editing of the DMD gene, inducing exon 23 skipping in dystrophin-expressing cardiac muscle, skeletal muscle, and brain tissue [79].

1.5 Aim of thesis

The CRISPR/Cas9 system has revolutionized biomedical research with its precision and versatility, offering unprecedented potential for therapeutic genome editing. Despite its promise in treating genetic disorders and cancer, clinical translation of CRISPR-based gene editing is still challenged by inefficient intracellular delivery of Cas9 ribonucleoprotein (RNP) complexes. Unlike plasmid DNA or mRNA-based strategies, direct RNP delivery avoids genomic integration and minimizes off-target effects. However, the large size and negative charge of RNP hinder their cellular uptake and endosomal escape, necessitating more efficient delivery platforms.

The first aim of this thesis focussed on the evaluation of a recently developed class of synthetic, dual pH-responsive LAF xenopeptides (LAF-XPs) as carriers for Cas9 RNP delivery. An XP library synthesized by Tobias Burghardt (PhD student, Pharmaceutical Biotechnology) with amphiphilic architectures, balancing hydrophobic and cationic domains to promote both complexation with Cas9 RNP and intracellular transport had to be tested. Through high-throughput screening in multiple reporter cell lines—including CT26-eGFP Luc, Hepa 1-6 Pcsk9tdTomato and HeLa eGFPd2—several lead XP backbones had to be identified.

Building on initial results, further optimization additional lipo-XPs, incorporating Stp analogs (e.g., dGtp and GEIPA) into the dual pH-responsive XP backbone, had to be tested. Nanoparticle stability, RNP loading efficiency, and gene editing performance, particularly under physiologically relevant conditions such as high serum incubation, had to be evaluated.

The second aim of the thesis addressed another critical barrier in precision genome editing: the inefficiency of homology-directed repair (HDR), which is required for precise gene correction. While non-homologous end joining (NHEJ) is the dominant DNA repair pathway in mammalian cells, it is error-prone and typically results in insertions or deletions

(indels). In contrast, HDR allows for accurate repair using a donor DNA template but is restricted to certain phases of the cell cycle and is inherently less efficient. To overcome this bottleneck, the study had to investigate the use of small-molecule modulators that could shift the balance toward HDR.

Specifically, the DNA-PKcs inhibitor Nu7441—traditionally used to suppress NHEJ—had to be tested in combination with optimized T shaped XP-Cas9 RNP/ssDNA complexes. Mechanistic investigations had to be performed to characterize enhanced genome editing. Detailed cellular and molecular analyses had to include cellular uptake, endosomal escape, and cell cycle progression, identifying HDR-permissive phases of cells. Complementary assays to be applied included co-delivery of plasmid DNA and mRNA reporters to verify the rule of nuclear entry.

2 Chapter I:

Dual pH-responsive CRISPR/Cas9 ribonucleoprotein xenopeptide complexes for genome editing

Xianjin Luo,[1+] Janin Germer,[1+] Tobias Burghardt,[1] Melina Grau,[1] Yi Lin,[1‡] Miriam Höhn,[1] Ulrich Lächelt,[2.3] Ernst Wagner[1,2,4*]

[1] Pharmaceutical Biotechnology, Department of Pharmacy, Ludwig-Maximilians-Universität Munich, Butenandtstrasse 5-13, 81377 Munich, Germany

[2] Center for Nanoscience (CeNS), LMU Munich, 80799 Munich, Germany

[3] Department of Pharmaceutical Sciences, University of Vienna, Josef-Holaubek-Platz 2, 1090 Vienna, Austria

[4] CNATM - Cluster for Nucleic Acid Therapeutics Munich, Germany

[+] Equally contributing first authors

[‡] Current address: Department of Biomedical Engineering, College of Future Technology, Peking University, Beijing 100871, China

The following sections are adapted from the submitted manuscript.

Sections may have been moved for consistency.

Contribution of PhD student colleagues: Janin Germer performed initial RNP formulations and testing; Tobias Burghardt synthesized the novel LAF-XPs, Melina Grau synthesized the initial LAF-XPs; Yi Lin provided initial supervision and introduction into cellular assays.

2.1 Abstract

Clustered regularly interspaced short palindromic repeat (CRISPR)/CRISPR associated (Cas) protein has been proved as a powerful tool for the treatment of genetic diseases. The Cas9 protein, when combined with single-guide RNA (sgRNA), forms a Cas9/sgRNA ribonucleoprotein (RNP) capable of targeting and editing the genome. However, the limited availability of effective carriers has restricted the broader application of CRISPR/Cas9 RNP. In this study, we evaluated dual pH-responsive amphiphilic xenopeptides (XPs) for delivering CRISPR/Cas9 RNP. These artificial lipo-XPs contain apolar cationizable lipoamino fatty acid (LAF) and polar cationizable oligoaminoethylene acid units such as succinoyl-tetraethylenepentamine (Stp) in various ratios and U-shaped topologies. The carriers were screened for functional Cas9/sgRNA RNP delivery in four different reporter cell lines, including a Duchenne muscular dystrophy (DMD) exon skipping reporter cell model. Significantly enhanced cellular uptake into HeLa cells, effective endosomal disruption in HeLa gal8-mRuby3 cells, and potent genome editing by several Cas9/sgRNA RNP complexes was observed in four different cell lines in the 5 nM sgRNA range. Comparing Cas9/sgRNA RNP complexes with Cas9 mRNA/sgRNA polyplexes in the DMD reporter cell model demonstrated similar splice site editing and high exon skipping of the two different molecular Cas9 modalities. Based on these studies, analogues of two potent U1 LAF_2-Stp and LAF_4-Stp_2 structures were deployed, tuning the amphiphilicity of the polar Stp group by replacement with the six oligoamino acids dmGtp, chGtp, dGtp, Htp, Stt, or GEIPA. The most potent LAF_2-Stp analogues (containing dGtp, chGtp or GEIPA) demonstrated further enhanced gene editing efficiency with EC50 values of 1 nM in the DMD exon skipping reporter cell line. Notably, the EC50 of LAF_2-dGtp reached 0.51 nM even upon serum incubation. Another carrier (LAF_4-$GEIPA_2$) complexing Cas9/sgRNA RNP and donor DNA, facilitated up to 43% of homology-directed repair (HDR) in HeLa eGFPd2 cells visualized by the switch from green fluorescent protein (eGFP) to blue fluorescent protein (BFP). This study presents a delivery system tunable for Cas9 RNP complexes or Cas9 RNP/donor DNA polyplexes, offering an effective and easily applicable strategy for gene editing.

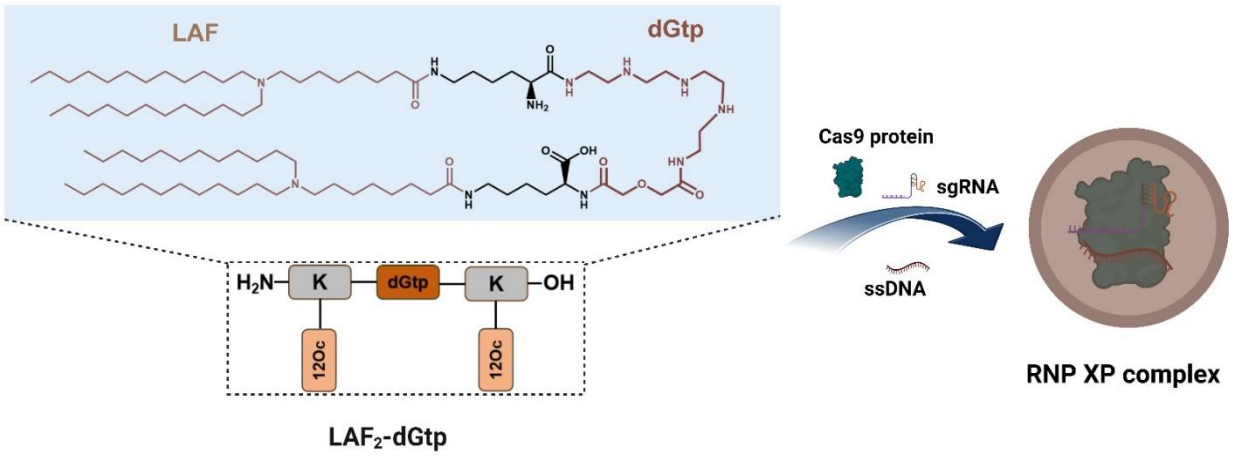

Schematic illustration depicting the chemical structure of LAF_2-dGTP and corresponding RNP XP complex.

2.2 Introduction

Recently, CRISPR-based gene therapy for Sickle Cell Disease (SCD) and beta thalassemia, CASGEVY (Exa-cel), was approved [64, 80, 81]. Obviously, CRISPR-based gene editing technologies are emerging as powerful tools for treating human diseases. Among them, CRISPR/Cas9 is the most commonly used system [82], serving as a groundbreaking genetic engineering tool. The programmable gene editing system comprises a Cas9 nuclease and single-guide RNA (sgRNA) that identifies specific target genomic loci and guides the Cas9 nuclease to cleave the recognized DNA sequence, resulting in a double-strand break (DSB). DSBs are repaired through either nonhomologous end joining (NHEJ) or homology-directed repair (HDR). NHEJ typically induces knockout mutations, while HDR can facilitate knock-in of sequences provided by a DNA repair template [11].

The CRISPR/Cas9 genome editing system can be applied using three forms of biomolecules, including plasmid DNA (Cas9 and sgRNA encoding plasmids), RNA (Cas9 mRNA and sgRNA), or ribonucleoprotein (Cas9/sgRNA RNP complex) [34, 83, 84]. While CRISPR/Cas9 plasmids are extensively employed in gene editing, the delivery of pDNA may potentially provoke more undesired side effects. Residual CRISPR genes may remain in host cells post-delivery and, along with sustained CRISPR expression, could trigger unintended genetic modifications and immune reactions. On the contrary, short-term RNP or mRNA delivery has the potential of decreased immunogenicity and side effects compared to plasmid-based delivery [85]. Additionally, in clinical settings, transient RNP exposure is highly desirable to ensure safety. Therefore, we primarily focused on

delivery of Cas9 RNP or Cas9 RNA nanoparticles as our research subjects.

However, achieving efficient Cas9/sgRNA RNP delivery [16, 74, 83, 86-88] remains an interesting but significant challenge due to its large size and structural instability, leading to inadequate cellular uptake. Like in the case of Cas9 mRNA, which is relatively unstable, it needs to be combined with sgRNA. Consequently, a delivery vehicle must be capable of loading either Cas9 protein or mRNA and sgRNA simultaneously for genome editing applications, posing challenges in both loading and release. These drawbacks can be effectively addressed with appropriate delivery systems. While viral vectors, notably lentiviruses or adeno-associated viruses, are extensively used in gene supplementation therapies and also utilized as vehicles for delivering the CRISPR/Cas9 machinery, they are not suitable for mRNA or ribonucleoprotein delivery. In addition, their inherently high viral immunogenicity presents a concern. Non-viral delivery strategies for Cas9 delivery [14, 89-92] utilize diverse materials, with lipid-based carriers being most advanced [93]. Synthetic nanoparticles have shown high nucleic acid loading capacity, low to moderate cytotoxicity and immunogenicity, and scalability [94-102]. Nevertheless, the efficacy measured at the nanoparticle level is often moderate and limited to specific organs and tissues.

Notably, peptide-like materials offer exceptional flexibility and precision in design and synthesis [103-106], making them a versatile platform for optimizing nucleic acid delivery systems by chemical evolution [107]. In our previous studies, we designed artificial peptides for nucleic acid delivery termed ‘xenopeptides’ (XPs), as they are primarily composed of artificial hydrophilic cationizable aminoethylene amino acids such as succinoyl-tetraethylenepentamine (Stp) [108-112]. A series of T-shaped lipo-XPs was further optimized by the chemical evolution strategy for Cas9 RNP delivery, providing top carriers with a 50% knockout efficacy in HeLa-GFP/tub reporter cells at sub-nanomolar sgRNA concentrations [76], demonstrating potent Cas9 RNP delivery capabilities. Entrapment within endosomes presents a significant barrier for nonviral formulations that needs to be overcome by various means [113]. Recently, we synthesized a series of dual pH-responsive amphiphilic lipo-XPs composed of lipophilic cationizable lipo amino fatty acid (LAF) and hydrophilic cationizable Stp units. By incorporating a central tertiary amine into the LAF unit, a pH-dependent tunable amphiphilicity of the XPs was achieved. Upon endosomal protonation, the lipophilic nature of LAF is disrupted, resulting in pH-dependent structural and physical alterations that result in the effective disruption of endosomes [78, 114, 115].

Based on their specific properties, Germer et al. applied such LAF-XPs for delivery of CRISPR/Cas9 mRNA and achieved over 50% gene editing efficiency at an ultra-low dose of 0.1 nM sgRNA [79]. We hypothesized that a subset of the dual pH-responsive amphiphilic XPs might also function as a powerful vehicle for the CRISPR/Cas9 RNP

delivery. In the current study, we assessed the suitability of the carrier class for gene editing via Cas9 protein/sgRNA RNP delivery. The nanocarriers were expected to substantially enhance cellular uptake of Cas9 RNP. The acidic environment of the endosome is supposed to trigger endosomal membrane disruption and escape of CRISPR/Cas9 RNP, ultimately resulting in significantly improved gene editing efficacy. Two U1-topology lipo-XPs (*1611* and *1719*) demonstrated robust gene editing efficiency in three different cell lines. Editing efficiencies of Cas9/sgRNA RNP were high and comparable with previously reported Cas9 mRNA/sgRNA efficiencies [[79], as evaluated here side-by-side in an DMD exon skipping reporter cell model [77]. As also reported in the following, chemical variation of the polar aminoethylene acid unit Stp by analogues resulted in new lipo-XP RNP complexes with further improved gene editing characteristics.

2.3 Materials and methods

2.3.1 Materials

4′,6-diamidino-2-phenylindole (DAPI), agarose, ampicillin, dimethyl sulfoxide (water free) (DMSO), 3-(4,5-dimethylthiazol-2-yl)-2,5-diphenyltetrazolium bromide (MTT), Dulbecco's Modified Eagle's Medium (DMEM), fetal bovine serum (FBS) and penicillin/streptomycin were bought from Life Technologies (Carlsbad, USA). 4-(2-hydroxyethyl)-1-piperazineethanesulfonic acid (HEPES) was bought from Biomol GmbH (Hamburg, Germany). Cas9 protein was produced in-house as described [75, 76]. Single guide RNA (sgRNA) with 2'-O-methyl modifications on the first and last three RNA bases, along with phosphorothioate modifications on the RNA bases. Single-stranded DNA (ssDNA) were procured from Integrated DNA Technologies (Coralville, USA) or AxoLabs GmbH (Kulmbach, Germany), with their sequences provided in Table S1. Cas9 mRNA (mCherry) were obtained from Trilink Biotechnologies (San Diego, USA). Deionized water, purified using a Millipore system (Simplicity Plus, Millipore Corp), was employed for solution preparation. The synthesis of the artificial amino acid Fmoc-Stp(Boc)3-OH (Stp) and its analogues as well as assembly of the LAF-xenopeptides (LAF-XPs) was performed as previously described [76] or will be separately described (Burghardt et al, in preparation).

Table 1. sgRNAs and ssDNA sequences utilized in this study.

sgRNA and ssDNA	Sequence 5'→ 3'
sgPcsk9	5'mC*mC*mC*AUACCUUGGAGCAACGGGUUUUAGAmGmCmUmAmGmAmAmAmUmAmGmCAAGUUAAAUAAGGCUAGUCCGUUAUCAmAmCmUmUmGmAmAmAmAmGmUmGmGmCmAmCmCmGmAmGmUmCmGmGmUmGmCmUmU*mU*mU* 3'
sgDMDEx23	5'mA*mU*mU*UCAGGUAAGCCGAGGUUGUUUUAGAGCUAGAAAUAGCAAGUUAAAAUAAGGCUAGUCCGUUAUCAACUUGAAAAAGUGGCACCGAGUCGGUGCmU*mU*mU*U
sgGFP1	5'mG*mA*mC*CAGGAUGGGCACCACCCGUUUUAGAGCUAGAAAUAGCAAGUUAAAAUAAGGCUAGUCCGUUAUCAACUUGAAAAAGUGGCACCGAGUCGGUGCmU*mU*mU*U3'
sgGFP2	5' mG*mC*mU*GAAGCACUGCACGCCGUGUUUUAGAGCUAGAAAUAGCAAGUUAAAAUAAGGCUAGUCCGUUAUCAACUUGAAAAAGUGGCACCGAGUCGGUGCmU*mU*mU*rU 3'
ssDNA	G*C*CACCTACGGCAAGCTGACCCTGAAGTTCATCTGCACCACCGGCAAGCTGCCCGTGCCCTGGCCCACCCTCGTGACCACCCTGAGCCACGGCGTGCAGTGCTTCAGCCGCTACCCCGACCACAT*G*A

Modification pattern: '*' denotes phosphorothioated RNA bases; 'm' indicates 2'-O-methyl nucleotide bases. sgGFP1 was employed in the CT26-eGFP Luc cell line for the eGFP knockout experiment, while sgGFP2 was utilized in the HeLa eGFPd2 cell line for both eGFP knockout and HDR experiments.

Table 2. Library of *1611* and *1719* XP analogues, with ID numbers and (N- to C-terminal) sequences.

Backbone	ID	sequence
1611 analogues	1840	K(12Oc)-dmGtp-K(12Oc)
	1841	K(12Oc)-chGtp-K(12Oc)
	1842	K(12Oc)-dGtp-K(12Oc)
	1843	K(12Oc)-Htp-K(12Oc)
	1844	K(12Oc)-Stt-K(12Oc)
	1845	K(12Oc)-GElPA-K(12Oc)
1719 analogues	1858	$[K(12Oc)]_2$-$(dmGtp)_2$-$[K(12Oc)]_2$
	1859	$[K(12Oc)]_2$-$(chGtp)_2$-$[K(12Oc)]_2$
	1860	$[K(12Oc)]_2$-$(dGtp)_2$-$[K(12Oc)]_2$
	1861	$[K(12Oc)]_2$-$(Htp)_2$-$[K(12Oc)]_2$
	1862	$[K(12Oc)]_2$-$(Stt)_2$-$[K(12Oc)]_2$
	1863	$[K(12Oc)]_2$-$(GElPA)_2$-$[K(12Oc)]_2$

2.3.2 Formulation of Cas9 ribonucleoprotein (RNP) complexes or Cas9 mRNA polyplexes

The expression, purification, and storage method of Cas9 protein were previously described [74-76]. For the preparation of Cas9 RNP complexes, the Cas9 protein was mixed with sgRNA at a 1:1 molar ratio, followed by an incubation period of 15 min at room temperature. Subsequently, the resulting RNP and the stored XP solution were individually diluted with HBG (20 mM HEPES, 5% glucose, pH 7.4) to equal volumes. The RNP was then added to the XP solution and thoroughly mixed by pipetting up and down 10 times. This mixture was further incubated for 15 min at room temperature to achieve the final Cas9 RNP complexes at a 375 nM or 500 nM sgRNA concentration. In the presence of a ssDNA HDR template, the different ssDNA amount was initially combined with the RNP. Subsequently, the XP was introduced to the mixture, followed by a 40-minute incubation period. Nitrogen to phosphate (N/P) ratio of the formulations are 12, 18, and 24.

In case of Cas9 mRNA polyplexes, Cas9 mRNA was combined with sgRNA at a 1:1 weight ratio and diluted in HBG. The appropriate amount of XP at a N/P ratio of 24 was then diluted in HBG. Equal volumes of the nucleic acid solution and XPsolution was mixed vigorously by pipetting up and down 10 times, followed by incubation for 40 min at room temperature. The final concentration of nucleic acids in the polyplex solution was 12.5 μg/mL (6.25 μg/mL Cas9 mRNA and 6.25 μg/mL sgRNA), corresponding to an sgRNA concentration of 375 nM.

2.3.3 Dynamic light scattering (DLS) and transmission electron microscopy (TEM) measurements of Cas9 RNP complexes

The size and zeta potential of nanocarriers were measured in a folded capillary cell (DTS1070) by Zetasizer Nano ZS (Malvern Instruments, Worcestershire, UK). The parameters of nanoparticle solutions were set as follow: equilibration time 30 sec, temperature 25°C, refractive index 1.330, viscosity 0.8872 mPa*s. The surface morphology of complex was measured by transmission electron microscopy (TEM). For sample preparation, the grid was positioned with the activated face downward onto 10 μL sample droplet. Subsequently, the sample was blotted away using filter paper and subjected to staining via a two-step process: initially, the grid was rinsed with 5 μL staining 1.0% uranyl formate solution, which was promptly removed. Subsequently, 5 μL of the same solution was retained on the grid. Subsequently, the solution was blotted away with filter paper, and the grid was allowed to air-dry for 20 min. Following this, samples were examined by a JEOL JEM-1100 electron microscope (Tokyo, Japan) with an acceleration voltage of 80 kV.

2.3.4 Ribogreen assay for encapsulation efficiency

The encapsulation efficiency of Cas9 RNP complexes was determined using the Quant-iTTM RiboGreen® RNA Assay Kit (Invitrogen, CA, USA). For each sample, 50 µL of RNP complexes (containing 125 ng sgRNA) was combined with 50 µL of TE buffer, either with or without 2% (v/v) Triton X-100 (Sigma Aldrich, UK), and incubated in a 96-well plate at 37 °C with shaking (150 rpm) for 10 min.

A standard curve was generated using various sgRNA concentrations. Following the incubation, 100 µL of RiboGreen solution (1:100 dilution) was added to each well, and the plate was incubated for an additional 5 min. Fluorescence was measured using a microplate reader (Spectrafluor Plus, Tecan, Switzerland) with excitation and emission wavelengths of 485 nm and 528 nm, respectively. The sgRNA concentrations in the complexes, with or without Triton X-100 treatment, were quantified using the standard curve. Encapsulation efficiency (%) was calculated using the formula: (1 − (nanocarriers without lysis / nanocarriers with lysis)) × 100 %.

2.3.5 Cell culture

HeLa WT, HeLa eGFPd2, CT26-eGFP Luc, Hepa 1-6 *Pcsk9*^{tdTomato} (exhibiting stable expression of tdTomato in the 3'UTR of the Pcsk9 gene), HeLa mCherry-DMD$_{Ex23}$ (stably expressing an artificial mCherry construct, containing a dystrophin exon 23 sequence interruption derived from the murine Duchenne muscular dystrophy (DMD) *mdx* model) and HeLa gal8-mRuby3 cells (stably expressing galectin8-mRuby3 fusion protein) were cultured in DMEM medium supplemented with 10% FBS, 100 U/mL penicillin, and 100 µg/mL streptomycin. These cells were incubated in ventilated flasks in a cell incubator set at 37°C and 5% CO_2 in a humidified atmosphere. Passage of the cells was performed at a confluency of approximately 80%.

2.3.6 Cellular uptake of Cas9 RNP complexes

To prepare the cellular uptake experiment of Cas9 RNP complexes, ATTO647N-labeled Cas9 protein was prepared as described previously (Lin et al., 2023a; Lin et al., 2023b). HeLa WT cells were first plated at a density of 2.5 × 10^4 cells per well in 24-well plates and cultured for 24 h. Afterwards, the cells were incubated with free Cas9 RNP or Cas9 RNP complexes containing 37.5 nM Cas9 protein for 2 h. Formulations were fabricated as outlined above using 20 % of ATTO647N-Cas9 protein. Following incubation, the medium was aspirated, and 500 µL of PBS containing 2000 IU heparin were added to dissociate any nanocarriers attached to the cell membrane. The cells were then incubated on ice for 30 min. After washing with 500 µL of PBS, the cell nuclei were stained with 4',6-diamidino-2-phenylindole (DAPI). Subsequently, the cells were harvested and prepared for analysis using a Beckman Coulter CytoFLEX S flow cytometer (Carlsbad, USA). All

experiments were conducted in triplicate. The DAPI signal was detected using 405 nm excitation and 450 nm emission wavelengths. ATTO647N fluorescence was measured with 640 nm excitation and 670 nm emission wavelengths. The uptake percentage was calculated based on the mean fluorescence intensity.

2.3.7 Gal8 endosomal escape assay of Cas9 RNP complexes by confocal laser scanning microscope (CLSM)

HeLa gal8-mRuby3 cells were seeded in 8-well Ibidi µ-slides (Ibidi GmbH, Germany) at a density of 2× 10^4 cells per well and cultured for 24 h. Following this, 60 µL of RNP complexes were added to each well, resulting in a final concentration of 10 nM Cas9 RNP, then incubated with cells for 2 h. Next, the cells were washed with 300 µL PBS and fixed with 4% paraformaldehyde at room temperature for 45 min. Subsequently, the cell nucleus was stained with 1 µg/mL DAPI in the dark for 15 min. Then, the staining solution was removed and 300 µL fresh PBS were added. The samples were analyzed using a Leica-TCS-SP8 confocal laser scanning microscope (Wetzlar, Germany).

The DAPI signal was recorded at 450 nm, while mRuby3 signal was recorded at 590 nm. The number of Gal8 spots per cell was analyzed using ImageJ software. Initially, cell nuclei and background were removed using the Clear tool. Subsequently, the image was converted to an 8-bit type. The parameters for identifying mRuby3/gal8 spots were further adjusted using the Threshold tool, and the number of spots in the cell cytosol per cell was counted using the Analyze Particles tool.

2.3.8 The gene editing efficiency of Cas9 RNP and Cas9 mRNA nanoparticles

To assess the gene editing efficiency of nanocarriers, Hepa 1-6 *Pcsk9*^{tdTomato}, CT26 eGFP-Luc, HeLa eGFPd2 and HeLa mCherry-DMD_{Ex23} cells were first plated at a density of 5 × 10^3 cells per well in Corning® Costar 96-well plates (Sigma-Aldrich, Germany) and cultured for 24 h. The medium was changed with 80 µL fresh medium and 20 µL formulation solution. The nanocarriers were fabricated at 375 nM sgRNA as outlined above. Subsequently, the formulation was diluted in HBS to ensure that the 20 µL solution contained the appropriate concentration. After 24 h of transfection, HeLa mCherry-DMD_{Ex23} cells were expanded and incubated for an additional 2 days. All other cell lines were transfected for 48 h and incubated for an additional 3 days. Subsequently, cells were trypsinized, centrifuged at 1000 g for 5 min, and washed with PBS. Finally, the cells were collected and resuspended in FACS buffer (10% FBS/90% HBG, v/v). The gene editing efficiency of the formulations was analyzed using a Beckman Coulter CytoFLEX S flow cytometer (Carlsbad, USA). Prior to measurement, 1 µg/mL DAPI was added to discriminate between viable and dead cells. A total of 2000 live cells per sample, identified through DAPI staining, were quantified. Gene editing efficiency was calculated using the formula: (A-B)/(100%-B)×100%, where A represents the percentage of GFP-negative cells

in the GFP cell model or mCherry-positive cells in the DMD cell model in the treated group, and B represents the corresponding percentage in the untreated group (incubated with HBG).

The DAPI signal was detected using 405 nm excitation and 450 nm emission wavelengths. The *Pcsk9* knock out efficiency was calculated as the percentage of tdTomato negative cells. The cellular tdTomato expression in Hepa 1-6 *Pcsk9t*^{tdTomato} cells was assayed using 561 nm excitation and 585 nm emission wavelengths. The GFP knockout efficiency was calculated as the percentage of GFP-negative cells, normalized to the control measurements with HBG buffer-treated cells. The cellular GFP expression in CT26 eGFP-Luc and HeLa eGFPd2 cells was evaluated using 488 nm excitation and 530 nm emission wavelengths. The transfection efficiency in HeLa mCherry-DMD$_{Ex23}$ cells was quantified as the percentage of mCherry-positive cells. Cellular mCherry expression was analyzed utilizing 561 nm excitation and 610 nm emission wavelengths.

2.3.9 Comparison of gene editing mediated exon skipping of Cas9 RNP complexes without or with pre-incubation in HBG or high serum

HeLa mCherry-DMD$_{Ex23}$ cells were seeded at a density of 5 × 10^3 cells per well in Corning® Costar 96-well plates and cultured 24 h. Subsequently, cells were transfected with 20 μL Cas9 RNP complexes for 24 h. Before transfection, the nanocarriers were fabricated at 500 nM sgRNA as outlined above. Subsequently, the complexes were diluted with HBG or 100% FBS, typically by a factor of over 10 times, followed by a 15-min incubation at room temperature. To ensure that the added 20 μL complex solution contained the appropriate concentration, additional HBG buffer or FBS was added for HBG-diluted or serum-incubated particles, respectively. HBG buffer served as the negative control. After 24 h transfection, the cells were incubated for 2 days. Then, cells were trypsinized, centrifuged at 1000 g for 5 min, and washed with PBS. Finally, the cells were collected and resuspended in FACS buffer. The gene editing efficiency of the formulations was analyzed using a Beckman Coulter CytoFLEX S flow cytometer (Carlsbad, USA). The details of measurement were conducted as outlined above.

2.3.10 Gene editing mediated exon skipping by Cas9 RNP complexes visualized by CLSM

HeLa mCherry-DMD$_{Ex23}$ cells were seeded at a density of 2 × 10^4 cells per well in Corning® Costar 24-well plates and cultured 24 h. The cells were then transfected with 10 nM Cas9 RNP complexes for 24 h and incubated for an additional 2 days. Following this, the cells were transferred to 8-well Ibidi μ-slides (Ibidi GmbH, Germany) and incubated overnight. The next day, the cells were washed with 300 μL PBS and fixed with 4% paraformaldehyde at room temperature for 45 min. The cytoskeleton was stained with Alexa Flour™ 488 phalloidin for 2 h, and the nuclei were stained with 1 μg/mL DAPI in the

dark for 15 min. After staining, the solution was removed and replaced with 300 µL of fresh PBS. The samples were then analyzed using a Leica TCS SP8 confocal laser scanning microscope (Wetzlar, Germany). The DAPI signal was recorded at 450 nm, the AF488 signal at 530 nm, and the mCherry signal at 610 nm.

2.3.11 eGFP to BFP conversion mediated by homology-directed repair (HDR)

Prior to the transfection for 24 h, HeLa eGFPd2 were plated at a density of 5×10^3 cells per well in Corning® Costar 96-well plates. Next, the medium was substituted with 80 µL fresh medium, supplemented with 20 µL of the formulation solution. Cas9 RNP/ssDNA complexes were fabricated at a 500 nM RNP as described above. And the formulation was diluted in HBG to ensure that the 20 µL solution contained the appropriate concentration. Then, cells were transfected for 48 h. Afterwards, the medium was replaced with 100 µL of fresh medium, and the cells were incubated for an additional 72 h. Then, cells were trypsinized, centrifuged at 1000 g for 5 min, and washed with PBS. Finally, the cells were harvested and resuspended in FACS buffer. Before measurement, the cells were stained with 1 µg/mL propidium iodide (PI) to discriminate between viable and dead cells. The cells with positive GFP (unedited cells), negative (NHEJ), and positive BFP (HDR) expression were quantified using a Beckman Coulter CytoFLEX S flow cytometer (Carlsbad, USA). The PI signal was detected using 561 nm excitation and 610 nm emission wavelengths. BFP fluorescence was measured with 405 nm excitation and 450 nm emission wavelengths. GFP fluorescence was assessed with 488 nm excitation and 530 nm emission wavelengths.

2.3.12 Assessment of the cytotoxicity of cells via MTT assay

Transfections were performed as described above. After 24 or 48 h of transfection, 10 µL of dimethylthiazol (MTT) solution (5 mg/mL) was added to each well, reaching a final concentration of 0.5 mg/mL. The supernatant was removed following a 2-hour incubation at 37 °C. The plates were then stored at –80 °C for at least 1 h. Subsequently, the purple formazan product was dissolved in 100 µL of DMSO. After a 30-minute incubation at 37 °C with constant shaking (125 rpm), the absorbance was measured photometrically using a Tecan microplate reader (Spectrafluor Plus, Tecan, Männedorf, Switzerland) at 590 nm, with background correction at 630 nm. Cell viability was calculated using the following equation: ***A/B×100%.*** Here, *A* represents the absorbance of the test sample group, while *B* represents the absorbance of the HBG group.

2.3.13 Statistical analysis

Statistical analysis was conducted using GraphPad Prism 8.0 software. Results are expressed as mean ± standard deviation (SD). The data were analyzed using an unpaired Student's two-tailed t-test, with significance indicated as * $p < 0.05$, ** $p < 0.01$, **** $p<$

0.0001 and "ns" denoting not significant.

2.4 Results and discussion

2.4.1 Screening of lipo-XPs for Cas9/sgRNA RNP delivery

In the current study we applied recently described LAF-XP carriers [78], which were synthesized through standard Fmoc solid-phase peptide synthesis, using the polar cationizable oligoamino acid succinoyl-tetraethylenepentamine (Stp) and apolar cationizable lipoamino fatty acid (LAF) units (Fig. 1A). Between Stp and LAF units, lysines were covalently connected as branching points to generate various topologies. In the current study, U-shape (U1, U3, U4) topologies as depicted in **Fig. 1B** were evaluated. In addition to the cationizable aminoethylene motif in Stp, the LAFs contain a protonatable tertiary amine, resulting in a pH-dependent switch of polarity in these hydrophobic moieties (**Fig.1C**). The sequences of evaluated lipo-XPs are listed in **Fig. 1D**. LAF-Stp XP based Cas9 RNP complexes were prepared by directly complexing LAF-Stp XP and Cas9 RNP at nitrogen-to-phosphate (N/P) ratio of 24 and incubation for 15 min. The N/P ratio refers at all protonatable nitrogens, irrespective of their actual protonation. At physiological pH, the LAF nitrogens and the majority of Stp nitrogens are non-protonated, and the C-terminal carboxylate is negatively charged. Thus, 6 to 11 nitrogens per molecule refer to only approximately 0.5 to 2 positive charges at neutral pH. For this reason, a high formal nitrogen-to-phosphate (N/P) ratio of 24 had to be applied to provide sufficiently positive charge for complexation of the negatively charged RNP. Most of the formed nanoparticles exhibited hydrodynamic sizes under 300 nm (**Fig. 2A**) and zeta potentials between +9 and +35 mV (**Fig. 2B**).

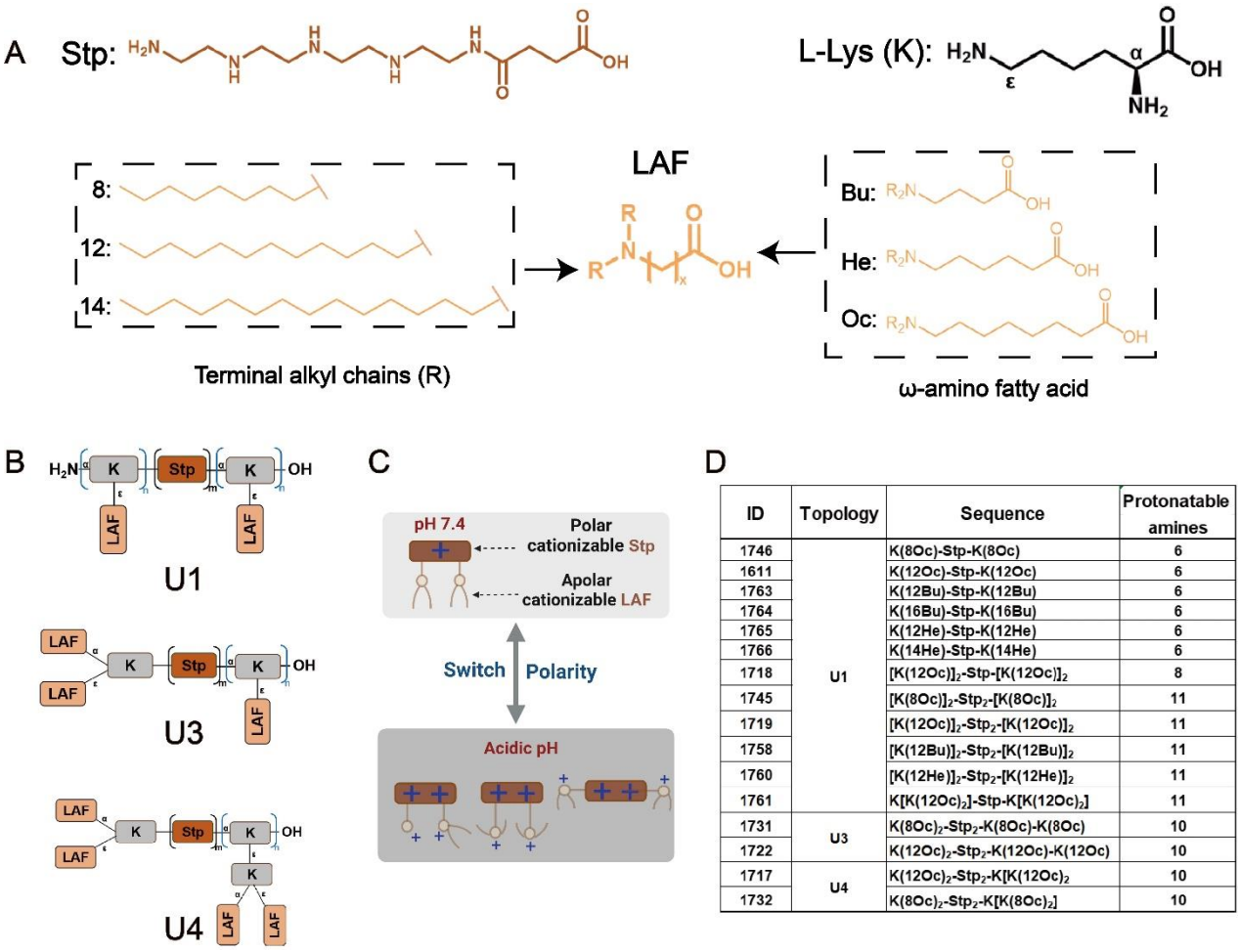

ID	Topology	Sequence	Protonatable amines
1746	U1	K(8Oc)-Stp-K(8Oc)	6
1611		K(12Oc)-Stp-K(12Oc)	6
1763		K(12Bu)-Stp-K(12Bu)	6
1764		K(16Bu)-Stp-K(16Bu)	6
1765		K(12He)-Stp-K(12He)	6
1766		K(14He)-Stp-K(14He)	6
1718		$[K(12Oc)]_2$-Stp-$[K(12Oc)]_2$	8
1745		$[K(8Oc)]_2$-Stp_2-$[K(8Oc)]_2$	11
1719		$[K(12Oc)]_2$-Stp_2-$[K(12Oc)]_2$	11
1758		$[K(12Bu)]_2$-Stp_2-$[K(12Bu)]_2$	11
1760		$[K(12He)]_2$-Stp_2-$[K(12He)]_2$	11
1761		K$[K(12Oc)_2]$-Stp-K$[K(12Oc)_2]$	11
1731	U3	$K(8Oc)_2$-Stp_2-K(8Oc)-K(8Oc)	10
1722		$K(12Oc)_2$-Stp_2-K(12Oc)-K(12Oc)	10
1717	U4	$K(12Oc)_2$-Stp_2-K$[K(12Oc)_2$	10
1732		$K(8Oc)_2$-Stp_2-K$[K(8Oc)_2]$	10

Figure 1. Chemical structures of LAF-Stp XPs.

(**A**) Chemical structures of xenopeptide building units. Stp: succinoyl tetraethylene pentamine; K: lysine; LAF: lipo amino fatty acid. The numbers (8, 12, and 14) indicate the count of carbon atoms in the terminal alkyl chains, while two letters denote the respective amino carboxylic acid used ("Oc" for 8-aminooctanoic acid, "He" for 6-aminohexanoic acid, "Bu" for 4-aminobutanoic acid). (**B**) Structure motifs of the three primary LAF-Stp carrier topologies. (**C**) Polarity switch of XPs upon protonation when exposed to an acidic environment. **(D)** Sequences of the peptide library comprising individual components of Stp, K, and LAF.

To further validate the potential of the dual pH-responsive XPs for Cas9 RNP delivery, gene knockout experiments were conducted using CT26-eGFP Luc, Hepa 1-6 Pcsk9^{tdTomato}, and HeLa eGFPd2 cells. Cas9 RNP complexes, formed using LAF-XPs at an N/P ratio of 24, were transfected at concentrations of 5 nM and 10 nM. After an additional three days of incubation, the cells were separately analyzed by flow cytometry. The results exhibited that the overall trend in gene knockout efficiency is similar in CT26-eGFP Luc, Hepa 1-6 *Pcsk9*^{tdTomato} and HeLa eGFPd2 (**Fig. 2C**). Particularly, Cas9 RNP

complexes with the U1 LAF_2-Stp topology *1611* exhibited the highest gene knockout efficiency (about 90%, 10nM) in CT26-eGFP Luc, Hepa 1-6 *Pcsk9*^{tdTomato}, and HeLa eGFPd2 cells. U3 and U4 topology carriers displayed moderate activity in CT26-eGFP Luc and Hepa 1-6 *Pcsk9*^{tdTomato} cells. Concurrently, Cas9 RNP complexes of *1611* and its pseudo-dimer analogue U1 LAF_4-Stp_2 *1719* exhibited negligible toxicity in all cell lines (**Fig. 8**). Additionally, DLS measurements revealed low polydispersity index (PDI) values of 0.2 for *1611* and *1719* Cas9 RNP complexes, indicating uniformity in particle size distribution. The hydrodynamic sizes of *1611* Cas9 RNP complexes (180 nm) and *1719* Cas9 RNP complexes (152 nm) were also relatively small. These results suggest that the U1 lipo-XPs *1611* and *1719* exhibit promising potential as nanocarriers for Cas9 delivery. Their encapsulation efficiencies were further measured, achieving approximately 96% for *1611* and 84% for *1719*. Both *1611* and *1719* are based on the LAF unit bis-dodecyl-amino octanoic acid (12Oc). Other U1 topologies also demonstrated efficient genome editing activity in at least two of three cell lines; the *1611* LAF_2-Stp analogue *1665* based on LAF 12He; and the *1719* LAF_4-Stp_2 analogues *1758* based on 12Bu and *1760* based on 12He. For practical reasons, further chemical evolution focused on the two 12Oc topologies *1611* and *1719*.

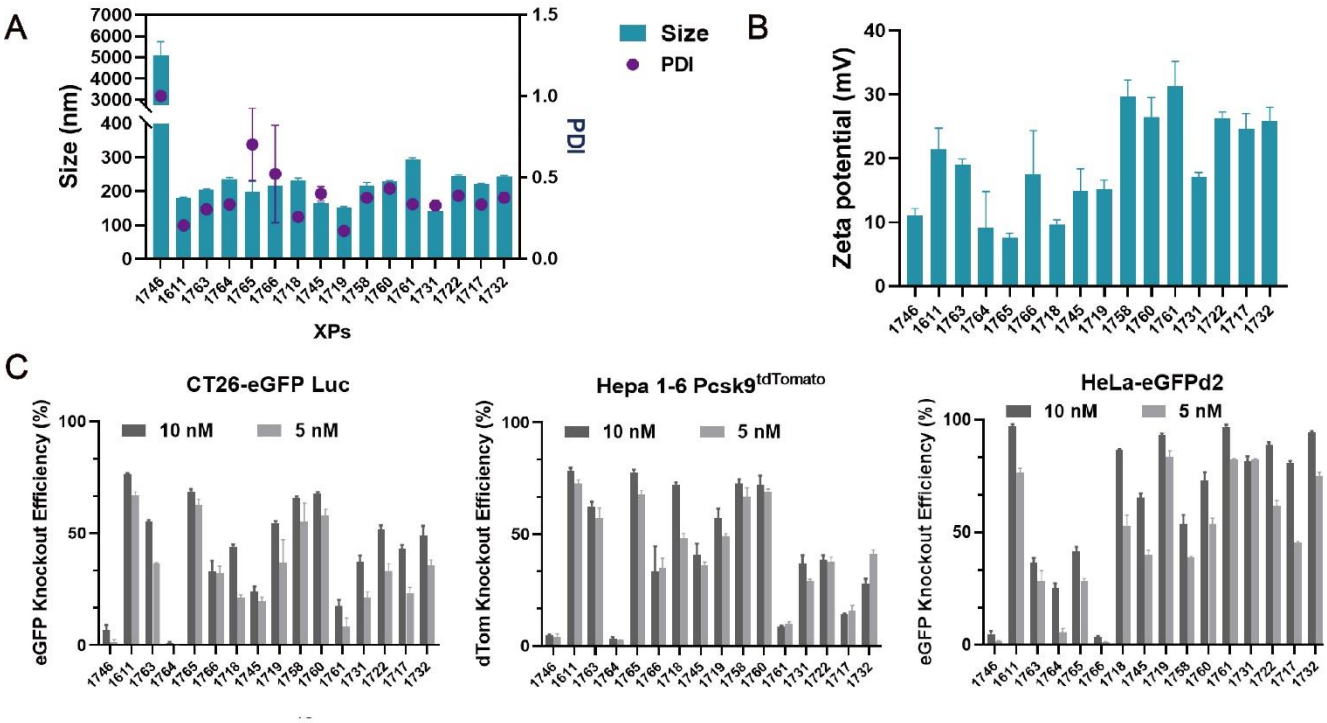

Figure 2. The screening of LAF-Stp XPs for Cas9 RNP delivery (**A**) Particle size, polydispersity index (PDI) and (**B**) zeta potential of XP-based Cas9 RNP complexes were measured using dynamic light scattering (DLS) at an N/P ratio of 24. (**C**) Gene editing efficiency in CT26-eGFP Luc, Hepa 1-6 *Pcsk9*^{tdTomato} and HeLa eGFPd2 cells after 48 h treatment with Cas9 RNP nanocarriers at RNP concentrations 5 nM and 10 nM. Data are presented as mean ± SD (n = 3).

2.4.2 Characterization and preliminary *in vitro* assessment of *1611* and *1719* Cas9 RNP complexes

To further characterize varied formulations of the two selected, representative potent LAF 12Oc U1 carrier candidates, LAF_2-Stp *1611* and LAF_4-Stp_2 *1719*, with Cas9 RNP complexes at different N/P ratios (24, 18, 12) were prepared and diluted to 10 nM RNP using HBG (20 mM HEPES, 5% glucose, pH 7.4). DLS measurements showed that all nanocarriers were between 150 to 180 nm in hydrodynamic size with zeta potentials ranging from +13 to +25 mV (**Fig. 3A,B**). Subsequently, transmission electron microscopy (TEM) was utilized to visualize Cas9 RNP complex morphology, revealing that *1611* and *1719* Cas9 RNP nanoparticles exhibited a spherical shape with a diameter of 50–80 nm (**Fig. 3C**).

Next, flow cytometry experiments were conducted to assess the cellular uptake of Cas9 RNP complexes labeled with fluorescent dye ATTO647N. Cells were treated with formulations containing 20% ATTO647N-labeled Cas9 protein at a final concentration of 37.5 nM and N/P ratio 24. as also described in our previous work [76]. After 2 h of incubation with HeLa-WT cells, flow cytometry analysis was performed. The results indicated that the nanocarriers *1611* and *1719* significantly enhanced the cellular uptake of Cas9 RNP compared to free Cas9 RNP. Moreover, *1611* Cas9 RNP complexes demonstrated higher cellular uptake than the *1719* Cas9 RNP complexes (**Fig. 3D**). This difference possibly is due to its higher zeta potential (+21 mV for *1611* compared to +15 mV for *1719*). Following that, HeLa gal8-mRuby3 reporter cells [76, 116, 117] were employed to assess capability of nanocarriers for endosomal destabilization. In this model, the rupture of endosomal membranes leads to the recruitment of a galectin-8 (gal8)-mRuby3 fluorescent fusion protein to galactan residues within endosomes, identifiable by intracellular punctate red spots. Herein, HeLa gal8-mRuby3 cells were treated with *1611* or *1719* Cas9 RNP complexes (N/P = 24) at a final concentration of 10 nM for 2 h of incubation. Subsequently, the cells were stained with 1 µg/mL DAPI in the dark and observed using confocal laser scanning microscopy (CLSM). The CLSM images depicted gal8-mRuby3 fusion proteins (red spots) that were induced by both *1611* and *1719* Cas9 RNP complexes (**Fig. 3E**), indicating enhanced endosomal disruption by these carriers. Additionally, the number of gal8 spots was quantified using ImageJ analysis software, showing a higher count in the *1719* Cas9 RNP group (**Fig. 3F**). Apparently, lipo-XP *1719* facilitated even more endosomal destabilization than *1611*.

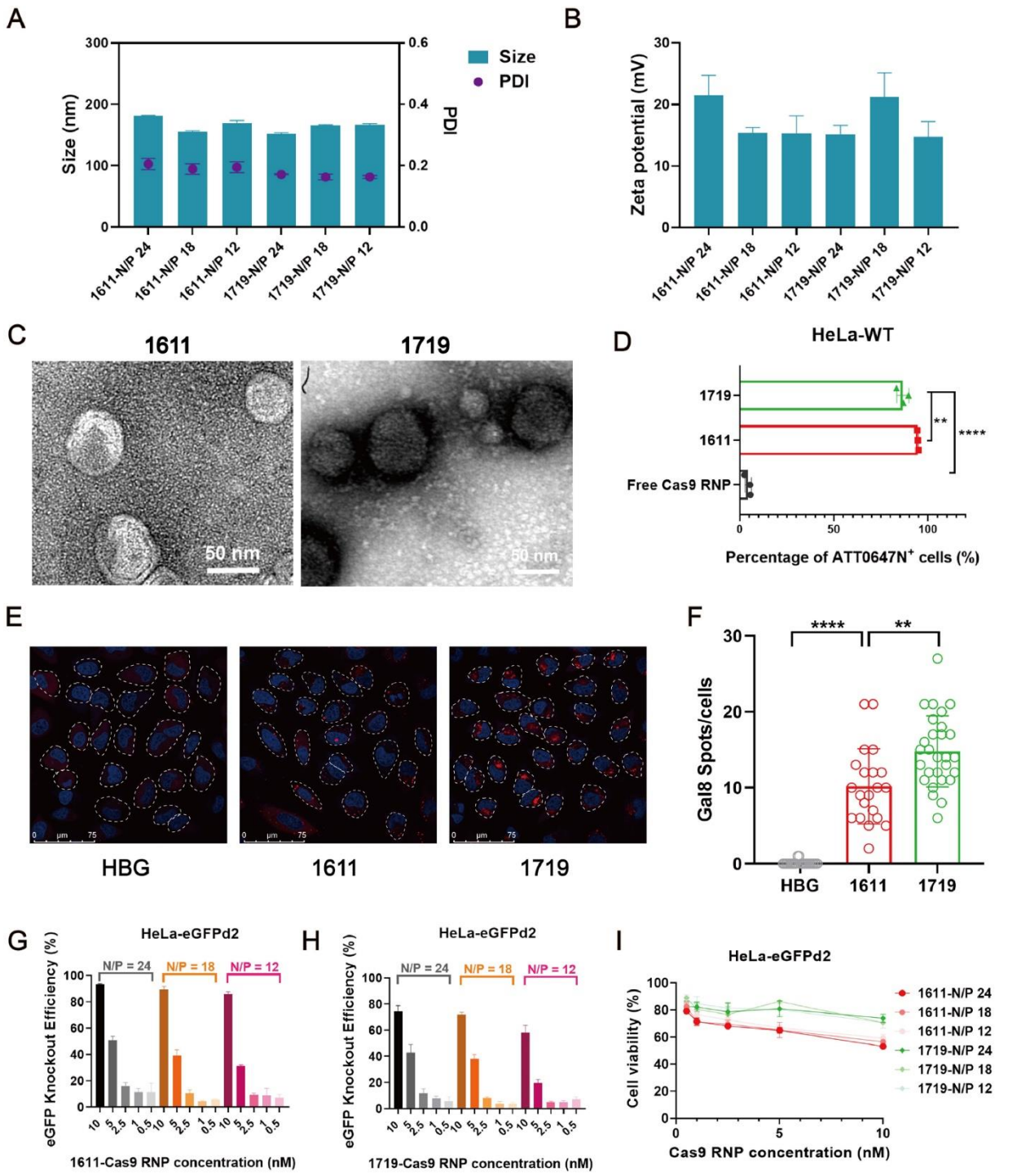

Figure 3. Characterization and evaluation of U1 *1611* and *1719* Cas9 RNP complexes. Particle size, PDI (**A**) and zeta potential (**B**) of Cas9 RNP complexes (*1611*, *1719*) with different N/P ratios (24, 18 and 12). (**C**) Surface morphology of *1611* and *1719* Cas9 RNP complexes (scale bar, 50 nm) as observed by TEM. (**D**) Cellular uptake of the formulations (37.5 nM RNP) containing 20% ATTO647N-Cas9 protein in HeLa-WT cells analyzed by flow cytometry after 2 h incubation. (**E**) CLSM images of HeLa gal8-mRuby3 cells treated with HBG, *1611* and *1719* Cas9 RNP

nanoparticles (10 nM RNP) for 2 h. Nuclei were stained with DAPI (blue). Red punctate distribution of gal8-mRuby3 fluorescence suggests damage of endosomal membranes. (**F**) The degree of endosomal disruption was quantified by counting gal8 spots via ImageJ analysis. (**G**) The efficiency of eGFP knockout in Hela eGFPd2 cells of *1611* Cas9 RNP complexes (**G**) or (**H**) *1719* Cas9 RNP complexes with RNP concentrations ranging from 0.5 to 10 nM and different N/P ratios (24, 18, 12). (**I**) Cell viability of HeLa eGFPd2 cells after treatment with complexes at varying RNP concentrations for 48 h, assessed by MTT assay ($n = 3$). Data are presented as means ± SD, the significant difference was analyzed by unpaired student's *t* test. ** $p < 0.01$, **** $p < 0.0001$.

This might be attributed to the doubled number of Stp and LAF units in the lipo-XP *1719*, along with the membrane-disrupting ability of the carriers in their protonated stage. Furthermore, to assess the impact of the N/P ratio on Cas9 RNP delivery, HeLa eGFPd2 cells were exposed to *1611* or *1719* Cas9 RNP complexes at varying concentrations (0.5, 1, 2.5, 5, 10 nM) and different N/P ratios (24, 18, 12) for 48 h, followed by evaluation after an additional three days of incubation. The results of GFP knockout efficiency indicated no significant differences in GFP knockout efficiency among different N/P ratios at the same concentration for the same LAF-XP, suggesting no significant influence of the N/P ratio on the gene editing efficiency of both *1611* and *1719* Cas9 RNP complexes. Concurrently, the highest gene editing efficiency approached 90% or 80% at 10 nM (N/P=24) for the *1611* (**Fig. 3G**) or *1719* Cas9 RNP complexes groups (**Fig. 3H**), respectively. Additionally, cytotoxicity experiments revealed minimal to moderate cytotoxicity associated with the complexes (**Fig. 3I**), despite the high N/P ratio of 24, indicating their suitability for further investigation.

2.4.3 Evaluation of Cas9 RNP delivery in DMD exon skipping reporter cells

Duchenne muscular dystrophy (DMD) is a severe, X-linked recessive disease with an average incidence of 1 in 5,000 live male births. The therapeutic potential of genome editing based on CRISPR/Cas9 has been investigated for DMD, particularly through removal of exon sequences on DNA level. However, it has been reported that utilizing RNA exon skipping may allow for the correction of DMD defects without the need for precise genetic modification [118, 119]. Hence, any indels introduced by NHEJ disrupting a splice donor or acceptor sequence of a mutant exon can lead to exon skipping. To further assess the potential of gene editing in the lipo-XP delivery system using a DMD cell model, we utilized the recently established HeLa mCherry-DMD_{Ex23} cell system [77, 79] in this study. The sgRNA sequence (sgDMDEx23) [119, 120] is displayed in **Table 1**, guiding Cas9 to the PAM sequence to induce a double-strand break (DSB) near the DMD exon 23 donor splice site in HeLa mCherry-DMD_{Ex23} cells. As a result of the mutation in the DMD exon 23 sequence, edited cells express functional mCherry, which is detectable as red fluorescence by flow cytometry (**Fig. 4A**).

To assess the potential of LAF-Stp XP Cas9 formulations for exon skipping efficiency, HeLa mCherry-DMD_{Ex23} cells were transfected with each formulation for 24 h and then detected after an additional two days of incubation. The results indicate that the majority of formulations exhibited high efficiency in gene editing mediated exon skipping for both Cas9 protein/sgRNA RNP complexes and Cas9 mRNA/sgRNA polyplexes, with similar overall trends observed (**Fig. 4B**). These findings highlight key points: amphiphilic LAF-XPs proved to be excellent delivery vehicles for both Cas9 protein/sgRNA RNP and mRNA/sgRNA. In addition, gene editing-positive HeLa mCherry-DMD_{Ex23} cells using *1611* or *1719* Cas9 RNP complexes were further observed by CLSM. The results suggested that the gene editing efficiency of the *1611* Cas9 RNP complexes was higher than that of the *1719* complexes (**Fig. 4C**), consistent with the flow cytometry results.

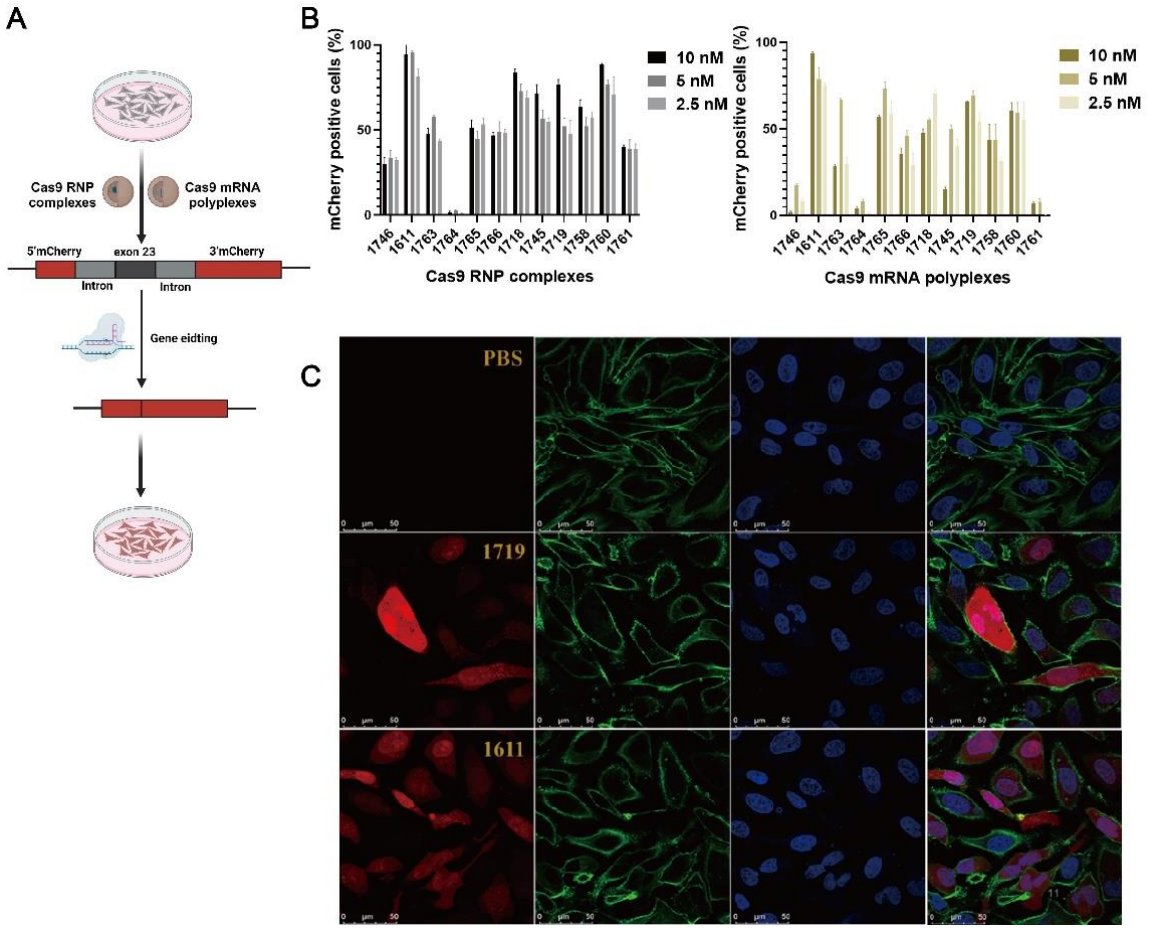

Figure 4. Comparison of gene editing mediated exon skipping efficiency of Cas9/sgRNA RNP complexes and Cas9 mRNA/sgRNA polyplexes in the DMD reporter cell model. (**A**) Structure of the mCherry-DMDEx23 construct and its gene editing mechanism in the presence of Cas9. (**B**) Gene editing efficiency with the mutated exon sequence using U1 peptide-based Cas9/sgRNA RNP complexes or Cas9 mRNA /sgRNA polyplexes in HeLa mCherry-DMD_{Ex23} cells. (**C**) CLSM images of HeLa mCherry-DMD_{Ex23} cells treated with *1611* and *1719* Cas9 RNP complexes at 10 nM RNP. Cell nuclei were stained with DAPI (blue) and the cytoskeleton with Alexa Fluor™ 488 phalloidin (green); mCherry fluorescence is indicated in red. The scale bar represents 50 µm. All complexes and polyplexes were prepared at N/P ratio 24 before transfection for 24 h. Data are presented as mean ± SD (*n* = *3*).

2.4.4 Optimization of dual pH-responsive amphiphilic XP architectures for Cas9 RNP delivery

The LAF-XP based CRISPR/Cas9 RNP delivery system exhibited high gene editing efficiency in above study, particularly with backbone *1611* and *1719*. Previous studies have suggested that the hydrophobicity of peptides plays a crucial role in achieving efficient Cas9 RNP delivery, with various building blocks influencing and inducing diverse hydrophobicity profiles [76]. Herein, to optimize LAF-XP *1611* (**Fig. 5A**) and *1719* (**Fig. 5B**), we evaluated a series of dual pH-responsive amphiphilic XPs where the hydrophilicity of polar subunit Stp had been modulated. This was achieved by replacement of tetraethylenepentamine (tp) with triethylenetetramine (tt) or 3,3′-ethylenediiminodipropylamine (EIPA), and/or exchange of succinic acid with alternative dicarboxylic acids. Chemical structures of the six Stp analogues (dmGtp, chGtp, dGtp, Htp, Stt and GEIPA) are depicted in (**Fig. 5C**). Solid-phase synthesis of the novel six LAF2-Stp *1611* and six LAF4-Stp2 *1719* analogues (**Table 2**) was performed according to established protocols [78]. Characterization of the novel LAF-XPs will be reported in detail elsewhere (Burghardt et al., in preparation).

Cas9 RNP complexes were prepared with these LAF-XPs at N/P = 24, yielding sizes between 100 and 319 nm, with a PDI around 0.23 and zeta potential ranging from +15 to +25 mV, measured by DLS (**Fig. 9**). Subsequently, the gene editing efficiency of the Cas9 RNP complexes was assessed in HeLa eGFPd2 cells. The cells were incubated with Cas9 RNP complexes at various final RNP concentrations (ranging from 0.5 to 10 nM) for 48 h. Following an additional three days of incubation, cells were analyzed using flow cytometry. **Fig. 5D** indicates that nanoparticles based on LAF-XPs *1842* (dGtp), *1844* (Htp), and *1845* (GEIPA) had higher GFP knockout efficiency compared to those based on the original XP compound *1611* (LAF_2-Stp). Particularly noteworthy was the gene editing efficiency of *1842* (LAF_2-dGtp), which reached 72 % at 2.5 nM with a size 319 nm. Consistently, also LAF_4-Stp_2 *1719* analogues demonstrated higher gene editing efficiency of RNP complexes compared to *1719* (**Fig. 5E**). This variation may be attributed to differences in hydrophobicity resulting from distinct backbones. In fact, the number of Stp units in backbone *1719* is double that of backbone *1611*, suggesting a greater impact of the Stp analogue. In summary, the efforts yielded a more effective Cas9 RNP delivery system by some of the six new oligoamino acid building blocks.

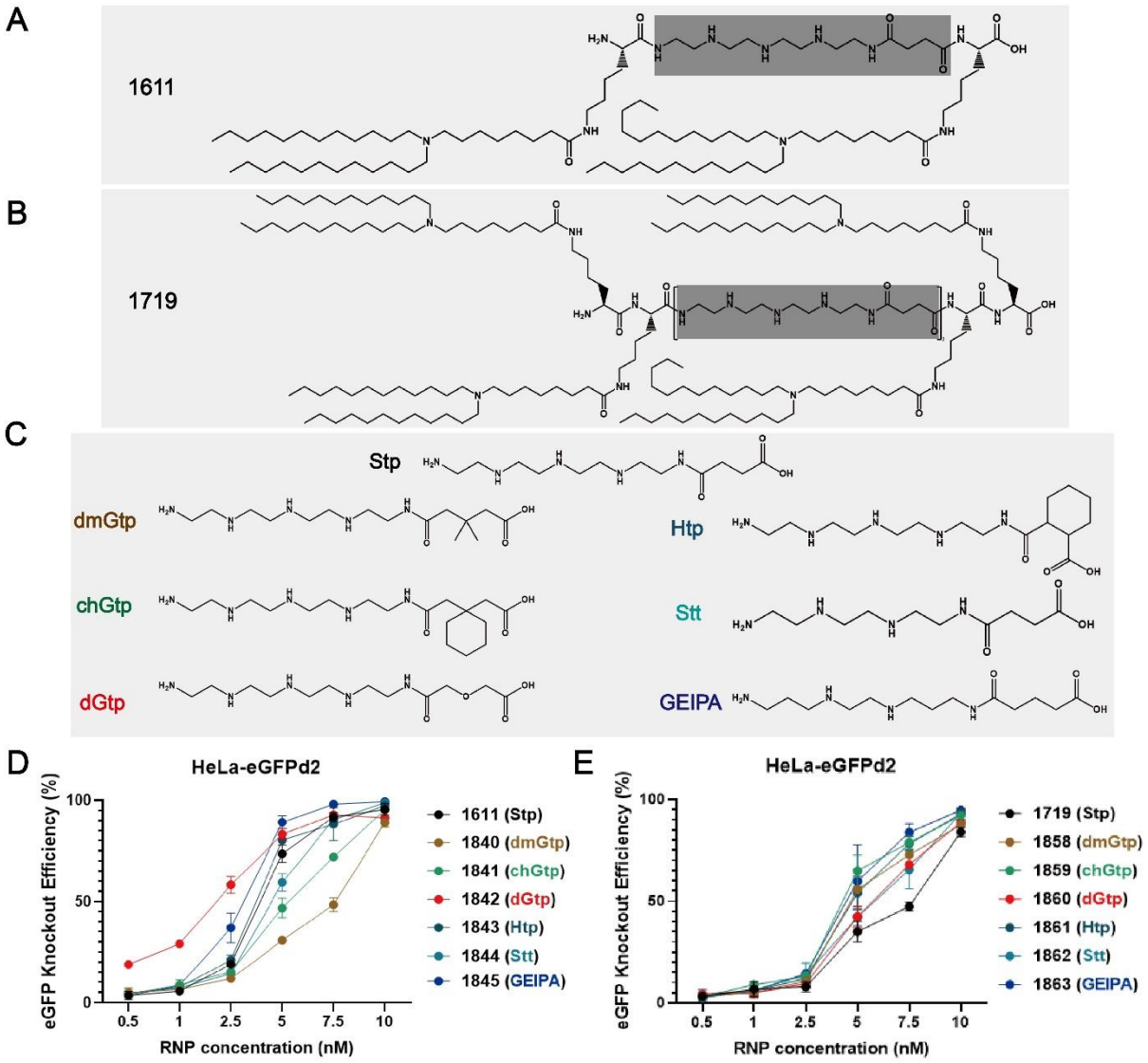

Figure 5. Amphiphilic LAF-XP architectures with enhanced gene editing efficacy. Chemical structure of *1611* (**A**) and *1719* (**B**). Structure of Stp and its analogues (dmGtp, chGtp, dGtp, Htp, Stt and GEIPA) depicted in (**C**). The gene editing efficacy of *1611* and analogue complexes (**D**) or *1719* and analogue complexes (**E**) at a series of RNP concentrations ranging from 0.1 nM to 10 nM in HeLa eGFPd2. Data are presented as mean ± SD (*n* = *3*). LAF-XP sequences are displayed in **Table 2**.

The most potent LAF-XPs (two LAF_2-XPs and two LAF_4-XPs) with their original LAF-XPs (*1611, 1719*) were subsequently screened under standard transfection conditions for Cas9 RNP delivery in HeLa mCherry-DMD_{Ex23} cells as a second reporter cell model (**Fig. 6A**). All XP carriers displayed high genome editing efficiency at 10 nM RNP concentration. The novel LAF-XPs *1842*, *1845*, and *1863* revealed a higher efficiency with EC50 values around 1 nM (**Fig. 6A**). For *in vivo* applications, interactions with plasma components are highly relevant, leading to the formation of a protein corona around the nanoparticles. Numerous nucleic acid complexes were previously shown to be inhibited serum [121, 122]. Hence, the functional activity of the RNP complexes was assessed by pre-incubation in high serum (over 90%, v/v) for 15 min at room temperature before standard transfection of HeLa mCherry-DMD_{Ex23} cells using RNP concentrations ranging from 0.05 to 10 nM (**Fig. 6C**). As control for the pre-incubation step, formulations were pre-incubated with HBG buffer under the same conditions before transfection in standard serum-containing medium (**Fig. 6B**).

The results showed that the HBG pre-incubation step (control groups, **Fig. 6B**) did not significantly change editing efficiencies as compared with the standard transfection. Importantly, pre-incubation of Cas9 RNP complexes with full serum fully maintained the high gene exon skipping activity (**Fig. 6C**), similar as previously found for mRNA LAF-XP polyplexes [78, 79]. Notably, the efficacy of the *1611* analogue LAF_2-dGtp (*1842*) slightly increased at low concentration, with EC50 reaching 0.51 nM. This indicates that Cas9 RNP complexes formulated with the dual pH-responsive LAF-XPs retain full functional activity in the presence of full serum, providing a promising foundation for *in vivo* studies.

A

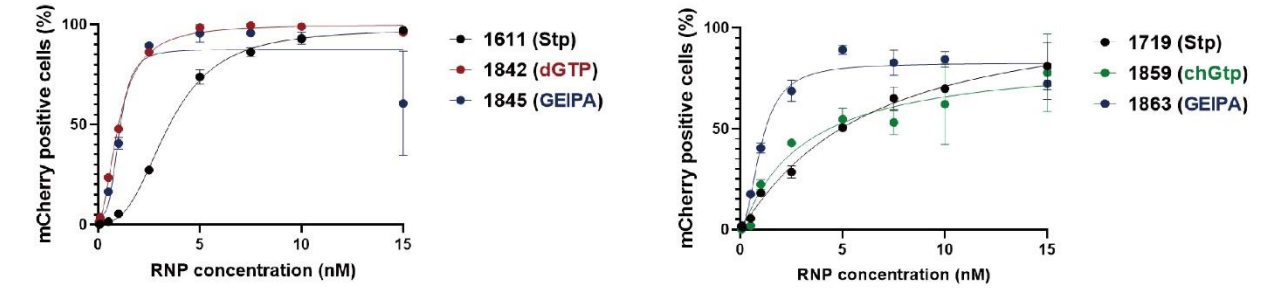

Standard transfection

	1611	1842	1845	1719	1859	1863
EC50 (nM)	3.48	1.03	1.04	5.83	2.97	1.02

B

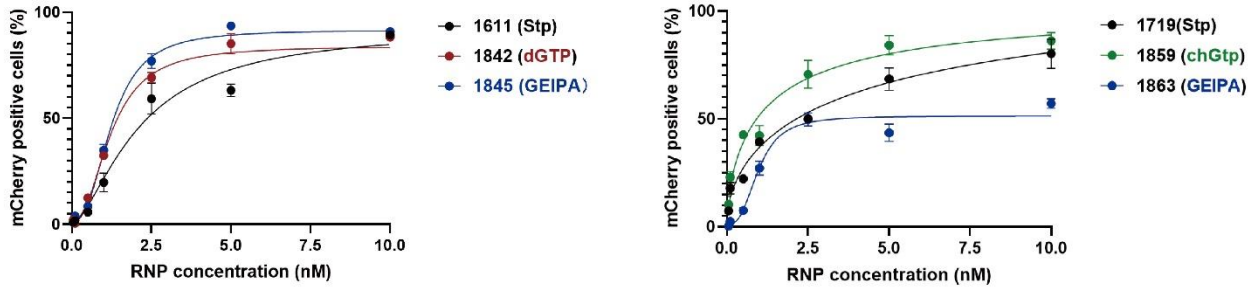

HBG pre-incubation

	1611	1842	1845	1719	1859	1863
EC50 (nM)	2.13	1.24	1.25	5.12	1.25	0.97

C

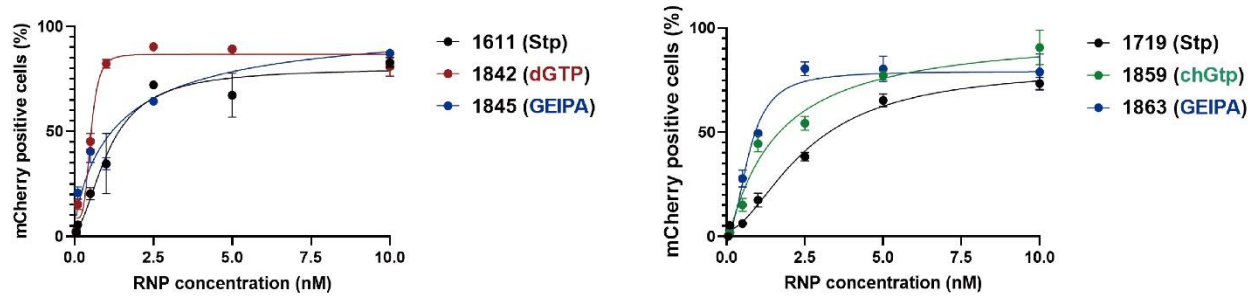

Serum pre-incubation

	1611	1842	1845	1719	1859	1863
EC50 (nM)	1.11	0.51	1.43	5.71	1.55	0.73

Figure 6. Comparison of RNP delivery by new LAF-XPs in the HeLa mCherry-DMD$_{Ex23}$ reporter cell model. (**A**) Gene editing mediated exon skipping of LAF$_2$-XP (*left*) and LAF$_4$-XP (*right*) Cas9 RNP complexes under standard conditions using RNP concentrations ranging from 0.05 to 10 nM. (**B**) Analogous experiment, with pre-incubation of Cas9 RNP complexes in HBG before adding them to standard transfection medium. (**C**) Pre-incubation of Cas9 RNP complexes in full serum (FBS) before adding them to standard transfection medium. The corresponding EC50 values (50% edited cells, in nM) for all XPs are listed. Data are presented as mean ± SD (*n* = *3*).

2.4.5 Gene correction by Cas9 RNP complexes via homology-directed repair (HDR)

Except for gene knockout (non-homologous end joining, NHEJ) treatment of genetic diseases, the CRISPR/Cas9 system is also meaningfully used to correct point mutations or insert expression cassettes via HDR-dependent knock-in. Different from the NHEJ mechanism, HDR also requires a DNA sequence that will be recognized by the HDR machinery and used as a template for repairing the DSB generated by Cas9. Therefore, the co-delivery of Cas9 protein/sgRNA RNP and a single-stranded DNA (ssDNA) template for HDR was explored in HeLa eGFPd2 cells. In this cell model, HDR-based genome editing at the 66th amino acid position of GFP (conversion of TAC into CAC) results in generation of blue fluorescent protein (BFP), allowing for the quantification of non-edited, NHEJ knock-out, and HDR conversion events as outlined in **Fig. 7A**. Due to the replacement of tyrosine (TAC) by histidine (CAC) at the specific location of GFP, the cells display blue instead of green fluorescence. Thus, during flow cytometry analysis, three types of cells were distinguished: non-edited cells (eGFP positive), NHEJ-mediated knockout cells (eGFP negative, BFP negative), and HDR-mediated gene-corrected cells (BFP positive).

Building on previous studies, an assessment of different RNP/ssDNA ratios is crucial to find most suitable conditions [76]. In the initial phase, LAF-XP *1611* was subjected to various RNP/ssDNA ratios and RNP concentrations. HeLa eGFPd2 cells were treated with RNP complexes for 48 h, with RNP/ssDNA molar ratios ranging from 1/0 to 1/4 and RNP concentrations between 0.1 nM to 5 nM. Following a 3-day incubation period, the cell population was analyzed using flow cytometry with a gating strategy as shown in **Fig. 7B**. As demonstrated in **Fig. 7C**, in the RNP control groups without ssDNA template (sgRNA/ssDNA = 1/0), higher RNP concentrations correlated with increased NHEJ efficiency (grey region). For the other *1611* complexes with sgRNA/ssDNA (sgRNA/ssDNA molar ratio = 1:0.5, 1:1, 1:2, 1:4) a similar dose dependence was observed: higher RNP concentrations were associated with increased HDR (blue region) as well as NHEJ efficiency (grey region). Notably, the highest HDR efficiency of 33 % was observed when *1611* complexes had a concentration of 2.5 nM RNP and an RNP/ssDNA ratio of 1:2. HDR efficiency also reached approximately 30% with 5 nM RNP and a 1:4 RNP/ssDNA ratio in this study. To further assess the potential of novel LAF-XPs for HDR-mediated gene correction, formulations with *1611* and *1719* analogues were prepared by complexation at a 1:4 Cas9 RNP/ssDNA ratio. Dynamic light scattering analysis revealed that the resulting complexes exhibited hydrodynamic sizes ranging from 155 nm to 225 nm, with zeta potentials ranging from +17 mV to +38 mV (**Fig.11**).

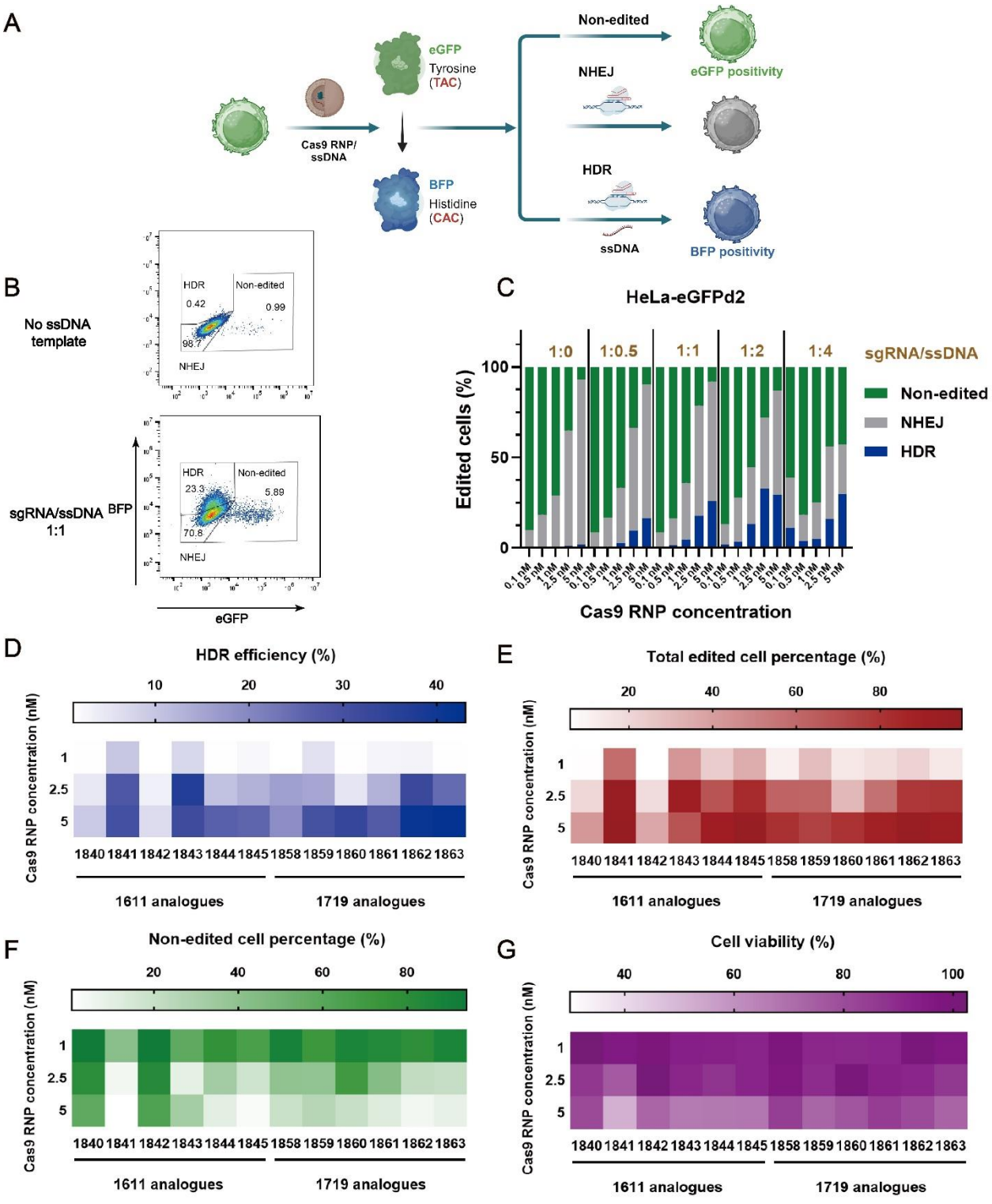

Figure 7. LAF-XP based Cas9 RNP complexes for enhanced HDR mediated genome editing in HeLa eGFPd2 cells. (**A**) Schematic illustration of eGFP to BFP conversion. GFP expression can be eliminated (NHEJ) or changed to native BFP (HDR). (**B**) The gating strategy was employed to distinguish between non-edited cells (eGFP positive), NHEJ (eGFP negative), and HDR (BFP

positive) cell populations, *1611* complexes, 5 nM RNP. (**C**) The amount and type of gene editing were assessed using FACS following transfection with *1611* RNP complexes. The formulations were prepared by different RNP concentration (0.1 nM to 10 nM) with different molar sgRNA to ssDNA ratios (1:0; 1:0.5; 1:1; 1:2; 1:4). Data are presented as mean ± SD (*n* = 3). (**D**) Analysis of HDR efficacy, (**E**) total gene editing efficacy, (**F**) non-edited cell percentages, and (**G**) cell viability after treatment with XP analogues of LAF_2-Stp *1611* and LAF_4-Stp_2 *1719* (sgRNA/ssDNA ratio = 4) at 1 nM, 2.5 nM, and 5 nM RNP concentrations. Cytotoxicity was measured using the MTT assay. The N/P ratio of all the formulations was 24, data are presented as mean (*n = 3*).

Subsequently, HeLa eGFPd2 cells were transfected with Cas9 RNP complexes containing analogues of *1611* and *1719* at concentrations ranging from 1 nM to 5 nM for 48 h. Flow cytometry assessment revealed that higher RNP concentrations were associated with increased HDR efficiency (**Fig. 7D, 12**), higher overall gene editing efficiency (**Fig. 7E, 13**) and decreased non-edited cell percentage (**Fig. 7F, 14**) for most analogue complexes. And cytotoxicity experiments revealed minimal to moderate cytotoxicity associated with the complexes (**Fig. 7G, 15**). Interestingly, while Cas9 RNP complexes based on *1719* analogues exhibited lower efficiency in gene knockout experiments (**Fig.5E**) than *1611* analogue Cas9 RNP complexes (**Fig. 5D**), they achieved higher HDR efficiency. Among the *1611* analogue Cas9 RNP complexes, the highest HDR efficiency, reaching up to 37%, was observed with LAF_2-Htp *1843* at 2.5 nM. In contrast, *1842* (LAF2-dGTP), which exhibited the highest gene editing efficiency in the absence of ssDNA, showed reduced activity for both gene knockout and HDR conversion in the presence of the ssDNA template. HDR efficiency of *1719* analogues surpassed 40%, particularly in case of LAF_4-Stt_2 *1862* (41%) and LAF_4-$GEIPA_2$ *1863* (43%). This difference may stem from the differing requirements between gene knockouts (using Cas9 protein/sgRNA RNP only) and knock-ins (requiring complexation of Cas9 protein/sgRNA RNP and ssDNA, favored by the double-sized XPs).

2.5 Conclusion

This study involved the screening of dual pH-responsive amphiphilic xenopeptides (XPs), identifying carriers tailored for the delivery of Cas9 protein/sgRNA RNP. Screening outcomes revealed that U1 backbone LAF_2-Stp XP *1611* and LAF_4-Stp_2 XP *1719* emerged as excellent candidates for Cas9 RNP delivery, displaying promising genome editing performance across various reporter cell lines. Physicochemical characterization of the nanosized RNP complexes demonstrated their favorable attributes, including small size and uniform distribution. Moreover, these RNP complexes demonstrated enhanced cellular uptake and facilitated endosomal destabilization, enabling endosomal escape of Cas9 protein/sgRNA. In a Duchenne muscular dystrophy (DMD) exon skipping reporter cell model, the XP carriers demonstrated their ability to deliver Cas9 protein with similar high potency as Cas9 mRNA. Additionally, amphiphilic modulation of LAF-XP nanocarriers by replacement of Stp with other oligoamino acids enabled further optimized genome editing, by either Cas9 RNP mediated gene knockout, or Cas9 RNP/ssDNA template-mediated HDR-based genetic knock-in (correction efficiency up to 43%). Interestingly, different XPs were required for gene knockout and knock-in, reflecting differing requirements between complexation of Cas9/sgRNA RNP without or with ssDNA. As a result, the most suitable carriers may vary for different applications. These LAF-XPs may also offer a potential solution for addressing the primary challenge of delivery for other related editing techniques [46], including base editors [123], prime editors [31], transcriptional modulators [124], and RNA editors [125].

2.6 Acknowledgements

The authors acknowledge support by the UPGRADE (Unlocking Precision Gene Therapy) project that has received funding from the European Union's Horizon 2020 research and innovation programme under grant agreement No 825825. This work was also supported by the German Research Foundation (DFG) SFB1032 (project-ID 201269156) sub-project B4, and BMBF Cluster for Future ‘CNATM - Cluster for Nucleic Acid Therapeutics Munich’ project number 03ZU1201AA. X.L. appreciates the fellowship of the China Scholarship Council that supports his Ph.D. study. We thank Susanne Kempter (Faculty of Physics, LMU Munich) for performing TEM measurements, Eric Weidinger for scientific discussions, Wolfgang Rödl and Olga Brück (Pharmaceutical Biotechnology, LMU Munich) for technical and organizational support.

2.7 Supporting information figures

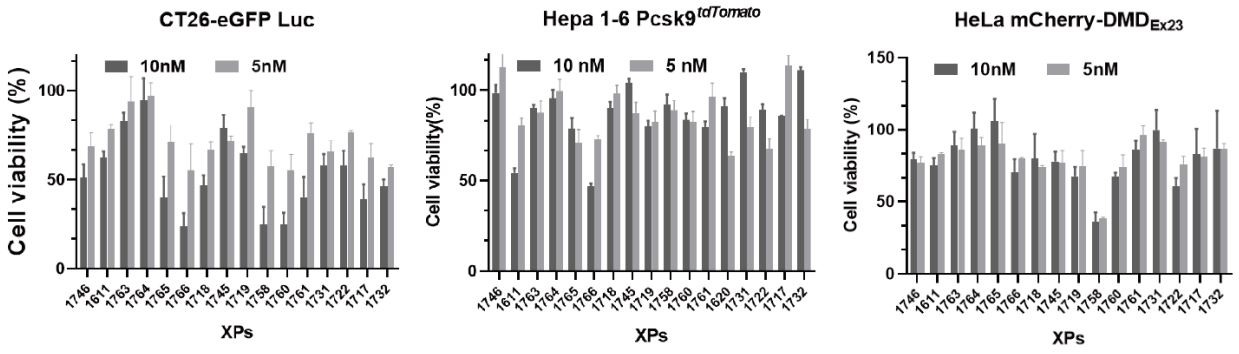

Figure 8. Cell viability of CT26-eGFP Luc, Hepa 1-6 *Pcsk9*^{tdTomato} and HeLa eGFPd2 after 48 h treatment with U-shape (U1, U3, U4) based Cas9 RNP complexes. Cytotoxicity was detected by MTT assay. Data are presented as mean ± SD (*n* = *3*).

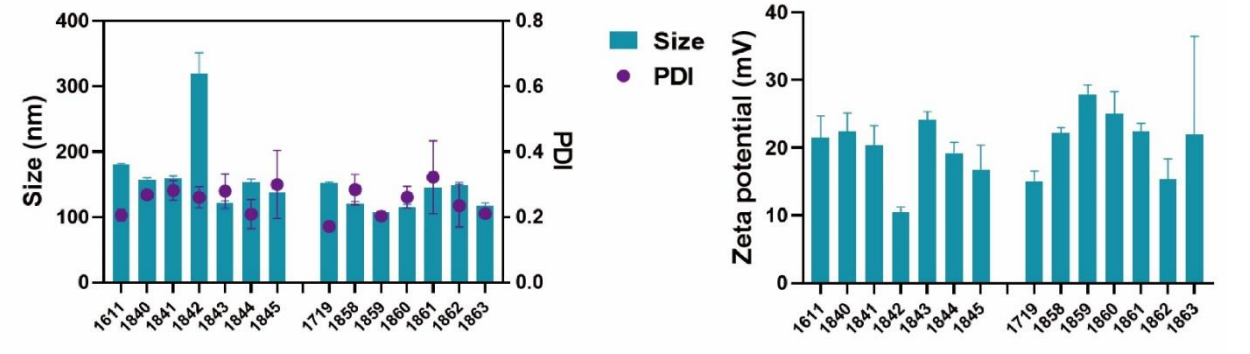

Figure 9. Particle size, PDI, and zeta potential of Cas9 RNP complexes were determined using DLS. The complexes were based on *1611* and *1719*, as well as *1611* analogues and *1719* analogues, all with an N/P ratio of 24. Data are presented as mean ± SD (*n* = *3*).

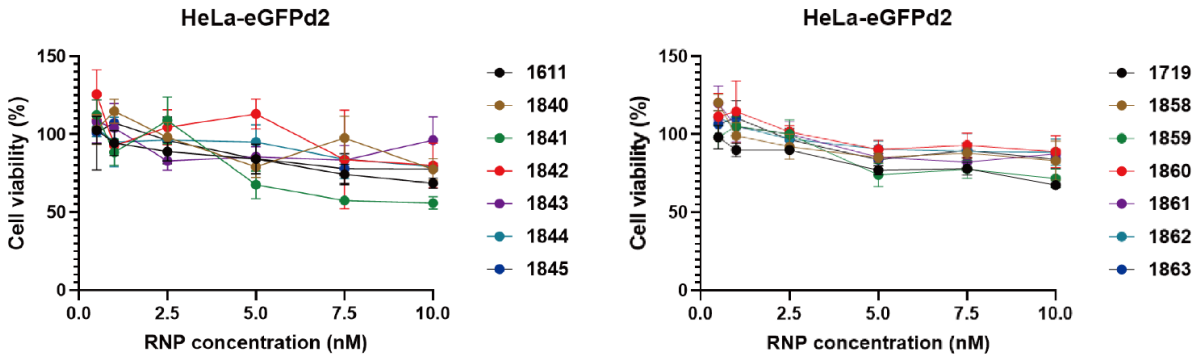

Figure 10. Effects of Cas9 RNP complexes on cell viability of HeLa-eGFPd2 were determined using MTT. The complexes were based on XP *1611* and *1719*, as well as *1611* analogues and *1719* analogues, all with an N/P ratio of 24. Data are presented as mean ± SD (*n* = *3*).

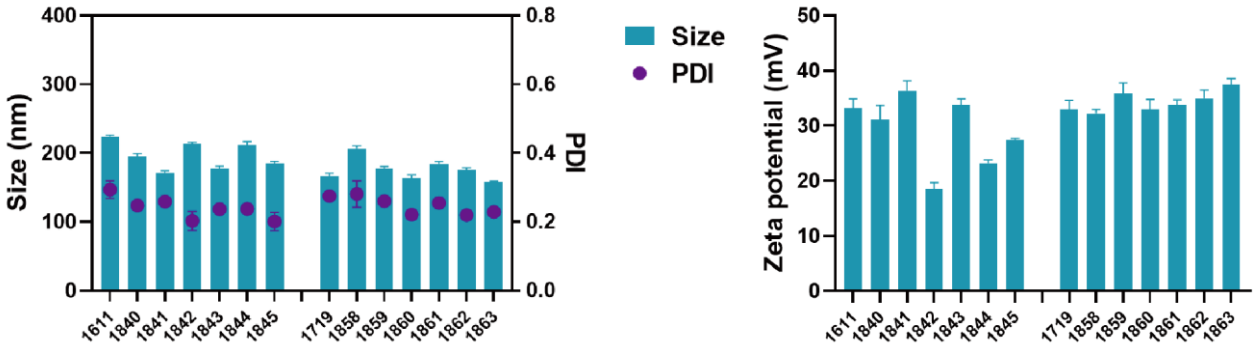

Figure 11. Particle size, PDI, and zeta potential of Cas9/sgRNA/ssDNA complexes formed with *1611* and *1719* analogue XPs were measured using DLS. The N/P ratio for all formulations was 24, sgRNA/ssDNA ratio was 4, and RNP concentrations were set at 2.5 nM. Data are presented as mean ± SD (*n* = *3*).

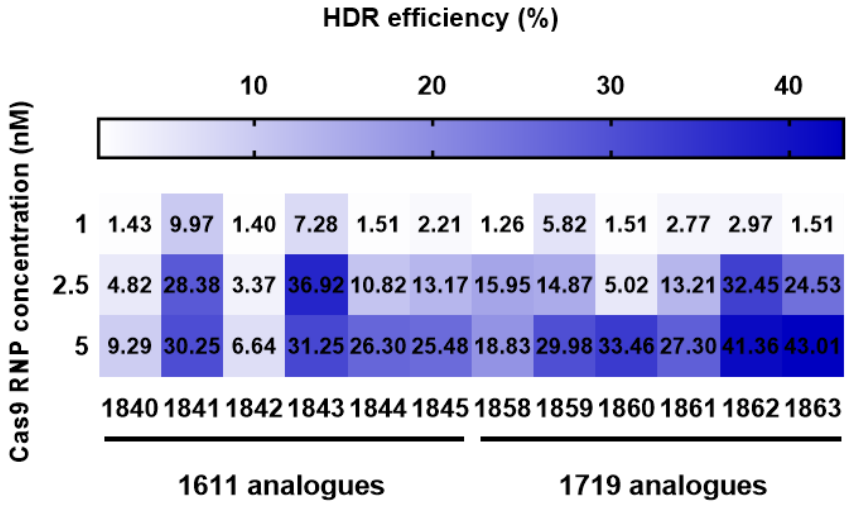

Figure 12. HDR efficacy in HeLa eGFPd2 cells after 48 h treatment with *1611* and *1719* analogue XPs (sgRNA/ssDNA = 4, N/P= 24) at 0.5 nM, 2.5 nM, and 5 nM RNP. Data are presented as mean (*n = 3*).

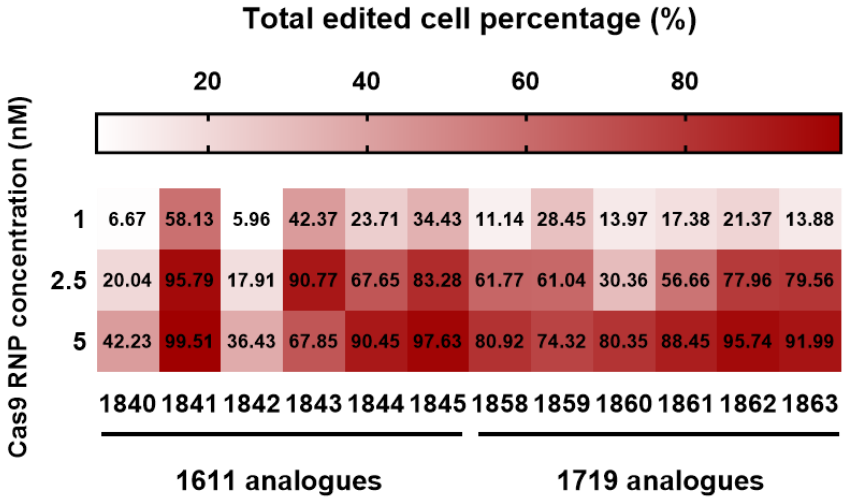

Figure 13. Total gene editing efficacy in HeLa eGFPd2 cells after 48 h treatment with *1611* and *1719* analogue XPs (sgRNA/ssDNA = 4, N/P= 24) at 0.5 nM, 2.5 nM, and 5 nM RNP. Data are presented as mean (*n = 3*).

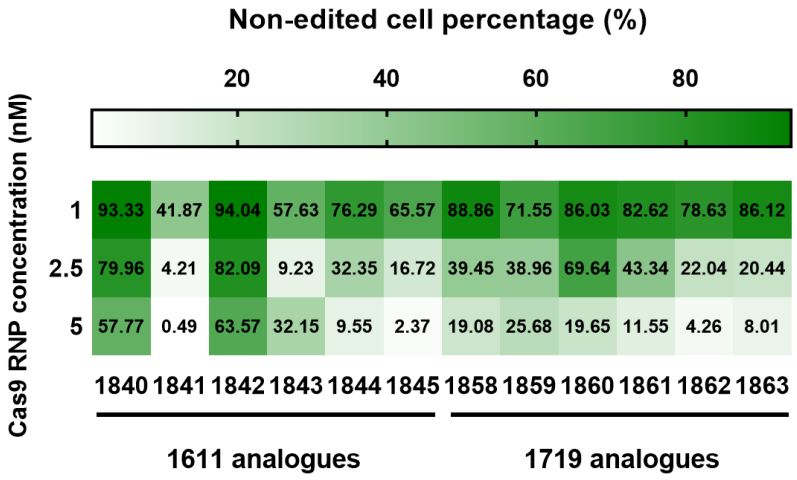

Figure 14. Non-edited cell percentages in HeLa eGFPd2 cells after 48 h treatment with *1611* and *1719* analogue XPs (sgRNA/ssDNA = 4, N/P= 24) at 0.5 nM, 2.5 nM, and 5 nM. Data are presented as mean (*n* = *3*).

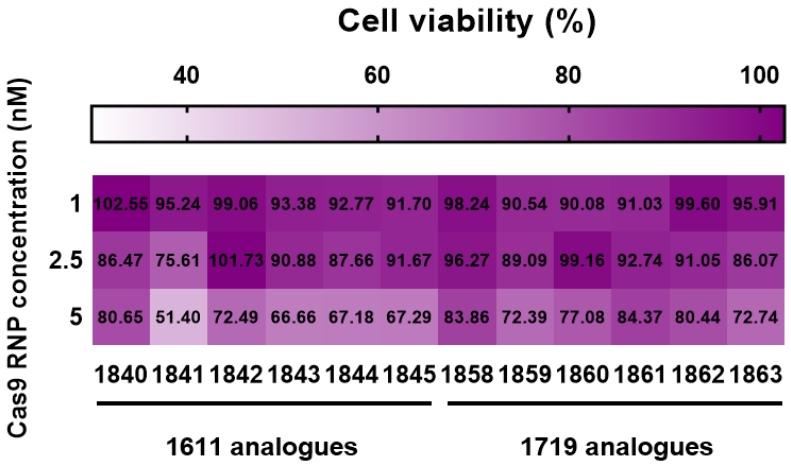

Figure 15. Cell viability of HeLa eGFP cells after 48 h treatment of *1611* and *1719* analogue XPs (sgRNA/ssDNA = 4, N/P= 24) at 0.5 nM, 2.5 nM, and 5 nM, was determined by MTT assay. Data are presented as mean (*n* = *3*).

3 Chapter II:

CRISPR/Cas9 ribonucleoprotein delivery enhanced by Lipo-Xenopeptide carriers and homology-directed repair modulators: Insights from reporter cell lines

Xianjin Luo [1], Eric Weidinger [1], Tobias Burghardt [1], Miriam Höhn [1], Ernst Wagner [1,2,3*]

1 Pharmaceutical Biotechnology, Department of Pharmacy, Ludwig-Maximilians-Universität Munich, Butenandtstrasse 5-13, 81377 Munich, Germany; xianjin.luo@cup.uni-muenchen.de (X.L.); eric.weidinger@cup.uni-muenchen.de (E.We); tobias.burghardt@cup.uni-muenchen.de (T.B.); miriam.hoehn@cup.uni-muenchen.de (M.H.)

2 Center for Nanoscience (CeNS), LMU Munich, 80799 Munich, Germany;

3 CNATM - Cluster for Nucleic Acid Therapeutics Munich, 81377 Munich, Germany;

* Correspondence: ernst.wagner@lmu.de

The following sections are adapted from the submitted manuscript.

Sections may have been moved for consistency.

Contribution of PhD student colleagues: Eric Weidinger conducted co-transfection studies using Cas9 mRNA/sgRNA and pDNA/mRNA. Tobias Burghardt synthesized several lipo-XPs.

3.1 Abstract

CRISPR-Cas9 genome editing is a versatile platform for studying and treating various diseases. Homology-directed repair (HDR) with DNA donor templates serves as the primary pathway for gene correction in therapeutic applications, but its efficiency remains a significant challenge. This study investigates strategies to enhance gene correction efficiency using a T-shaped lipo-xenopeptide (XP)-based Cas9 RNP/ssDNA delivery system combined with various HDR enhancers. Nu7441, a known DNA-PKcs inhibitor, was found most effective in enhancing HDR-mediated gene correction. An over 10-fold increase in HDR efficiency was achieved by Nu7441 in HeLa-eGFPd2 cells, with a peak HDR efficiency of 53% at a 5 nM RNP concentration, and up to 61% efficiency confirmed by Sanger sequencing. Surprisingly, also total gene editing efficiency including non-homologous end joining (NHEJ) was improved. For example, Nu7441 boosted exon skipping via NHEJ mediated splice site destruction by 30-fold in a DMD reporter cell model. Nu7441 modulated the cell cycle by reducing cells in the G1 phase and extending the S and G2/M phases without compromising cellular uptake or endosomal escape. The enhancement of genome editing by Nu7441 was widely applicable across several cell lines, several Cas9 RNP/ssDNA carriers (LAF-XPs), and also Cas9 mRNA/sgRNA/ssDNA polyplexes. These findings highlight a novel and counterintuitive role for Nu7441 as an enhancer of both HDR and total gene editing efficiency, presenting a promising strategy for Cas9 RNP-based gene therapy.

Keywords: CRISPR Cas9; Cas9 ribonucleoprotein; Cas9 mRNA/sgRNA; Homology-directed repair; enhancer; cell cycle

3.2 Introduction

Genome engineering using nucleases offers a powerful platform for generating both gene knock-outs and knock-ins through the repair of DNA double-strand breaks (DSBs) [8, 126]. These genetic modifications rely on two primary pathways: non-homologous end joining (NHEJ) and homology-directed repair (HDR) [127]. For gene knock-outs, the error-prone NHEJ pathway functions without a template, introducing random insertions or deletions [128]. In contrast, HDR is essential for precise gene correction in therapeutic applications, enabling accurate repair and template-guided insertions [139-145]. Additionally, emerging Cas9-based approaches, such as base editing [22, 24] and prime editing [22, 129], facilitate targeted gene modifications and small insertions (<50 bases) without requiring DSBs. However, unlike base and prime editing, HDR-mediated editing is not constrained by sequence length and supports insertions spanning several kilobases [130], making it the most versatile method for achieving complex targeted substitutions and insertions. Despite its advantages, CRISPR/Cas9 HDR efficiency remains relatively low at standard editing conditions, and far lower as compared to NHEJ mediated editing, posing a significant challenge to its widespread application. As a result, the development of effective delivery platforms is critical to advancing HDR-mediated gene therapy.

Traditional CRISPR/Cas9 delivery methods, such as microinjection and electroporation, are effective for *in vitro* applications but often cause cell membrane damage due to the need for individual cell manipulation. These methods are also less suitable for tissue-level or *in vivo* applications [131, 132]. In contrast, viral and non-viral vectors present promising alternatives for delivering Cas9 in both *in vitro* and *in vivo* contexts. Viral vectors, such as lentiviral, adenoviral, and adeno-associated viral vectors, have been developed as gene editing tools by researchers like Merienne [133], Xu [134], and Ibraheim [135]. However, these vectors are constrained by cargo size limitations and the risk of immune activation [136]. Non-viral delivery systems, on the other hand, are emerging as versatile platforms with broad applications and are poised to dominate future delivery strategies [14, 34, 85, 88, 95, 97, 99, 102, 137-140]. For instance, Zhang et al. developed lipid-based Cas9 mRNA nanoparticles that effectively knocked out PD-L1 in tumors, significantly reducing tumor growth and metastasis in a mouse model [141]. Similarly, Tan et al. engineered a dual-functionalized polymer incorporating boronate and lipoic acid moieties, which served as a Cas9 RNP carrier targeting NLRP3, successfully disrupting inflammasomes and mitigating inflammation in a psoriasis mouse model [165]. Building on chemical evolution of sequence-defined xenopeptides (XPs) generated by solid phase-supported synthesis [75, 107], our previous work introduced synthetic T-shaped lipo-XPs as CRISPR/Cas9 RNP carriers with high gene editing and correction potential. Notably, the lipo-XP ID *1738* (dGtp) and ID *1636* (Gtt) based Cas9 nanocarriers demonstrated high delivery efficiency, with the 1636-based RNP complex achieving an HDR efficiency of 40% [76].

Furthermore, studies have demonstrated that various HDR enhancers based on small molecules have been utilized to improve CRISPR/Cas9 HDR-mediated gene editing efficiency. These enhancers include NHEJ pathway inhibitors, HDR pathway stimulators, and cell cycle synchronization agents [142]. The NHEJ pathway is triggered by DSBs, which recruit the Ku70/80 heterodimer and the catalytic subunit of DNA-dependent protein kinase (DNA-PKcs) [143, 144]. Together, these components tether the DNA ends, initiating a cascade of reactions including resection, extension, and ligation. Inhibiting key factors of the NHEJ pathway, such as Ku70/80 [145], DNA-PKcs [146], and ligase IV [147], has proven to be an effective strategy for enhancing HDR. For instance, the DNA-PKcs inhibitors Nu7441 and KU-0060648 have been shown to significantly increase HDR repair events while reducing NHEJ frequency in Cas9-mediated gene editing [148]. Similarly, SCR7, a ligase IV inhibitor, has achieved up to a 19-fold improvement in HDR efficiency when combined with Cas9 in mammalian cell lines and mouse models across four target genes [147]. On the HDR pathway side, RAD51, a key factor in DNA strand exchange, plays a central role by forming presynaptic filaments with the accumulation of other proteins on single-stranded DNA (ssDNA). Rs-1, identified from a screen of 10,000 compounds, enhances RAD51 binding to DNA, thereby stimulating HDR [149]. In this study, we primarily investigated strategies to improve HDR efficiency using both NHEJ pathway inhibitors and HDR pathway stimulators in combination with T-shaped peptide-based Cas9 RNP complexes. The evaluated enhancers included Pevonedistat, Rs-1, M3814, KU-0060648, and Nu7441.

Overall, we developed an improved gene correction and editing platform for treating genetic disorders. This platform integrates one of the top T-shaped lipo-XP candidates, in combination with the DNA-PKcs inhibitor Nu7441. Remarkably, this system enhanced both knock-in-mediated gene correction and knock-out-based total gene editing efficiency. Mechanistically, Nu7441 modulated the cell cycle by inhibiting the G1 phase and extending the S and G2/M phases without compromising cellular uptake or endosomal escape. In GFP-to-BFP conversion models, the platform achieved a more than 10-fold increase in HDR efficiency by Nu7441 treatment. The HDR-mediated gene editing efficiency reached 53% in flow cytometry analysis when using the *1636* (Gtt)-based Cas9 nanocarriers. Notably, gene sequencing confirmed that the HDR efficiency peaked at 61%. Beyond HDR enhancement, Nu7441 also amplified exon skipping by 30-fold in a DMD exon 23 reporter cell model and exhibited broad compatibility across various cell lines and LAF-XP oligomers for gene correction and editing. These findings highlight the platform's significant potential as an efficient and versatile tool for future gene therapy applications.

3.3 Materials and methods

3.3.1 Materials

Nu7441 (KU-57788), Rs1, KU-0060648, Scr7, Pevonedistat (MLN4924), and M3814 (nedisertib) were purchased from MedChemExpress (Monmouth Junction, NJ, USA). Reagents including 4′,6-diamidino-2-phenylindole (DAPI), propidium iodide (PI), ampicillin, dimethyl sulfoxide (water-free) (DMSO), Dulbecco's modified Eagle's medium (DMEM), fetal bovine serum (FBS), penicillin/streptomycin, and 3-(4,5-dimethylthiazol-2-yl)-2,5-diphenyltetrazolium bromide (MTT) were obtained from Life Technologies (Carlsbad, CA, USA). Minimum essential medium (MEM) and Lipo 3k were procured from Thermo Fisher Scientific (Waltham, MA, USA), and 4-(2-hydroxyethyl)-1-piperazineethanesulfonic acid (HEPES) was sourced from Biomol GmbH (Hamburg, Germany). HEPES-buffered glucose solution (HBG, pH 7.4) was prepared by dissolving 20 mM HEPES and 5% (*w*/*v*) glucose in water. Cas9 protein was harvested and labeled with ATTO647N, as previously described [75, 76]. Cas9 mRNA (mCherry) was obtained from Trilink Biotechnologies (San Diego, CA, USA). Single guide RNA (sgRNA) with 2′-O-methyl modifications on the first and last three RNA bases, along with phosphorothioate modifications on the RNA bases, Cas9 mRNA, and single-stranded DNA (ssDNA) were procured from Integrated DNA Technologies (Coralville, IA, USA) or AxoLabs GmbH (Kulmbach, Germany), with sequences described in prior studies [78, 176]. pEGFP-N1 plasmid was obtained from addgene (https://www.addgene.org/178088/, accessed on 25 August 2022).

Deionized water, purified using a Millipore system (Simplicity Plus, Millipore Corp Burlington, MA, USA), was employed for solution preparation. The synthesis of the artificial amino acid Fmoc-Stp(Boc)3-OH (Stp) and its analogues was performed as previously described [76, 150].

The lipo-XPs *1738* (dGtp) and *1636* (Gtt) were synthesized using standard Fmoc solid-phase synthesis and detected by MALDI, as previously described [18]. Sequences of all tested lipo-XPs are listed in **Tables 2** and **3**. The synthesized oligomers were stored at a concentration of 10 mg/mL at −20 °C.

Table 1 The sequences of the sgRNA, ssDNA and GFPd2 gene sequence used for GFP conversion, as well as the sgRNA and mcherry-DMDEX 23 gene sequence for exon skipping in this study.

Name	Sequence 5'→ 3'
sgGFP	5′ mG*mC*mU*GAAGCACUGCACGCCGUGUUUUAGAGCUAGAAAUAGCAAGUUAAAAUAAGGCUAGU CCGUUAUCAACUUGAAAAAGUGGCACCGAGUCGGUGCmU*mU*mU*U 3′
ssDNA	5′ G*C*CACCTACGGCAAGCTGACCCTGAAGTTCATCTGCACCACCGGCAAGCTGCCCGTGCCCTGGCCCAC CCTCGTGACCACCCTGAGCCACGGCGTGCAGTGCTTCAGCCGCTACCCCGACCACAT*G*A 3′
sgDMDEx23	5′ mA*mU*mU*UCAGGUAAGCCGAGGUUGUUUUAGAGCUAGAAAUAGCAAGUUAAAAUAAGGCUAG UCCGUUAUCAACUUGAAAAAGUGGCACCGAGUCGGUGCmU*mU*mU*U 3′
GFPd2 gene sequence	5′ ATGGTGAGCAAGGGCGAGGAGCTGTTCACCGGGGTGGTGCCCATCCTGGTCGAGCTGGACGGCGACGTA AACGGCCACAAGTTCAGCGTGTCCGGCGAGGGCGAGGGCGATGCCACCTACGGCAAGCTGACCCTGAAG TTCATCTGCACCACCGGCAAGCTGCCCGTGCCCTGGCCCACCCTCGTGACCACCCTGACCTACGGCGTGC AGTGCTTCAGCCGCTACCCCGACCACATGAAGCAGCACGACTTCTTCAAGTCCGCCATGCCCGAAGGCTA CGTCCAGGAGCGCACCATCTTCTTCAAGGACGACGGCAACTACAAGACCCGCGCCGAGGTGAAGTTCGA GGGCGACACCCTGGTGAACCGCATCGAGCTGAAGGGCATCGACTTCAAGGAGGACGGCAACATCCTGGG GCACAAGCTGGAGTACAACTACAACAGCCACAACGTCTATATCATGGCCGACAAGCAGAAGAACGGCATC AAGGTGAACTTCAAGATCCGCCACAACATCGAGGACGGCAGCGTGCAGCTCGCCGACCACTACCAGCAG AACACCCCCATCGGCGACGGCCCCGTGCTGCTGCCCGACAACCACTACCTGAGCACCCAGTCCGCCCTGA GCAAAGACCCCAACGAGAAGCGCGATCACATGGTCCTGCTGGAGTTCGTGACCGCCGCCGGGATCACTC TCGGCATGGACGAGCTGTACAAGAAGCTTAGCCATGGCTTCCCGCCGGAGGTGGAGGAGCAGGATGATG GCACGCTGCCCATGTCTTGTGCCCAGGAGAGCGGGATGGACCGTCACCCTGCAGCCTGTGCTTCTGCTAG GATCAATGTGTAG3′
mCherry-DMDEx23 gene sequence	5′ ATGGAGGGCTCCGTGAACGGCCACGAGTTCGAGATCGAGGTAAGGGCACTGAGCAGAAGGGAAGAAGC TCCGGGGGCTCTTTGTAGGGTCCTCCAGTCAGGACTCAAACCCAGTAGTGTCTGGTTCCAGGCACTGACC TTGTATGTCTCCTGGCCCAAATGCCCACTCAGGGTAGGGGTGTAGGGCAGACAACGAGTCTTTTGTCATC TACAGGCTCTGCAAAGTTCTTTGAAAGAGCAATAAAATGGCTTCAACTATCTGAGTGACACTGTGAAGGA GATGGCCAAGAAAGCACCTTCAGAAATATGCCAGAAATATCTGTCAGAATTTGAAGAGATTGAGGGGCAC TGGAAGAAACTTTCCTCCCAGTTGGTGGAAAGCTGCCAAAAGCTAGAAGAACATATGAATAAACTTCGAA AATTTCAGGTAAGCCGAGGTTTGGCCTTGGAAGAAGCTCCGGGGGCTCTTTGTAGGGTCCTCCAGTCAGG ACTCAAACCCAGTAGTGTCTGGTTCCAGGCACTGACCTTGTATGTCTCCTGGCCCAAATGCCCACTCAGG GTAGGGGTGTAGGGCAGACAACGAGTCTTTTGTCATCTACAGGGCGAGGGCGAGGGCCGCCCCTACGAG GGCACCCAGACCGCCAAGCTGAAGGTGACCAAGGGTGGCCCCCTGCCCTTCGCCTGGGACATCCTGTCC CCTCAGTTCATGTACGGCTCCAAGGCCTACGTGAAGCACCCCGCCGACATCCCCGACTACTTGAAGCTGT CCTTCCCCGAGGGCTTCAAGTGGGAGCGCGTGATGAACTTCGAGGACGGCGGCGTGGTGACCGTGACCC AGGACTCCTCCCTGCAGGACGGCGAGTTCATCTACAAGGTGAAGCTGCGCGGCACCAACTTCCCCTCCGA CGGCCCCGTAATGCAGAAGAAGACCATGGGCTGGGAGGCCTCCTCCGAGCGGATGTACCCCGAGGACGG CGCCCTGAAGGGCGAGATCAAGCAGAGGCTGAAGCTGAAGGACGGCGGCCACTACGACGCTGAGGTCA AGACCACCTACAAGGCCAAGAAGCCCGTGCAGCTGCCCGGCGCCTACAACGTCAACATCAAGTTGGACAT CACCTCCCACAACGAGGACTACACCATCGTGGAACAGTACGAACGCGCCGAGGGCCGCCACTCCACCGG CGGCATGGACGAGCTGTACAAGTAAGGATCC3′

Modification pattern: '*' denotes phosphorothioated RNA bases; 'm' indicates 2'-O-methyl nucleotide bases.

Table 2 The xenopeptide (XP) library in this study, consisting of *1392*-, *1396*-, and *1445*-analogues, includes IDs and sequences (N- to C-terminus).

Backbone	ID	Sequence
1392 analogues	1392	$K(N_3)$-Y_3-Stp-K(K(LinA)$_2$)-Stp-Y_3
	1737	$K(N_3)$-Y_3-chGtp-K(K-(LinA)$_2$)-chGtp-Y_3
	1738	$K(N_3)$-Y_3-dGtp-K(K-(LinA)$_2$)-dGtp-Y_3
1396 analogues	1396	$K(N_3)$-Y_3-H-Stp-H-K(K(LinA)$_2$)-H-Stp-H-Y_3
	1653	$K(N_3)$-Y_3-H-GEIPA-H-K(K(LinA)$_2$)-H-GEIPA-H-Y_3
	1743	$K(N_3)$-Y_3-H-TFE-H-K(K(LinA)$_2$)-H-TFE-H-Y_3
1445 analogues	1445	$K(N_3)$-C-Y_6-Stp$_2$-K(K-(OleA)$_2$)-Stp$_2$-Y_6-C
	1636	$K(N_3)$-C-Y_3-Gtt$_2$-K(K(OHSteA)$_2$)-Gtt$_2$-Y_3-C
	1637	$K(N_3)$-C-Y_3-GEIPA$_2$-K(K(OHSteA)$_2$)-GEIPA$_2$-Y_3-C

Table 3 The XP ID and list of sequences (N- to C-terminus) of *1218* and LAF-XPs *(1611* and *1719)*.

ID	Sequence
1218	$K(N_3)$-Y_3-(H-Stp)$_2$-H-K(G-ssbb-K(OleA)$_2$)-H-(Stp-H)$_2$-Y_3
1611	(12Oc)K-Stp-K(12Oc)
1719	[K(12Oc)]$_2$-Stp$_2$-[K(12Oc)]$_2$

3.3.2 Cell culture and cell construction

HeLa (ACC57, DSMZ, Germany), HeLa eGFPd2, C2C12 (ACC565, DSMZ, Germany), HeLa mCherry-DMD$_{Ex23}$ (which stably expresses an artificial mCherry construct containing a dystrophin exon 23 sequence interruption derived from the murine Duchenne muscular dystrophy (mdx) model) [77], and HeLa gal8-mRuby3 cells (stably expressing a galectin8-mRuby3 fusion protein) [75, 117] were maintained in DMEM supplemented with

10% FBS, 100 U/mL penicillin, and 100 µg/mL streptomycin. Meanwhile, 16HBE14o- (SCC150, Sigma-Aldrich, USA) cells were cultured in MEM with the same supplementation.

To construct the C2C12 eGFPd2, and 16HBE14o-eGFPd2 cell lines, cells were transfected using lipo-XP *1218* polyplex (**Table 3**) [121] or Lipo 3K gene delivery for 48 h. After additional three days of incubation, flow cytometry was performed to sort GFP-positive cells. Subsequently, following an additional seven days of incubation, a second round of sorting was conducted. If the percentage of GFP-positive cells exceeded 20%, cells were seeded at a density of one cell per well in 96-well plates. Finally, single-cell sorting was performed to isolate GFP-positive clones for subsequent experiments. A similar single-cell sorting approach was employed to construct the purified BFP cell line. In these experiments, the reporter cell lines were generated using a PiggyBac transposon system by co-transfecting a transposase-expressing plasmid and a GFP reporter plasmid. To minimize the chance of multiple integrations, a low donor-to-transposase ratio (1:1, W/W) was used. After transfection, monoclonal cell lines were established by single-cell sorting. Flow cytometry analysis showed a single, uniform GFP-positive population without multiple peaks, which is consistent with single-copy integration.

3.3.3 Fabrication of Cas9 ribonucleoprotein (RNP) complexes or mRNA/sgRNA polyplexes

To prepare the Cas9 RNP/ssDNA complex, pre-stored Cas9 protein and sgRNA solution were mixed and incubated for 15 min at room temperature. The resulting Cas9 RNP solution was then diluted with HBG buffer (pH 7.4). Subsequently, an equal volume of ssDNA template solution was added to the diluted Cas9 RNP solution and thoroughly mixed by pipetting 10 times. The mixture was further combined with an equal volume of the oligomer solution and incubated at room temperature for 40 min.

For the preparation of the Cas9 RNP complex (without ssDNA), the pre-mixed Cas9 RNP solution was directly added to the oligomer solution in equal volume, followed by incubation at room temperature for 15 min.

The final Cas9 RNP/ssDNA complexes were prepared at concentrations of 100 nM or 75 nM with a nitrogen-to-phosphate (N/P) ratio of 12, while the Cas9 RNP complexes were formulated with an N/P ratio of 24. These formulations were then used in subsequent experiments.

Cas9 mRNA nanoparticles were prepared by diluting Cas9 mRNA, sgRNA and ssDNA at a weight ratio of 1:1:1.2 in HBG. The final concentration of nucleic acid in HBG was 25 ng/µl. The lipo-XP *1611* was diluted in water to a final concentration of 0.4 mg/ml. Equal

amounts of nucleic acid dilution and lipo-XP dilution were rapidly mixed and the obtained polyplexes were incubated for 40 min at room temperature.

3.3.4 Characterization of Cas9 RNP/ssDNA complexes

The size and zeta potential of the Cas9 RNP/ssDNA complexes were determined using a Zetasizer Nano ZS (Malvern Instruments, Worcestershire, UK) under the following conditions: equilibration time of 30 s, temperature at 25 °C, refractive index of 1.330, and viscosity of 0.8872 mPa·s. Additionally, the morphology of the Cas9 RNP/ssDNA complex was analyzed using transmission electron microscopy (TEM).

For TEM sample preparation, the grid was positioned with its activated side facing a 10 µL droplet of the sample. Excess liquid was gently removed using filter paper. The staining process was performed in two steps: first, the grid was rinsed with 5 µL of 1.0% uranyl formate solution, which was immediately removed. Then, another 5 µL of the same staining solution was applied to the grid. After blotting away, the excess solution with filter paper, the grid was allowed to air-dry for 15 min. The samples were then analyzed using a JEOL JEM-1100 electron microscope (Tokyo, Japan) operated at an acceleration voltage of 80 kV.

3.3.5 GFP to BFP conversion mediated via homology-directed repair (HDR)

HeLa-eGFPd2, C2C12-eGFPd2, and 16HBE14o-eGFPd2 cells were seeded individually into Corning® Costar 96-well plates one day prior to the experiment. HeLa-eGFPd2 and C2C12-eGFPd2 cells were plated at a density of 5×10^3 cells per well, while 16HBE14o-eGFPd2 cells were seeded at a density of 1×10^4 cells per well. After 24 h of cell attachment, Cas9 RNP/ssDNA complexes or Cas9 mRNA/sgRNA/ssDNA polyplexes, prepared at specified concentrations optimized for each cell line, were added to each well containing fresh culture medium. Simultaneously, 10 µL of various enhancers, pre-diluted in medium to the desired working concentrations, were added to the wells. The resulting mixtures were incubated with the cells at 37°C for 24 h under standard culture conditions.

The cells were collected by trypsinization, centrifuged at 1000× *g* for 5 min, washed with PBS, and resuspended in FACS buffer (10% FBS in PBS, *v*/*v*). Before measurement, 1 µg/mL propidium iodide (PI) (Thermo Fisher Scientific, Waltham, MA, USA) was added to distinguish viable cells from dead cells. GFP-positive (unedited), GFP-negative (NHEJ), and BFP-positive (HDR) cells were quantified from 3000 viable cells using a Beckman Coulter CytoFLEX S flow cytometer (Carlsbad, CA, USA). PI, BFP, and GFP signals were detected with excitation/emission wavelengths of 561/610 nm, 405/450 nm, and 488/530 nm, respectively.

3.3.6. Cellular uptake and endosomal escape of Cas9 RNP/ssDNA complexes

In the case of the cellular uptake, HeLa cells were seeded at a density of 2.5 × 10^4 cells per well in 24-well plates and allowed to grow overnight prior to the experiment. The following day, the cells were incubated with *1738*-based Cas9 RNP/ssDNA complexes (37.5 nM, including 20% ATTO647N-labeled Cas9 protein) in the presence or absence of 50 nM Nu7441 for 2 h. To remove any nanoparticles bound to the cell membrane, the cells were rinsed with 500 µL of PBS containing 2000 IU heparin (Sigma-Aldrich, Merck, Darmstadt, Germany). Subsequently, they were kept on ice for 30 min. The cells were then washed with PBS to prepare for nuclear staining with DAPI (Thermo Fisher Scientific, Waltham, MA, USA). Afterward, they were harvested and analyzed using a Beckman Coulter CytoFLEX S flow cytometer. Each experiment was performed in triplicate. Fluorescence detection was carried out with excitation at 405 nm and emission at 450 nm for DAPI and excitation at 640 nm with emission at 670 nm for ATTO647N.

For the endosomal escape experiment, HeLa Gal8-mRuby3 cells were placed at a density of 2 × 10^4 cells per well in 8-well Ibidi µ-slides (Ibidi GmbH, Gräfelfing, Germany) and incubated for 24 h prior to transfection. Subsequently, 280 µL new medium, 80 µL of RNP complexes, and 40 µL of Nu7441 (50 nM) were added to each well, followed by an incubation period of 2 h. Cells were further washed with 300 µL PBS, fixed with 4% paraformaldehyde (Sigma-Aldrich, Merck, Darmstadt, Germany) at room temperature for 45 min, and stained with 1 µg/mL DAPI in the dark for 15 min. After replacing the staining solution with 300 µL fresh PBS, the samples were analyzed using a Leica TCS SP8 confocal microscope (Leica Microsystems, Wetzlar, Germany). DAPI signals were recorded at 450 nm and mRuby3 signals at 590 nm. Gal8 spots per cell were quantified using ImageJ (version 1.48, National Institutes of Health, Bethesda, MD, USA) by removing nuclei and background, converting the image to 8 bit, adjusting thresholds, and counting cytosolic spots with the Analyze Particles tool.

3.3.7 Cellular cell cycle assay

HeLa cells were seeded at a density of 1.2 × 10^4 cells per well in Corning® Costar 96-well plates (Corning Inc., Corning, NY, USA) one day prior to treatment. For the pre-Nu5 group, cells were pre-incubated with 5 nM Nu7441 for 24 h on the first day. After incubation, the cells were washed with PBS and treated with Cas9 RNP/ssDNA complexes on the second day for an additional 24 h. For the co-Nu5 group, cells were simultaneously treated with Cas9 RNP/ssDNA complexes and 5 nM Nu7441 for 24 h on the second day. The single *1738* group (control) was treated with Cas9 RNP/ssDNA complexes alone under the same conditions on the second day. For the normal transfection protocol in HeLa-GFPd2, the cells were directly incubated with the *1738* RNP complex/ssDNA and 5 nM Nu7441, as described above. On the last day, cells from all groups were collected and suspended

dropwise into 90 µL of cold 70% ethanol. The suspensions were incubated at 4 °C for 2 h. Subsequently, the cells were centrifuged and resuspended in 100 µL of PI staining buffer (comprising 0.1% sodium citrate, 0.1% Triton X-100, 180 U/mL RNase stock solution, and 50 µg/mL PI). The suspensions were incubated for 3 h at 4 °C. Finally, the cells were washed with PBS and analyzed using flow cytometry.

3.3.8 Preparation and transfection evaluation of mRNA/pDNA polyplexes by flow cytometry

The *1611*-based mRNA/pDNA polyplex was prepared by mixing mCherry mRNA and pEGFP-N1 at a fixed weight ratio of 1:1, followed by dilution in HBG. The lipo-XP *1611* applied at an N/P ratio of 18 was separately diluted in purified water, then rapidly mixed with the nucleic acid solution and incubated for 40 min at room temperature. The final nucleic acid concentration in the polyplex solution was 12.5 µg/µL. HeLa cells were seeded in 24-well plates at 2.5 × 10^4 cells per well and cultured for 24 h before transfection. After incubation, the medium was replaced with fresh, pre-warmed medium and polyplex solutions were added to achieve final concentrations of 62.5 ng, 125 ng, or 250 ng of nucleic acid and 50 nM Nu7441 in the cell culture. HBG buffer was used as a negative control.

After 24 h of treatment, cells were collected, resuspended in FACS buffer, and analyzed using a CytoFLEX S Flow Cytometer. DAPI staining was used to distinguish viable from dead cells, with excitation at 405 nm and emission detected at 450 nm. Only isolated viable cells were analyzed. The median fluorescence intensity (MFI) of mCherry- and eGFP-positive cells indicated mRNA and pDNA transfection efficiency, respectively. Fluorescence expression was measured by exciting mCherry at 561 nm and eGFP at 488 nm, with emission detected at 610 nm and 530 nm, respectively.

3.3.9 Gene editing mediated exon skipping of Cas9 RNP complexes with or without Nu7441

HeLa mCherry-DMD_{Ex23} cells were plated at a density of 5 × 10^3 cells per well in Corning® Costar 96-well plates and maintained for 24 h before treatment. Cas9 RNP complexes (20 µL) formed with sgDMDEx23 as described in prior studies [79, 150] with or without Nu7441 (10 µL) were then applied to the cells for 24 h. Prior to transfection, nanocarriers were assembled as previously detailed and diluted with HBG to achieve the desired concentration in the final 20 µL solution. Following the transfection period, cells were further cultured for two days. Subsequently, the cells were detached using trypsin, centrifuged at 1000 × g for 5 min, and rinsed with PBS. The collected cells were resuspended in FACS buffer and analyzed for gene editing efficiency using a Beckman Coulter CytoFLEX S flow cytometer (Carlsbad, USA) according to the previously

described protocol. DAPI and mCherry signals were recorded at 450 nm and 610 nm, respectively.

3.3.10 Gene editing mediated exon skipping by Cas9 RNP complexes visualized by CLSM

HeLa mCherry-DMD_{Ex23} cells were seeded at 2 × 10^4 cells per well in Corning® Costar 24-well plates and cultured for 24 h. The cells were then transfected with 10nM Cas9 RNP complexes, with or without 5 nM Nu7441, for 24 h, followed by two additional days of incubation. Afterward, the cells were transferred to 8-well Ibidi µ-slides and incubated overnight. The following day, cells were washed with 300 µL PBS, fixed with 4% paraformaldehyde for 45 min, and stained for 2 h with Alexa Fluor™ 488 phalloidin to label the cytoskeleton. Nuclei were stained with 1 µg/mL DAPI in the dark for 15 min. After staining, the solution was replaced with fresh PBS. Samples were then analyzed using a Leica TCS SP8 confocal microscope. DAPI, Alexa Fluor™ 488, and mCherry signals were recorded at 450 nm, 530 nm, and 610 nm, respectively.

3.3.11 Genome extraction

The treated HeLa eGFPd2 cells underwent the 'GFP to BFP conversion mediated via homology-directed repair (HDR)' process as described. The cells were transferred into 24- and 6-well plates to promote growth expansion. After sufficient growth, the cells were harvested and DNA was extracted using the QIAamp DNA Mini Kit (Hilden, Germany). The cells were washed with PBS and resuspended in 100 µL of PBS. Subsequently, 10 µL of proteinase K and 100 µL of buffer AL were added to the cell suspension. The mixture was incubated at 56 °C for 10 min. Following incubation, 100 µL of ethanol was added to the sample, which was vortexed for 15 seconds. The mixture was then transferred into a spin 2.0 column and centrifuged at 8000 g for 1 min. The liquid from the collection tube was discarded, and 500 µL of buffer AW1 was added to the column, followed by centrifugation at 8000 g for 1 min. The sample was subsequently washed with 500 µL of buffer AW2 and centrifuged at 13300 g for 3 min. The waste buffer was discarded, and the column was centrifuged empty for an additional 1 min to ensure complete removal of residual buffer. Finally, 50 µL of nuclease-free water was added to the column, and centrifugation was performed to obtain the purified DNA sample.

3.3.12 PCR amplification and sequencing

To obtain the target gene sequence for gene sequence measurement, primers (TGGGCAACGTGCTGGTTATT, CACGAACTCCAGCAGGACCATG) were designed for PCR amplification. The harvested DNA sample (100 ng) was mixed with 10× Thermopol standard buffer, 10 mM dNTPs, 10 µM forward/reverse primer, nuclease-free water, and Taq DNA polymerase. The mixture was added to a PCR tube and subjected to the

following PCR conditions: initial denaturation (94 °C, 30 s), 37 cycles (94 °C, 30 s; 58 °C, 1 min), and final extension (68 °C, 1 min).

Subsequently, a 2% (w/v) agarose gel was prepared by dissolving agarose (Sigma-Aldrich, Merck, Darmstadt) in TBE buffer (containing 18.0 g tris(hydroxymethyl)aminomethane, 5.5 g boric acid, and 0.002 M disodium ethylenediaminetetraacetic acid (EDTA) at pH 8, in 1 L of water). After cooling to approximately 50°C, 1× GelRed™ (Hayward, CA, USA) was added. The agarose solution was cast into an electrophoresis unit and allowed to solidify. For the PCR products, 5 µL of 6× loading buffer (6 mL glycerol, 1.2 mL 0.5 M EDTA, 2.8 mL water, and 0.02 g bromophenol blue) was added to 25 µL of PCR product. Samples were loaded into the gel wells, and electrophoresis was performed at 100 V for 3 h in TBE buffer. The unedited cell PCR products served as a control. The peqGold 1 kb DNA Ladder (VWR International, Pennsylvania, USA) was used to estimate DNA fragment sizes and confirm the accuracy of PCR amplification and cloning.

The final PCR products were analyzed by agarose gel electrophoresis (2% agarose gel; 100 V; 3 h). Individual band intensities were quantified and compared to the full-length band of 769 bp using ImageJ software. The targeted band was excised using a scalpel, and the PCR products were purified using a QIAquick PCR purification kit (Hilden, Germany) before being sent to Eurofins for Sanger sequencing. Final gene sequence results were analyzed using the Synthego ICE tool (https://ice.synthego.com/#/).

3.3.13 Assessment of the cytotoxicity of cells via MTT assay

Following 24 or 48 h of transfection as described above, 10 µL of MTT solution was added to achieve a final concentration of 0.5 mg/mL. After 3 h of incubation at 37 °C, the supernatant was discarded, and the plates were stored at –80 °C for at least 1 h. Formazan crystals were dissolved in 100 µL of DMSO and incubated at 37 °C for 30 min with shaking at 125 rpm. Absorbance was recorded at 590 nm with a background correction at 630 nm using a Tecan Spectrafluor Plus microplate reader (Tecan, Männedorf, Switzerland). Cell viability (%) was calculated as (***A***/***B***) ×100, where ***A*** and ***B*** represent the absorbance of the test sample and HBG group, respectively.

3.3.14 Statistical analysis

Statistical analysis was performed using GraphPad Prism 8.0 software, with results presented as mean ± standard deviation (SD). Data were evaluated through an unpaired, two-tailed Student's t-test, where statistical significance was denoted as * $p < 0.05$, ** $p < 0.01$, *** $p < 0.001$, **** $p < 0.0001$ and "ns" representing no significance.

3.4 Results

3.4.1 Characterization of T shape Cas9 RNP/ssDNA complexes and the selection of enhancers

In this study, to identify various HDR enhancers, a recently designed gene-editing T-shaped lipo-XP, ID *1738* (dGtp), was selected as main delivery carrier (**Fig. 1A**). This oligomer demonstrated excellent gene editing efficiency with minimal cellular toxicity. Lipo-XP *1738* has the peptidic sequence (N- to C- terminus) K(N_3)-Y_3-dGtp-K(K(LinA)$_2$)-dGtp-Y_3. It is composed of C- and N-terminal tyrosine tripeptides and central branching lysines as natural amino acids, modified with two linoleic acids in T-shape configuration, and two units of the artificial amino acid diglycoloyl tetraethylene pentamine (dGtp). Lipo-XP *1738* was synthesized using standard Fmoc based solid-phase peptide synthesis, purified and characterized as previously described [76]. The T-shaped Cas9 RNP/ssDNA complexes (**Fig. 1B**) were then prepared by mixing *1738* and Cas9 RNP/ssDNA at a nitrogen-to-phosphate (N/P) ratio of 12, with an RNP/ssDNA ratio of 1:1, followed by 40-minute incubation. The resulting nanoparticles had a hydrodynamic size of 150 nm (**Fig. 1C**) and a zeta potential of +20.1 mV (**Fig. 1D**). To visualize the Cas9 RNP/ssDNA complexes, the sample was stained with 5 µL of 1.0% uranyl formate solution, dried for 15 min, and analyzed using a JEOL JEM-1100 electron microscope. The results revealed a spherical shape with a diameter of 50-60 nm (**Fig. 1E**).

The *1738*-based Cas9 RNP/ssDNA complexes were evaluated in a GFP-to-BFP conversion model (**Fig. 1F**) using previously described HeLa-eGFPd2 cells [76]. Applied sgRNA, ssDNA and reporter gene sequences are listed in the **Table 1**. To identify potential compounds that could further enhance the genome correction efficiency, we screened a range of small-molecule modulators targeting either the HDR or NHEJ pathways in HeLa-eGFPd2 cells. The cells were treated with *1738*-based Cas9 RNP/ssDNA complexes (18.75 nM) in the absence ('*1738*') or presence of selected enhancers for 24 h. The tested compounds included HDR pathway stimulators—Pevonedistat (CtIP stimulator; 0.5, 1, 2 nM) [151] and RS-1 (RAD51 stimulator; 1, 2.5, 10 nM) [152, 153]—as well as NHEJ pathway inhibitors—SCR7 (ligase IV inhibitor; 1, 5, 10 nM) [154-156] and three DNA-PKcs inhibitors: M3814 (5, 10, 20 nM) [157, 158], KU-0060648 (0.1, 0.25, 1 nM) [148, 159], and

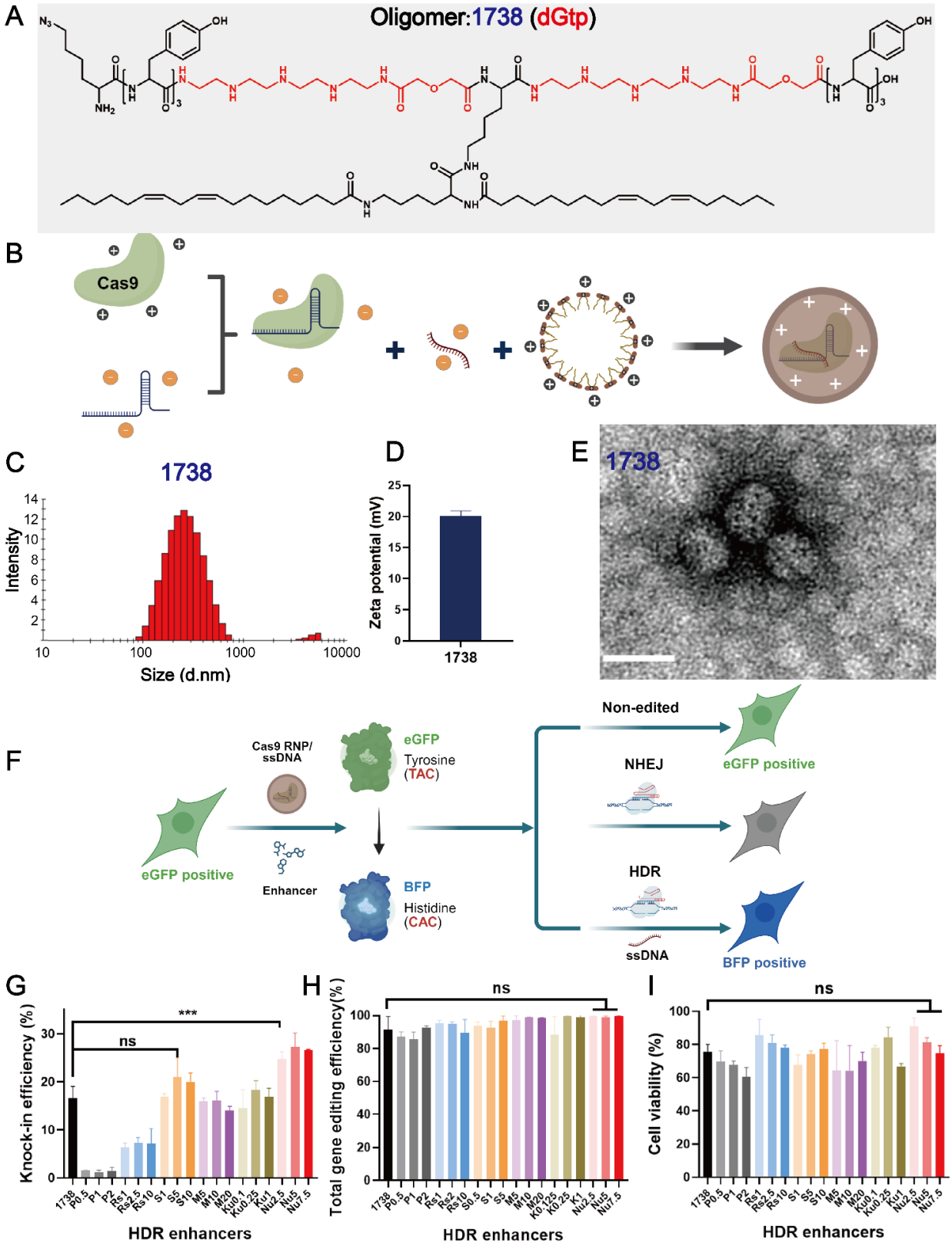
A
Oligomer:1738 (dGtp)
B
Cas9
C
1738
Intensity
Size (d.nm)
D
Zeta potential (mV)
1738
E
1738
F
Cas9 RNP/
ssDNA
eGFP
Tyrosine
(TAC)
eGFP positive
Enhancer
BFP
Histidine
(CAC)
Non-edited
NHEJ
eGFP positive
HDR
ssDNA
BFP positive
G
Knock-in efficiency (%)
***
ns
HDR enhancers
H
Total gene editing efficiency(%)
ns
HDR enhancers
I
Cell viability (%)
ns
HDR enhancers

Figure 1. Characterization of Cas9 RNP complexes and selection of gene correction enhancers. (**A**) The chemical structure of T-shaped lipo-XP *1738* (dGtp). (**B**) Schematic illustration depicting T-shaped lipo-XP-based Cas9 RNP complexes prepared by mixing Cas9 protein with sgRNA, ssDNA, and lipo-XP *1738*. Dynamic light scattering (DLS) intensity size distribution (**C**) and zeta potential (**D**) of *1738*-based Cas9 RNP/ssDNA complexes at an RNP/ssDNA ratio of 1:1 and N/P = 12. (**E**) Transmission electron microscopy (TEM) image of *1738*-based Cas9 RNP/ssDNA complexes at an RNP/ssDNA ratio of 1:1 and N/P = 12 (scale bar, 80 nm). (**F**) Schematic illustration of eGFP-to-BFP conversion in eGFPd2 cells. GFP expression can be eliminated via NHEJ, or the 66th amino acid, tyrosine (TAC), can be changed to histidine (CAC) through HDR to produce BFP expression. (**G**) HDR efficiency, (**H**) total gene editing efficiency (both HDR and NHEJ events), and (**I**) cell viability of HeLa-eGFPd2 cells treated with *1738*-based Cas9 RNP/ssDNA complexes (18.75 nM, RNP) with various gene correction enhancers, including Pevonedistat (0.5, 1, 2 nM), Rs-1 (1, 2.5, 10 nM), SCR7 (1, 5, 10 nM), M3814 (5, 10, 20 nM), KU-0060648 (0.1, 0.25, 1 nM), and Nu7441 (2.5, 5, 7.5 nM). "*1738"* refers to treatment with *1738* Cas9 RNP/ssDNA complexes without enhancer. Enhancer abbreviations represent the enhancer name followed by its concentration in nM. *** $p < 0.001$ vs. *1738*; ns denotes no significant difference. Data are shown as means ± SD *(n = 3*), with statistical significance determined by unpaired Student's *t*-test.

Nu7441 (2.5, 5, 7.5 nM) [148, 160, 161]. Following treatment, the cells were washed with PBS and incubated for an additional five days in fresh medium. Flow cytometry analysis identified eGFP-positive (non-edited), eGFP-negative (NHEJ), and BFP-positive (HDR) populations (**Fig.1F**). Among the enhancers tested, only Nu7441 significantly improved HDR efficiency, increasing it from 16.5% in the *1738* nanocarrier group to around 25% (**Fig. 1G**), without a substantial difference in the total gene editing efficiency (both HDR and NHEJ events) (**Fig. 1H**). Additionally, all enhancers exhibited minimal cytotoxicity (**Fig. 1I**). Based on these findings, Nu7441 was selected for further development in subsequent experiments.

3.4.2 HDR and gene editing efficiency with various T shape XPs or enhancer combinations

To further investigate the effects of Nu7441, gene-editing efficacies (knock-in and knock-out) of nine recently developed T-shaped lipo-XPs minus/plus Nu7441 were compared on HeLa eGFPd2 cells (**Fig. 2A**). These carriers (**Table 2**) derive from three lipo-XPs (*1392*, *1396* and *1445*) with the artificial amino acid succinoyl tetraethylene pentamine (Stp) in their backbone. Within a subsequent chemical evolution process, carriers were further optimized by replacement of Stp by other artificial amino acids including chGtp, dGtp, GEIPA, TFE, or Gtt (see **Table 2**) as recently published [76]. After 24 h of treatment, the cells were washed with PBS and incubated with fresh medium for an additional five days. The results demonstrated that 5 nM Nu7441 improved BFP-conversion efficiency for all T-shaped XP, except for the already highly potent *1653* (**Fig. 2A**). Notably, the HDR efficiency was increased more than tenfold by addition of Nu7441 to RNP/ssDNA complexes formed with *1396*. Interestingly, Nu7441 also increased the total gene editing

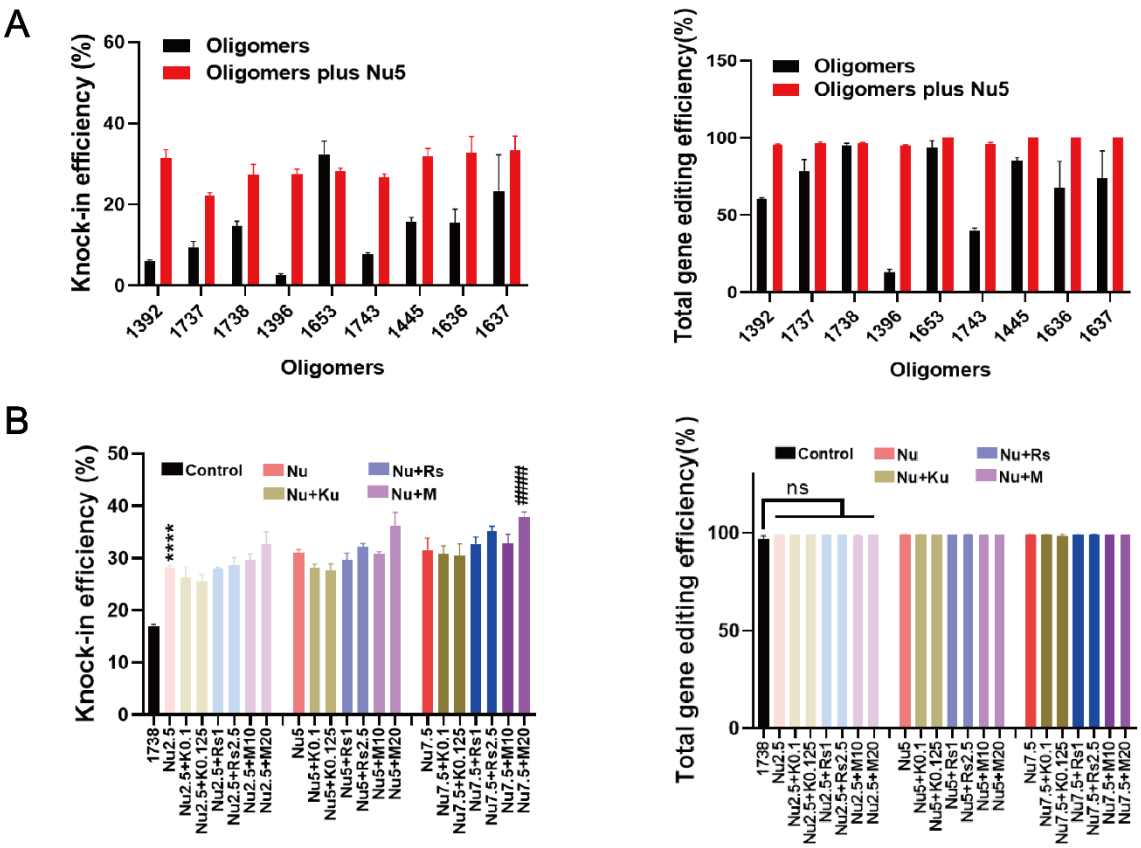

Figure 2. HDR and gene editing efficiency of Cas9 RNP/ssDNA complexes formed with nine different lipo-XP carriers and tested without or with enhancers in HeLa-GFPd2 cells. HDR and gene editing efficiency of Cas9 RNP/ssDNA complexes formed with nine different lipo-XP carriers and tested without or with enhancers in HeLa-GFPd2 cells. (**A**) HDR efficiency and total gene editing efficiency of T-shaped oligomer-derived Cas9 RNP/ssDNA complexes (18.75 nM RNP), transfected with or without 5 nM Nu7441. (**B**) HDR efficiency and total gene editing efficiency of *1738* Cas9 RNP/ssDNA complexes (18.75 nM RNP), in combination with enhancer mixtures, added for 24 h transfection. Enhancer mixtures include Nu7441 (2.5, 5, 7.5 nM), Rs1 (1, 2.5 nM), KU-0060648 (0.1, 0.25 nM), or M3814 (10, 20 nM). '*1738*' refers to treatment with *1738* Cas9 RNP/ssDNA complexes without enhancer. Enhancer abbreviations represent the enhancer name followed by its concentration in nM. **** $p < 0.0001$ vs. *1738*; #### $p < 0.0001$ vs. group Nu2.5; ns denotes no significant difference. Data are shown as means ± SD ($n = 3$), with statistical significance determined by unpaired Student's *t*-test.

efficiency by T-shaped lipo-XP. Specifically, in the *1396* group, the overall gene editing efficiency increased approximately 7-fold, from 13.1% to 95.1%. These findings suggest that the DNA-PKcs inhibitor Nu7441 surprisingly also works for enhancement of NHEJ-mediated gene editing efficiency.

In addition, studies have shown that combining various enhancers represents an effective strategy for improving gene correction [151, 162, 163]. In our study, Rs1, KU-0060648, and M3814 at various concentrations were co-incubated with Nu7441 and *1738*-based Cas9 RNP/ssDNA complex for 24 h. After an additional five days of incubation, the cells were analyzed. The results indicate that the enhancer combination improved HDR efficiency beyond the *1738*/Nu7441 group, resulting in almost 40% BFP-positive cells for the combination of 7.5 nM Nu7441 plus 20 nM M3814. Total gene editing efficiency reached almost 100% (**Fig. 2B**). However, cell viability, assessed via MTT assay after one day of incubation, revealed increased cytotoxicity (**Fig. 9)**. Consequently, Nu7441 alone, without additional enhancers, was identified as the preferable option for further development in subsequent studies.

3.4.3 Mechanistic investigation of Nu7441 for gene editing improvement

To further investigate the mechanism of Nu7441 in the gene editing process, cellular uptake experiments were conducted in standard HeLa cells. The cells were treated with *1738*-based Cas9 RNP/ssDNA complexes containing 37.5 nM RNP (20% ATTO647N-labeled Cas9 protein) for 2 h, with or without 5 nM Nu7441. The results demonstrated no significant difference in cellular uptake between *1738*/Nu7441 and *1738* alone group (**Fig. 3A**), suggesting that Nu7441 does not influence cellular uptake. Similarly, endosome destabilization was analyzed in HeLa gal8-mRuby3 cells [75, 117] as previously described [113, 150]. After a 4-hour treatment with HBG, *1738*-based Cas9 RNP/ssDNA complexes, or *1738* plus 5 nM Nu7441, the cells were stained with DAPI and endosomal rupture was detected by CLSM. Upon endosomal disruption, cytosolic galectin-8 translocates to the damaged endosomes, where it binds to membrane-associated galactan residues [164]. The images revealed comparable gal8-mRuby3 fusion protein signals (red spots) in both groups (**Fig. 3B,C**), indicating that Nu7441 does not alter endosomal escape activity.

Next, a PI-based cell-cycle analysis was performed to investigate whether the gene-editing enhancement by Nu7441 is associated with alterations in cell cycle (**Fig. 3D**). The cells were treated with *1738*-based Cas9 RNP/ssDNA complexes (18.75 nM) and 5 nM Nu7441 for various incubation methods (**Fig. 3D**). Flow cytometry analysis revealed that Nu7441 significantly increased the proportion of cells in the S and G2/M phases while decreasing the G1 phase population (**Fig. 3E**). Besides, the cell cycle was further analyzed on day 6 using standard transfection protocols in HeLa-eGFPd2 cells. The results were consistent with above findings, showing a similar cell cycle distribution (**Fig.**

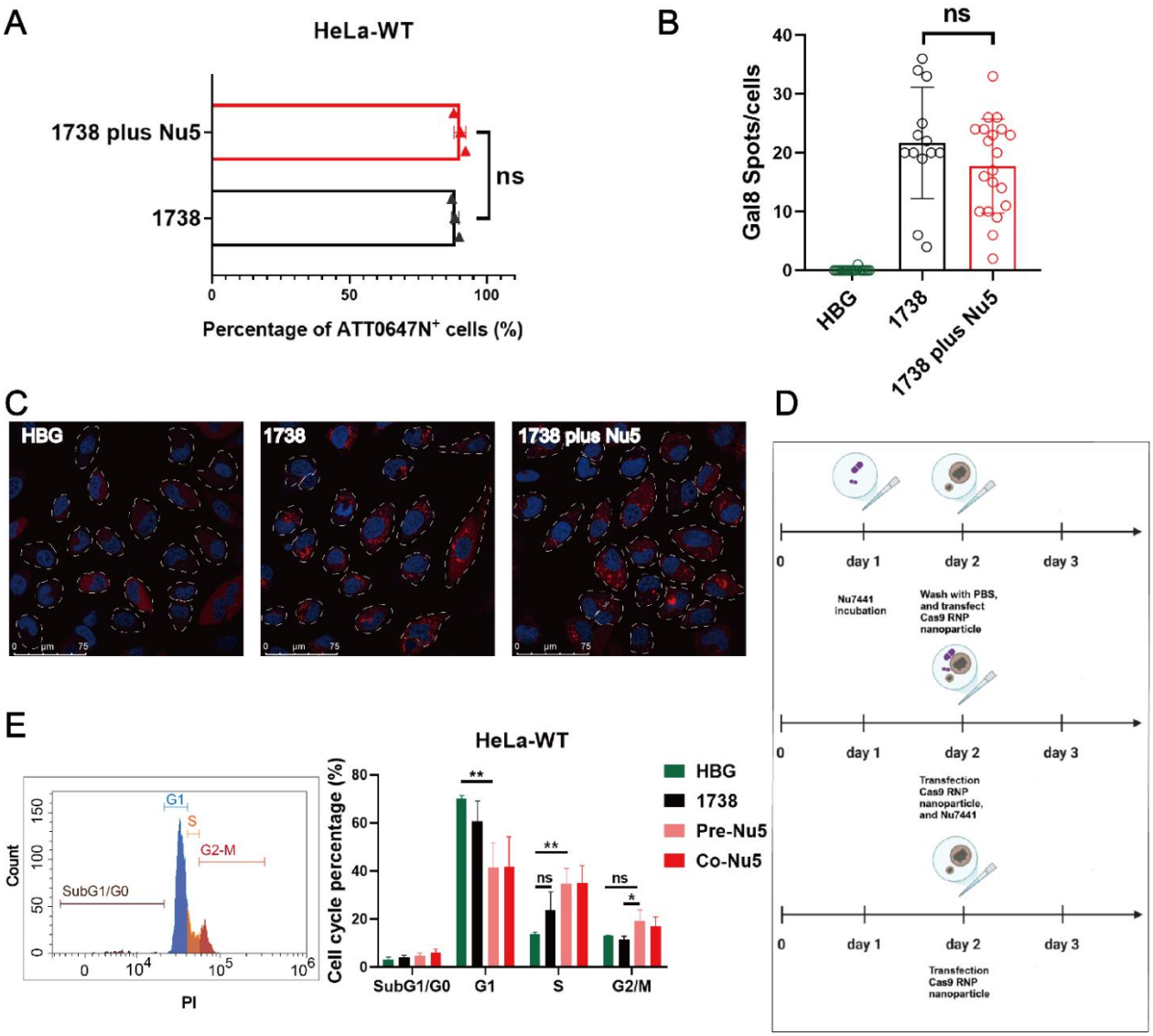

Figure 3. Mechanistic investigation of the Nu7441 effect. (**A**) Cellular uptake of *1738* Cas9 RNP/ssDNA complexes (37.5 nM) containing 20% ATTO647N-labeled Cas9 protein, with or without 5 nM Nu7441, in HeLa cells, analyzed by flow cytometry after 2 h of incubation. (**B**) Quantification and (**C**) confocal laser scanning microscopy (CLSM) imaging of gal8 puncta in HeLa gal8-mRuby3 cells treated with HBG or Cas9 RNP/ssDNA nanoparticles (37.5 nM), with or without 5 nM Nu7441 for 4 h. Nuclei were stained with DAPI (blue), while red punctate gal8-mRuby3 fluorescence indicates endosomal membrane disruption. Gal8 puncta were quantified using ImageJ analysis. (**D**) Experimental design for cell cycle analysis. (**E**) PI-based cell cycle analysis of HeLa cells treated with various *1738*-based nanocarriers (18.75 nM Cas9 RNP), analyzed on day 3 after treatment. Data are shown as means ± SD ($n = 3$), with statistical significance determined by unpaired Student's *t*-test. * $p < 0.05$; ** $p < 0.01$; ns denotes no significant difference.

10). Previous studies have shown that HDR is predominantly active in the S and G2 phases, coinciding with the availability of homologous sequences that can serve as repair templates during DNA damage [165, 166]. Additionally, the G2/M stage has previously been demonstrated to facilitate transfection due to breakdown of the nuclear membrane during the M phase and an easier access to the nuclear genomic compartment [167-170]. To investigate whether Nu7441 can facilitate such a nuclear entry process, a mCherry mRNA and GFP pDNA co-transfection experiment was carried out with or without Nu7441 (5 nM). The results (**Fig. 11**) demonstrated that Nu7441 enhanced pDNA transfection (which requires nuclear entry) but reduced mRNA transfection (where nuclear entry is not desired).

3.4.4 Exon skipping efficiency of *1738* Cas9 RNP complexes with 5 nM Nu7441 in a DMD exon 23 reporter cell model

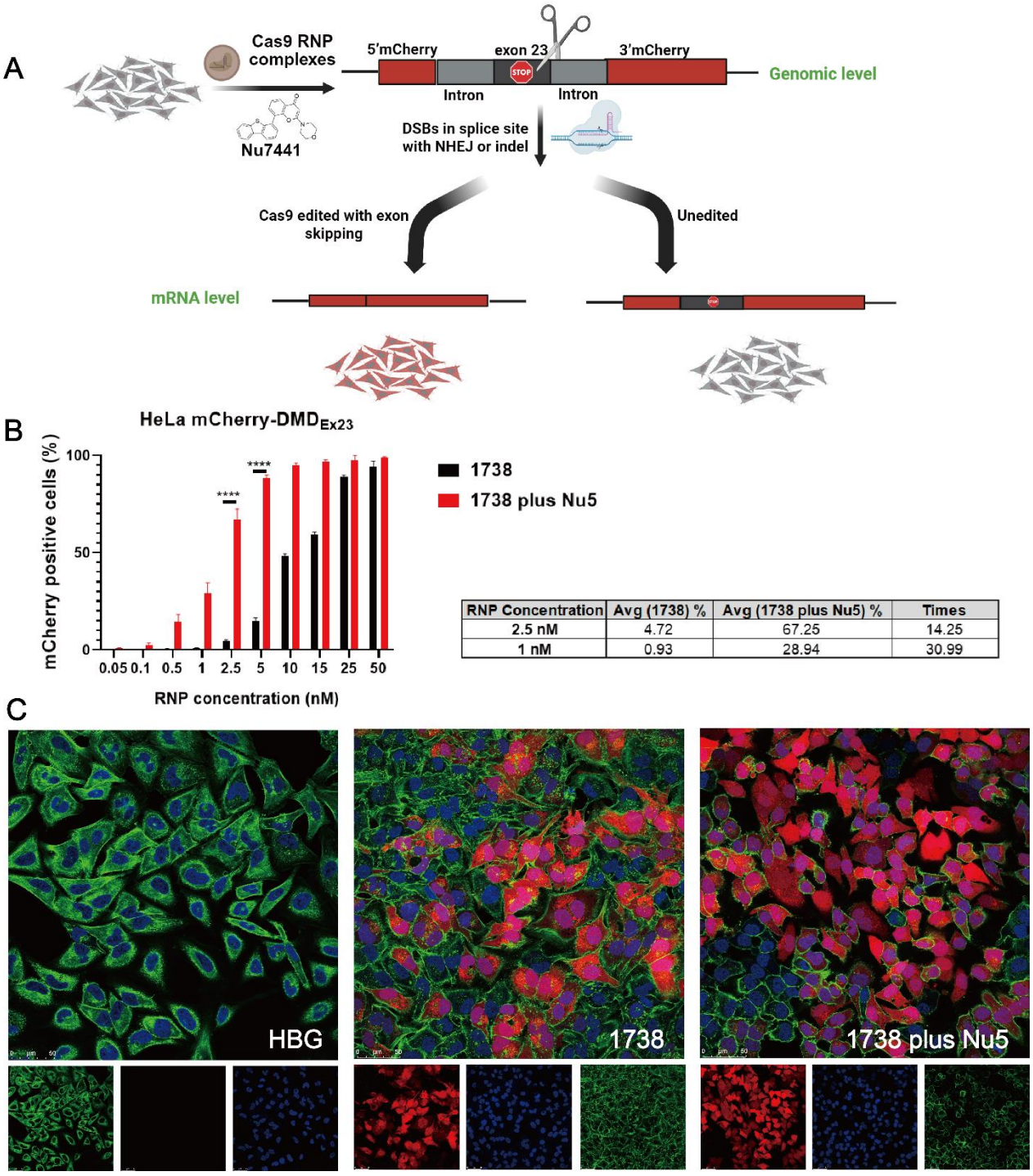

RNP Concentration	Avg (1738) %	Avg (1738 plus Nu5) %	Times
2.5 nM	4.72	67.25	14.25
1 nM	0.93	28.94	30.99

Figure 4. Exon skipping efficiency of Cas9 RNP complexes with NU7441 in a DMD reporter cell model. (**A**) Schematic representation of the exon 23 skipping mechanism using Cas9 RNP

complexes in the absence or presence of 5 nM Nu7441. (**B**) Comparison of exon skipping efficiency between single *1738* Cas9 RNP complexes and the group supplemented with 5 nM Nu7441. Cas9 RNP concentrations ranged from 0.05 to 50 nM. The column chart illustrated significant improvements in exon skipping efficiency with Nu7441. (**C**) CLSM images of HeLa mCherry-DMD_{Ex23} cells treated with *1738* Cas9 RNP complexes at 10 nM RNP, either with or without 5 nM Nu7441. Cell nuclei were stained with DAPI (blue), the cytoskeleton with Alexa Fluor™ 488 phalloidin (green), and mCherry fluorescence (red). The scale bar represents 50 µm. All complexes were prepared at an N/P ratio of 24 and transfected for 24 h. Data are shown as means ± SD (*n* = *3*). Statistical significance is indicated as ****$p < 0.0001$.

In our previous work, HeLa mCherry-DMD_{Ex23} cells [77] were validated as a DMD exon 23 reporter cell model, demonstrating high exon-skipping efficiency using LAF-XPs Cas9 mRNA/sgRNA [79] or Cas9 protein/sgRNA complexes [150] even in serum-containing conditions and at low sgRNA concentration. Exon skipping at the mRNA level was also confirmed in these studies by Germer et al. [79] and Lessl et al. [77]. The exon-skipping mechanism is illustrated in **Fig. 4A**. To assess whether Nu7441 enhances exon skipping, HeLa mCherry-DMD_{Ex23} cells were treated with *1738*-based Cas9 RNP nanocarriers at varying concentrations (0.05–50 nM), with or without 5 nM Nu7441, for 24 h. After treatment, the cells were washed with PBS and incubated in fresh medium for an additional two days. Flow cytometry analysis was subsequently performed to distinguish between mCherry-negative cells (non-edited, negative cells) and mCherry-positive cells (edited, red cells), evaluating exon-skipping efficiency under the experimental conditions.

The data revealed that the EC50 of exon skipping for the single *1738* group was 11.18 nM RNP, whereas the EC50 for the *1738* plus Nu7441 group significantly decreased to 1.65 nM, as shown in **Fig. 12**. These results indicated that Nu7441 markedly enhanced exon skipping in the DMD model. Similarly, exon-skipping efficacies in the *1738* group reached 0.93% at 1 nM RNP and 4.72% at 4 nM RNP. Whereas additional treatment with Nu7441 resulted in 28.94% and 67.25%, reflecting 29.99-fold and 13.25-fold improvements, respectively (**Fig. 4B**).

Additionally, the DMD reporter cell model was further analyzed using CLSM to visually assess exon skipping efficiency. After treatment with 10 nM RNP, as described above, the cells were examined under a confocal microscope. The CLSM images (**Fig. 4C**) revealed that in the single *1738* group, a limited proportion of cells displayed mCherry fluorescence, indicating exon skipping activity. In contrast, the *1738* plus Nu7441 group demonstrated a significantly higher proportion of mCherry-positive cells, aligning with the enhanced exon skipping efficiency observed in the flow cytometry results. In summary, Nu7441 enhanced NHEJ-mediated exon skipping in the DMD reporter cell model, consistent with its role in promoting NHEJ activity.

3.4.5 General applicability of Nu7441 in different settings

Nu7441 exhibited high enhancement of gene editing including HDR with the T-shaped lipo-XP-based Cas9 RNP/ssDNA system in the HeLa-eGFPd2 cell line. To further examine Nu7441's role in HDR and gene editing under different conditions, we constructed C2C12-eGFPd2 and 16HBE14o-eGFPd2 cell lines. The cells were separately seeded and treated with the *1738*-based formulation under the same conditions as before (18.75 nM, RNP/ssDNA = 1/1), with or without 5 nM Nu7441. The results indicated that Nu7441 significantly improved total gene editing efficiency in both C2C12-eGFPd2 (**Fig. 5A**, p = 0.0256) and 16HBE14o-eGFPd2 cell lines (**Fig. 5B**, p = 0.0182). However, HDR efficiency was only improved in the 16HBE14o-eGFPd2 cells, not in the C2C12-eGFPd2 cells. This could be attributed to cell-specific differences, such as variations in cell cycle dynamics or DNA repair machinery. Furthermore, we explored the impact of material structure on

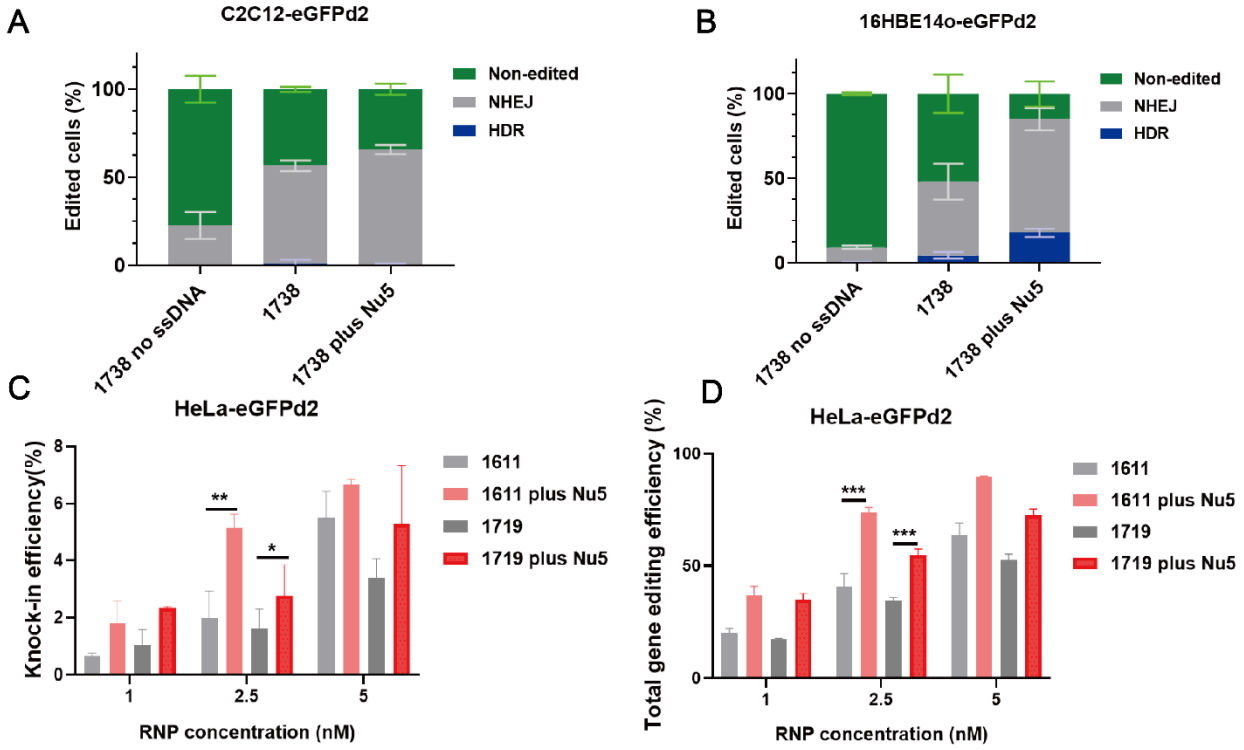

Figure 5. Gene correction and editing efficiency of Cas9 RNP/ssDNA complexes with NU7441 under various conditions. Gene editing was evaluated by flow cytometry in C2C12-eGFPd2 (**A**) and 16HBE14o-eGFPd2 (**B**) cell lines following transfection with *1738* Cas9 RNP complexes without a DNA template (referred to as *1738* no ssDNA, 18.75 nM), or *1738* Cas9 RNP/ssDNA complexes (18.75 nM) in the presence or absence of 5 nM Nu7441. The HDR efficiency (**C**) and total gene editing efficiency (**D**) of LAF Cas9 RNP/ssDNA complexes (*1611* and *1719*) with or without 5 nM Nu7441 in HeLa-eGFPd2. All complexes were prepared at an N/P ratio

of 12 and transfected for 24 h. Data are shown as means ± SD (*n* = *3*). Statistical significance is indicated as * $p < 0.05$, ** $p < 0.01$ and *** $p < 0.001$.

Nu7441's performance. U-shaped lipo-amino fatty acid (LAF)-based XPs (*1611*, *1719*) [79, 113, 150] were formulated into Cas9 RNP/ssDNA complexes at a 1-5 nM RNP concentration and tested in HeLa-eGFPd2 cells. Results showed that Nu7441 continued to enhance HDR and gene editing efficiency across structurally different delivery systems (**Fig. 5C,D**). Similarly, Nu7441 strongly improved HDR and overall gene editing efficiency in HeLa-eGFPd2 cells using a Cas9 mRNA based editing platform, specifically applying Cas9 mRNA/sgRNA/ssDNA polyplexes [150] formed with the LAF-XP carrier *1611* (**Fig. 13**). This consistent enhancement highlights Nu7441 as a robust enhancer for both Cas9 protein/sgRNA /ssDNA and Cas9 mRNA/sgRNA/ssDNA delivery, making it a promising candidate for gene correction therapy.

3.4.6 Gene correction efficiency of an optimized T-shape carrier *1636*-based Cas9 RNP/ssDNA formulation with Nu7441

In our previous work, *1636* (Gtt) Cas9 RNP/ssDNA complexes achieved the highest HDR-mediated genome editing efficiency, reaching about 40% at a 25 nM RNP concentration and an RNP/ssDNA ratio of 1:4 after a 48-hour transfection [76]. To evaluate the gene correction potential of Nu7441 in combination with these Cas9 RNP/ssDNA complexes, Cas9 RNP/ssDNA complexes were tested under similar conditions. HeLa- eGFPd2 cells were treated with the complexes, either with or without 5 nM Nu7441, for 24 h. Following treatment, the cells were incubated for an additional five days before analysis. The results demonstrated that the single *1636* group achieved over 26% HDR efficiency at a 25 nM RNP concentration and an RNP/ssDNA ratio of 1:8 (**Fig. 6A** and **14A**). When supplemented with 5 nM Nu7441, HDR efficiency was consistently improved in each group. For instance, at the lower RNP concentration of 5 nM and the same RNP/ssDNA ratio (1:8), the *1636* plus Nu7441 group achieved a remarkable HDR efficiency of 53% (**Fig. 6A** and **14A**), highlighting Nu7441's strong HDR enhancement effect. A similar trend was observed for total gene editing efficiency (**Fig. 6B** and **14B**). Finally, MTT assays revealed improved cell metabolism in the *1636* plus Nu7441 group compared to the single *1636* group (**Fig. 6C** and **14C**). This finding suggests that Nu7441 not only enhances HDR efficiency but also reduces cytotoxicity associated with Cas9 RNP delivery, further supporting its potential as a versatile enhancer for genome correction and editing applications.

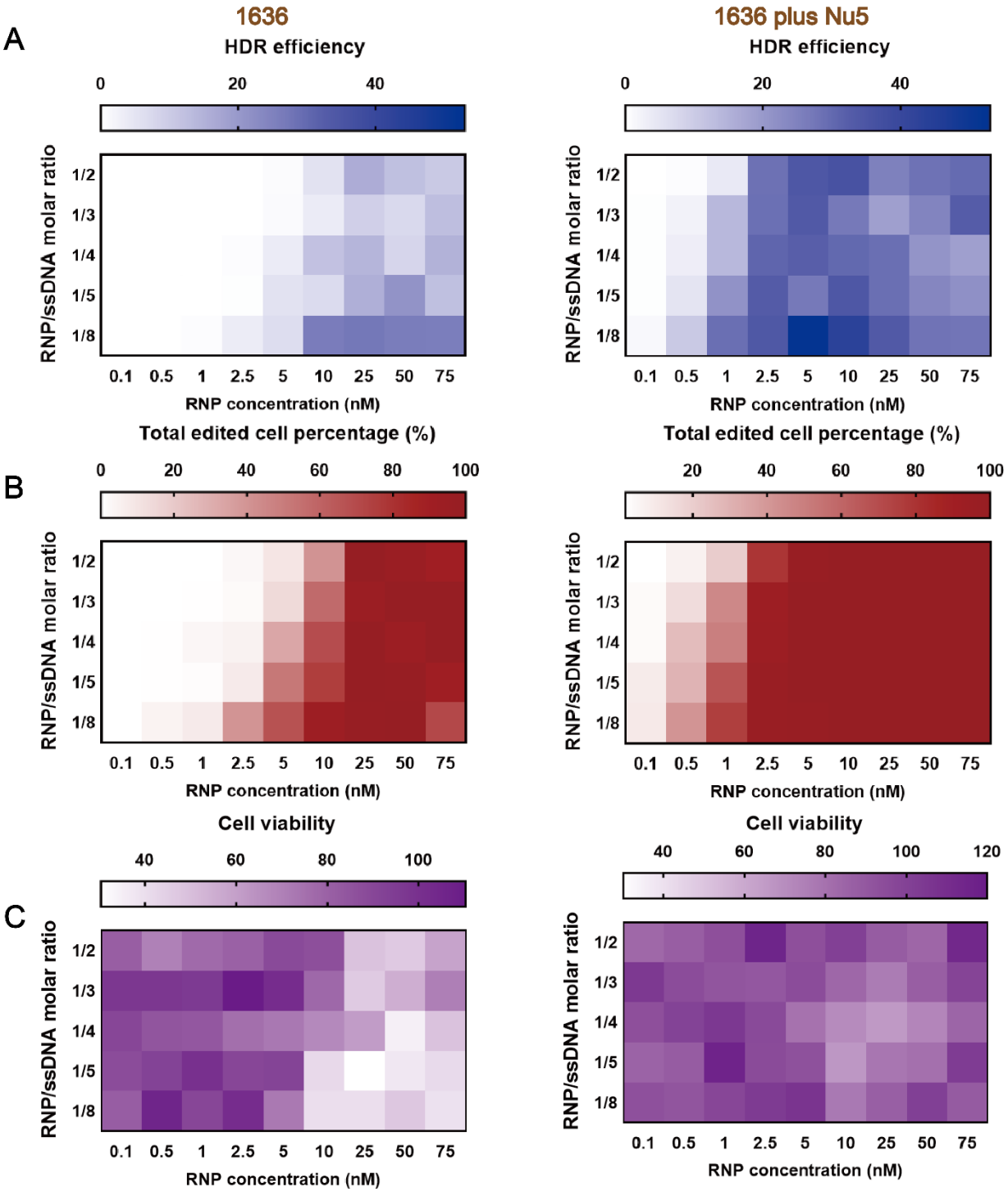

Figure 6. Enhanced HDR-mediated genome editing of HeLa-eGFPd2 applying the optimized HDR T-shape XP (*1636*)-based Cas9 RNP/ssDNA complexes with Nu7441. (**A**) Assessment of HDR efficiency, (**B**) total gene editing performance, and (**C**) cellular viability were evaluated after treatment with *1636*-based Cas9 RNP/ssDNA complexes at varying sgRNA/ssDNA ratios (1/2, 1/3, 1/4, 1/5, 1/8) and RNP concentrations ranging from 0.1 nM to 75 nM. Cytotoxicity was assessed

using MTT assay. All formulations maintained an N/P ratio of 12. Data are presented as mean (n = 3). Numeric percentages are listed in **Fig. 14**.

3.4.7 Comparison of HDR efficiency in flow cytometry and gene sequence measurement

HDR efficiency as measured by flow cytometry was further validated through gene sequence analysis. As depicted in **Fig. 7A**, following the 24-hour treatment and additional incubation, a portion of the HeLa-eGFPd2 cells was transferred to a 6-well plate for continued incubation. The cells were then harvested for DNA extraction. The extracted DNA was amplified using PCR, and the PCR products were purified before Sanger sequencing to confirm the HDR efficiency and validate the gene editing results. **Fig. 7B** shows the gating strategy applied in all flow cytometry evaluations, indicating around 51% HDR efficiency. After DNA extraction and PCR amplification of BFP in sample shown in **Fig.7B** (50.7% HDR in FACs assay), a 769 bp target band was detected in an agarose gel electrophoresis experiment (**Fig. 7C**). The purified PCR product was then subjected to Sanger sequencing, and ICE analysis revealed that this band contained a mixture of HDR (BFP), unedited (GFP), and NHEJ sequences. Subsequently, comparison with the untreated control group using the Synthego ICE tool, as described in previous studies [10, 171], detected an HDR efficiency of 61% (**Fig. 7D-F**), confirming the high level gene sequence correction. This demonstrates that this platform could serve as a powerful tool for gene therapy. To further validate the gene sequence accuracy, purified HeLa-BFPd2 cells and an additional 50% sample were also analyzed, and the results confirmed the reliability of the findings (**Fig. 15**). Additionally, part of the samples was also detected using CLSM for further confirmation (**Fig. 16**).

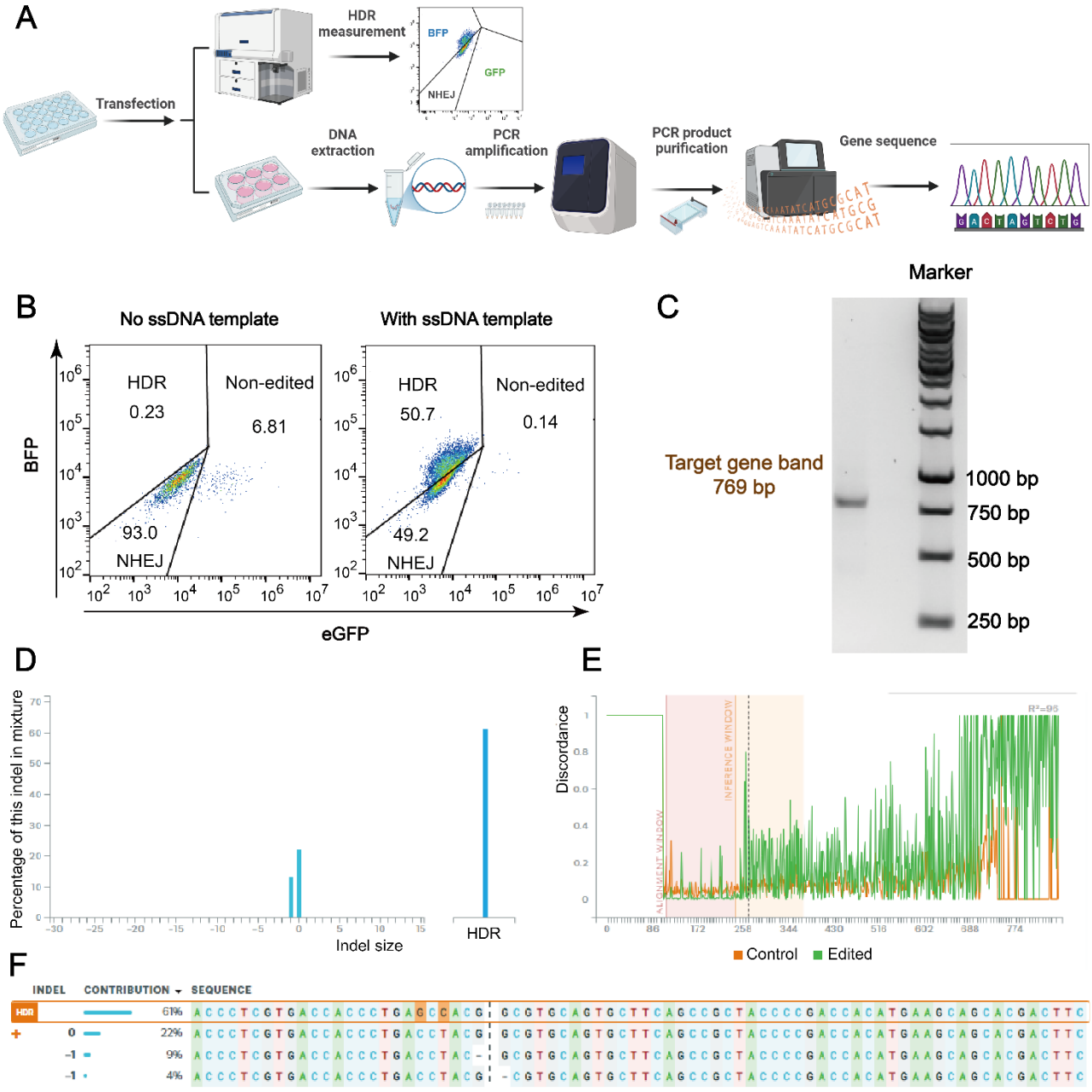

Figure 7. Gene sequence analysis of HeLa-eGFPd2 cells treated with Cas9 RNP/ssDNA complexes and Nu7441. (**A**) Schematic representation of the HDR evaluation process using flow cytometry and Sanger sequencing. (**B**) Flow cytometry gating strategy used to differentiate between eGFP-positive (non-edited), eGFP-negative (knock-out) and BFP-positive (knock-in) populations in samples treated with *1636* RNP/ssDNA complexes and 5 nM Nu7441. (**C**) Gel electrophoresis of PCR-amplified target region (769 bp) from a sample with 50.7% HDR, as shown in **Fig. 7B**. (**D**) Distribution of indel sizes. (**E**) Alignment of Sanger sequencing, control group is untreated HeLa-GFPd2 cells. (**F**) Contribution of each sequence after GFP to BFP conversion.

Sanger sequencing results analyzed using the Synthego ICE tool (https://ice.synthego.com/#/, accessed on 18 October 2023).

3.5 Discussion

DNA-PKcs pathway inhibitors, such as NU7026, Nu7441 and M3814, are known to effectively inhibit the NHEJ pathway, thereby enhancing HDR efficiency. These inhibitors have been extensively studied in various cell models, including SW620, hiPSCs, K562, HEK293T, zebrafish embryos, and in $CD34^+$ progenitor and $CD4^+$ T cells, demonstrating a 3- to 13-fold improvement in HDR efficiency [172]. For instance, NU7026 increased targeted gene fragment insertion efficiency by 3-fold in HEK293 cells, 4-fold in K562 cells, 3-fold in $CD4^+$ T cells, and 1.7-fold in $CD34^+$ progenitor cells [151]. Similarly, M3814 enhanced HDR efficiency to 81% by suppressing NHEJ in K562 cells [157], and Nu7441 improved HDR efficiency by 3-fold in HEK293T cells [148] and up to 13.4-fold in zebrafish embryos [173]. However, the effects of these inhibitors seem to be cell-type dependent, as seen in our enhancer selection results (**Fig. 1E**), which may limit their broader application.

In this study (see **Fig. 8**), we developed a highly efficient gene correction and editing platform by combining lipo-XPs for CRISPR/Cas9 delivery with Nu7441. Our findings suggest that Nu7441 not only enhanced HDR efficiency, as previously reported [148], but also improved overall gene editing efficiency including NHEJ. Closer analysis revealed that the combination of Nu7441 with Cas9 RNP/ssDNA complexes did not affect the cellular uptake or endosomal escape of Cas9 RNP (**Fig. 3A,B**), it did modulate the cell cycle by shifting more cells into the S and G2/M phases while reducing the G1 phase population (**Fig. 3E** and **10**). Previous studies have shown that HDR is predominantly active in the S and G2 phases, which coincide with the availability of homologous sequences that can serve as repair templates during DNA damage [165, 166]. Moreover, Jennifer A. Doudna's group demonstrated that blocking the cell cycle at the M phase in HEK293T cells using nocodazole improved HDR efficiency by up to 38% [170]. They speculated that delivering Cas9 RNP into nocodazole-synchronized cells might effectively target two daughter cells upon release from mitotic arrest. Another possibility is that the breakdown of the nuclear envelope during mitosis facilitates easier access for Cas9 RNP to the genomic DNA. Previous studies demonstrated that pDNA mediated gene transfer is strongly promoted by transfection in S or G2 phases close to M phase, facilitated by nuclear membrane breakdown [167].

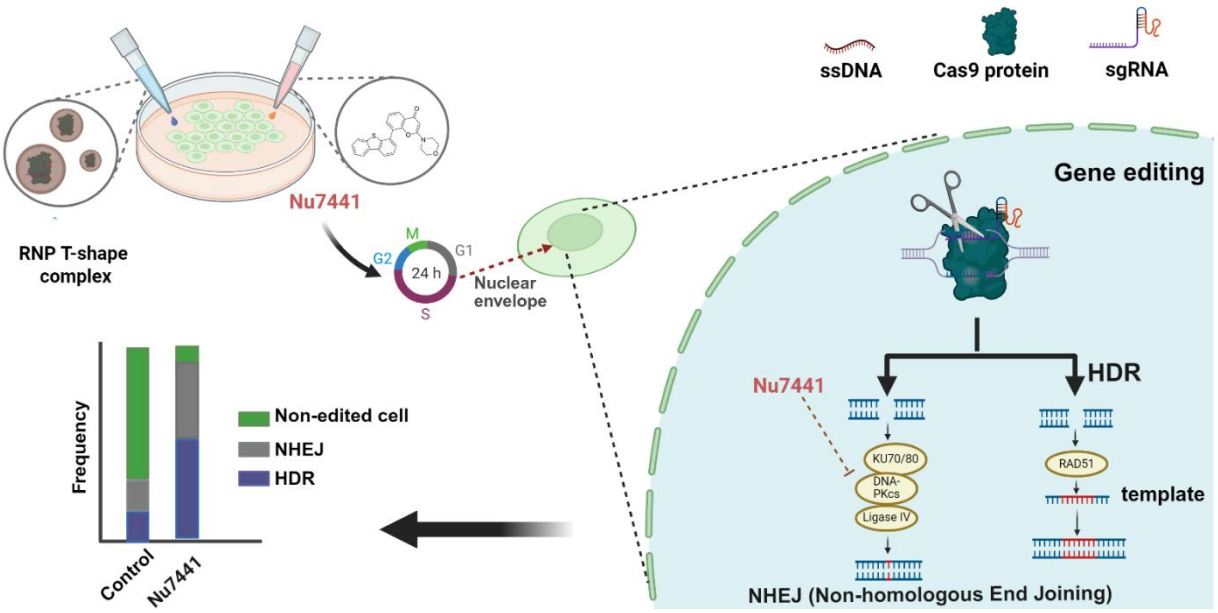

Figure 8. Schematic illustration of the gene editing process utilizing the lipo-xenopeptide based RNP complex and the HDR enhancer Nu7441, with additional possible impact on cell cycle and breakdown of nuclear envelope.

To generate indirect evidence, we co-transfected pDNA (GFP) and mRNA (mCherry) within the same nanoparticles in the presence or absence of Nu7441. According to our hypothesis, pDNA transfection (requiring nuclear entry) but not mRNA (requiring ribosomal translation in cytosol) should be enhanced by Nu7441. Indeed, we observed that Nu7441 enhanced pDNA transfection while reducing mRNA expression (**Fig. 11**). Therefore, it is reasonable to hypothesize that Nu7441 enhances HDR efficiency by arresting cells in the S and G2/M phases, thereby extending DNA repair time in these phases and promoting Cas9/sgRNA nuclear entry. The mechanism likely ensures that more Cas9 reaches the nucleus at the optimal stage of the cell cycle and extends the repair time, which contribute to increased overall gene editing efficiency including HDR.

This modulation of the cell cycle also resulted in more efficient and specific gene knock-in or knock-out in HeLa, C2C12, and 16HBE14o- cells. Notably, gene correction efficiency improved more than 10-fold in a GFP to BFP gene conversion model in HeLa cells and achieved over 50% at an RNP concentration of just 5 nM with *1636* based formulation, as measured by flow cytometry, with a corresponding 61% HDR efficiency observed in Sanger sequencing. Cas9-mediated exon skipping therapy has emerged as a promising approach for treatment of Duchenne muscular dystrophy (DMD) [174]. In a DMD exon 23 reporter model, co-treatment with Nu7441 exhibited a 30-fold increase in exon skipping efficiency as shown in **Fig. 4** and **12**.

Although Nu7441 treatment reduced exogenous mRNA translation (**Fig.11**), the Cas9 mRNA/sgRNA/ssDNA polyplexes still exhibited higher HDR and gene editing efficiency when combined with Nu7441 (**Fig. 13**). This suggests that Nu7441 provides a high potential for genomic DNA editing irrespective of the format of the gene editing cargo [95]. Moreover, gene correction and editing strategies based on NHEJ, transposon-mediated knock-in, prime editing (Cas nickases and reverse transcriptase), and base editing (Cas nickases and DNA deaminase) might also benefit from such effects. Therefore, we speculate that Nu7441 holds significant potential as a gene editing enhancer.

To quantify editing outcomes, we primarily relied on the Synthego ICE tool for analyzing Sanger sequencing data. While ICE is widely used for indel quantification, it has known limitations, particularly in detecting subtle HDR edits involving 1-3 bp base changes. In our GFP-to-BFP conversion model, HDR introduces a precise point mutation that often produces minimal chromatogram shifts, which may be interpreted as "unedited" if the signal deviation falls below ICE's detection threshold [175]. This limitation is particularly relevant when analyzing heterogeneous populations with mixed outcomes. For instance, while flow cytometry in **Fig. 7B** indicated 49.2% NHEJ and only 0.14% unedited cells, ICE analysis in **Fig. 7F** detected just 13% NHEJ and a higher unedited fraction (~22%). These discrepancies likely reflect inherent limitations of the algorithm in accurately resolving subtle HDR events or low-frequency indels, as well as its reduced sensitivity to larger deletions and complex or mixed chromatogram signals. Moreover, Sanger sequencing itself may fail to capture complex editing patterns or deletions >30 bp due to read collapse in pooled samples [176]. Together, these considerations highlight the need to interpret ICE-based DNA-level analysis with caution in HDR-focused studies.

Another critical consideration is the potential for off-target effects. Although CRISPR/Cas systems are powerful tools, they are not without risk. Cas9 can cleave unintended genomic regions, particularly when up to three mismatches exist between the sgRNA and target DNA [177, 178]. In silico tools are therefore essential for genome-wide off-target prediction [179]. In our study, NU7441 extends the DNA repair window and synchronizes cells in HDR-permissive phases (S and G2/M). While this enhances on-target HDR (**Fig. 7**), it may also inadvertently increase susceptibility to off-target events by prolonging Cas9 activity or enabling unintended integration during extended repair periods. These findings underscore the importance of further evaluating the off-target profile of this approach, especially when applying it to therapeutic contexts.

In parallel with concerns about off-target genome editing, the safety profile of NU7441 must also be carefully considered. Although NU7441 remains a preclinical compound and has not yet entered clinical trials, several studies have reported its potential side effects based on animal models and combination treatments in cancer research. Zhao etal reported NU7441 exhibited high hepatic accumulation, could be raising concerns about

potential hepatotoxicity [180]. Moreover, its poor aqueous solubility may pose formulation challenges [181]. When used in combination with chemotherapy agents (e.g., etoposide) [182] or radiation [183], NU7441 has been shown to enhance the therapeutic effect by sensitizing cancer cells to DNA damage. However, this radiosensitization or chemosensitization effect may also exacerbate systemic toxicity, potentially increasing side effects such as nausea, vomiting, diarrhea, and fatigue.

Additional limitations of our current study should also be acknowledged. First, our experiments were primarily performed using a limited set of target sites and gene sizes. Thus, the generalizability of Nu7441's effect across different genomic loci, especially larger or clinically relevant genes, remains to be evaluated. Second, although we expanded the scope beyond cancer cell lines by including non-transformed 16HBE14o- and C2C12- cells, we did not extend validation to a broader range of tissue types or primary cells lacking functional reporters. In particular, assessing genome editing at endogenous loci across diverse cell types—including patient-derived primary cells or iPSC-derived models—would be critical for evaluating therapeutic potential in more physiologically relevant contexts. Third, a more comprehensive evaluation of potential off-target effects was beyond the scope of this study. Future work involving genome-wide off-target profiling (e.g., GUIDE-seq or DISCOVER-seq) [184, 185] and application of our editing strategy in primary or disease-relevant cell models will be essential for advancing the translational relevance of these findings.

In conclusion, this study presents a highly efficient gene editing platform combining most recently developed lipo-XPs for CRISPR/Cas9 delivery with Nu7441, a DNA-PKcs pathway inhibitor. The platform enhances HDR efficiency and overall gene editing by modulating the cell cycle, specifically by extending DNA repair time in the S and G2 phase and promoting Cas9 RNP nuclear entry upon mitosis in M phase. This strategy results in efficient gene knock-in or knockout across various cell models and nonviral delivery systems. Thus, the platform demonstrates great potential for improving gene editing and offers significant promise for advancing gene therapy applications.

3.6 Acknowledgements

The authors acknowledge support by the UPGRADE (Unlocking Precision Gene Therapy) project that has received funding from the European Union's Horizon 2020 research and innovation programme under grant agreement No 825825. This work was also supported by the German Research Foundation (DFG) SFB1032 (project-ID 201269156) sub-project B4, and BMBF Cluster for Future ‘CNATM - Cluster for Nucleic Acid Therapeutics Munich’ project number 03ZU1201AA. X.L. appreciates the fellowship of the China Scholarship Council that supports his Ph.D. study.

We thank Susanne Kempter (Faculty of Physics, LMU Munich) for performing TEM measurements, Yi Lin (Department of Biomedical Engineering, College of Future Technology, Peking University), Fengrong Zhang, Wolfgang Rödl, Olga Brück, Lorina Bawej and Melinda Kiss (Pharmaceutical Biotechnology, LMU Munich) for technical and organizational support.

3.7 Supplementary Materials

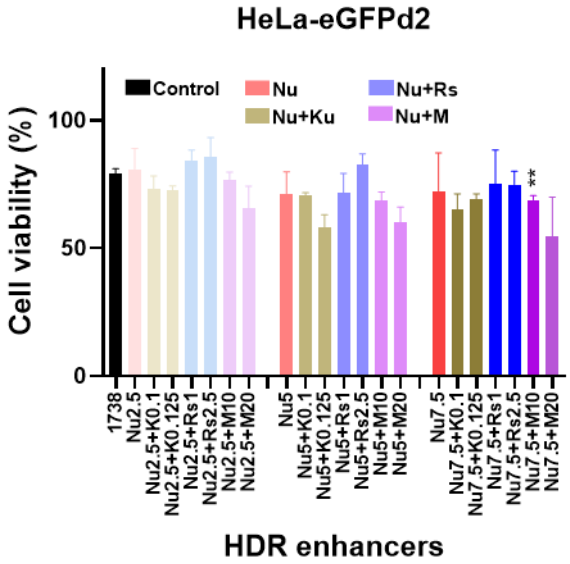

Figure 9. Cell viability of HeLa-eGFPd2 post-transfection with *1738* Cas9 RNP/ssDNA complexes and enhancer mixtures. Cell viability was assessed for 18.75 nM *1738* Cas9 RNP/ssDNA complexes, with or without enhancer mixtures, 24 h post-transfection. The enhancer mixtures included Nu7441 (2.5, 5, 7.5 nM), Rs1 (1, 2.5, 10 nM), KU-0060648 (0.1, 0.25, 1 nM), or M3814 (5, 10, 20 nM). Enhancer abbreviations represent the enhancer name followed by its concentration in nM. The experiment was performed using the MTT assay. ** $p < 0.01$ vs *1738*; Data are presented as mean ± SD ($n = 3$).

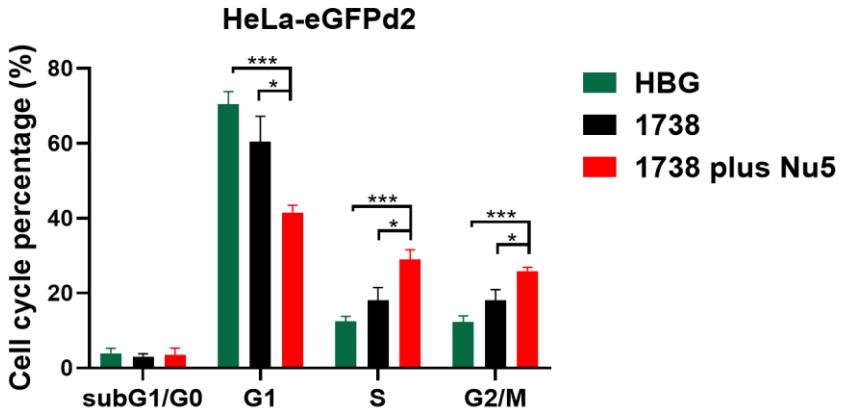

Figure 10. Cell cycle analysis of HeLa-GFPd2 cells post-transfection with *1738* RNP/ssDNA complex and Nu7441. The analysis was performed using PI staining following a 24-hour transfection with *1738*-based RNP/ssDNA complex (18.75 nM RNP) with or without 5 nM Nu7441 and an additional 5-day incubation in HeLa-GFPd2 cells. Data are presented as mean ± SD (*n* = *3*). Statistical significance is indicated as * $p < 0.05$ and *** $p < 0.001$.

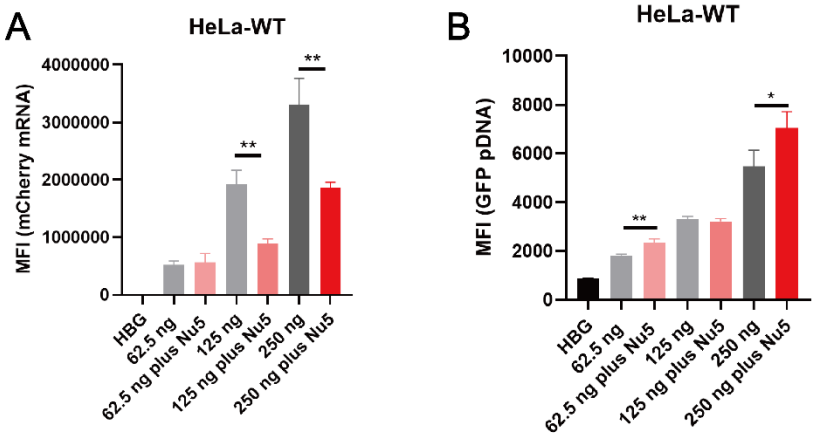

Figure 11. Median Fluorescence Intensity (MFI) analysis of mRNA and DNA co-transfection in HeLa cells with or without Nu7441. The analysis of mRNA and DNA co-transfection in HeLa cells without or with Nu7441. (**A**) mRNA (mCherry) and (**B**) pDNA (GFP) MFI results after 24 h of treatment with *1611*-based mRNA/pDNA polyplexes, in the presence or absence of 5 nM Nu7441. The polyplexes were formed at an N/P ratio of 18 and contained a total of 62.5 ng, 125 ng, or 250 ng of nucleic acid (mCherry mRNA: GFP pDNA; weight ratio 1:1). Data are presented as mean ± SD (*n* = *3*). Statistical significance is indicated as * $p < 0.05$ and ** $p < 0.01$.

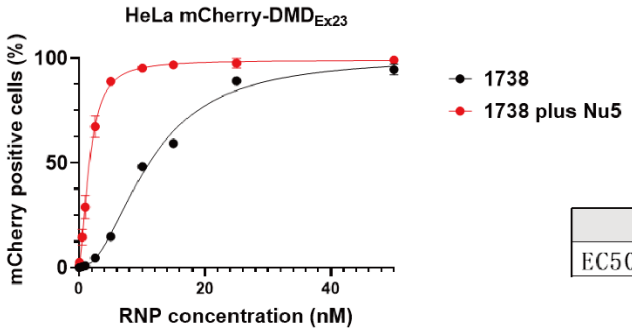

	1738	1738 plus Nu5
EC50 (nM)	11.18	1.65

Figure 12. Exon skipping dose titration of *1738* and *1738* plus Nu5 in HeLa mCherry-DMD_{Ex23}. Cas9 RNP concentrations ranged from 0.05 to 50 nM. EC50 value calculated as dose for 50% mCherry positive cells. Addition of 5 nM Nu7441 reduced EC50 by 6.8 fold. Data are presented as mean ± SD (*n* = *3*).

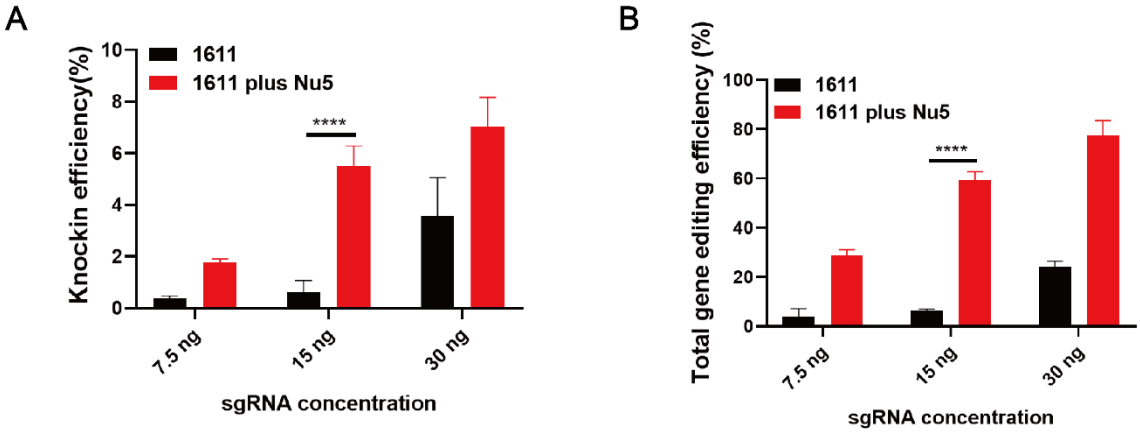

Figure 13. Gene correction and editing of Cas9 mRNA/sgRNA/ssDNA polyplexes with Nu7441 in HeLa-eGFPd2 cells. Cas9 mRNA/sgRNA/ssDNA polyplexes, based on *1611*, were formed at N/P ratio 18 and a dose of 7.5 ng, 15 ng, and 30 ng of total nucleic acid was transfected for 24 h. Data are presented as mean ± SD (*n* = *3*). Statistical significance is indicated as **** $p < 0.0001$.

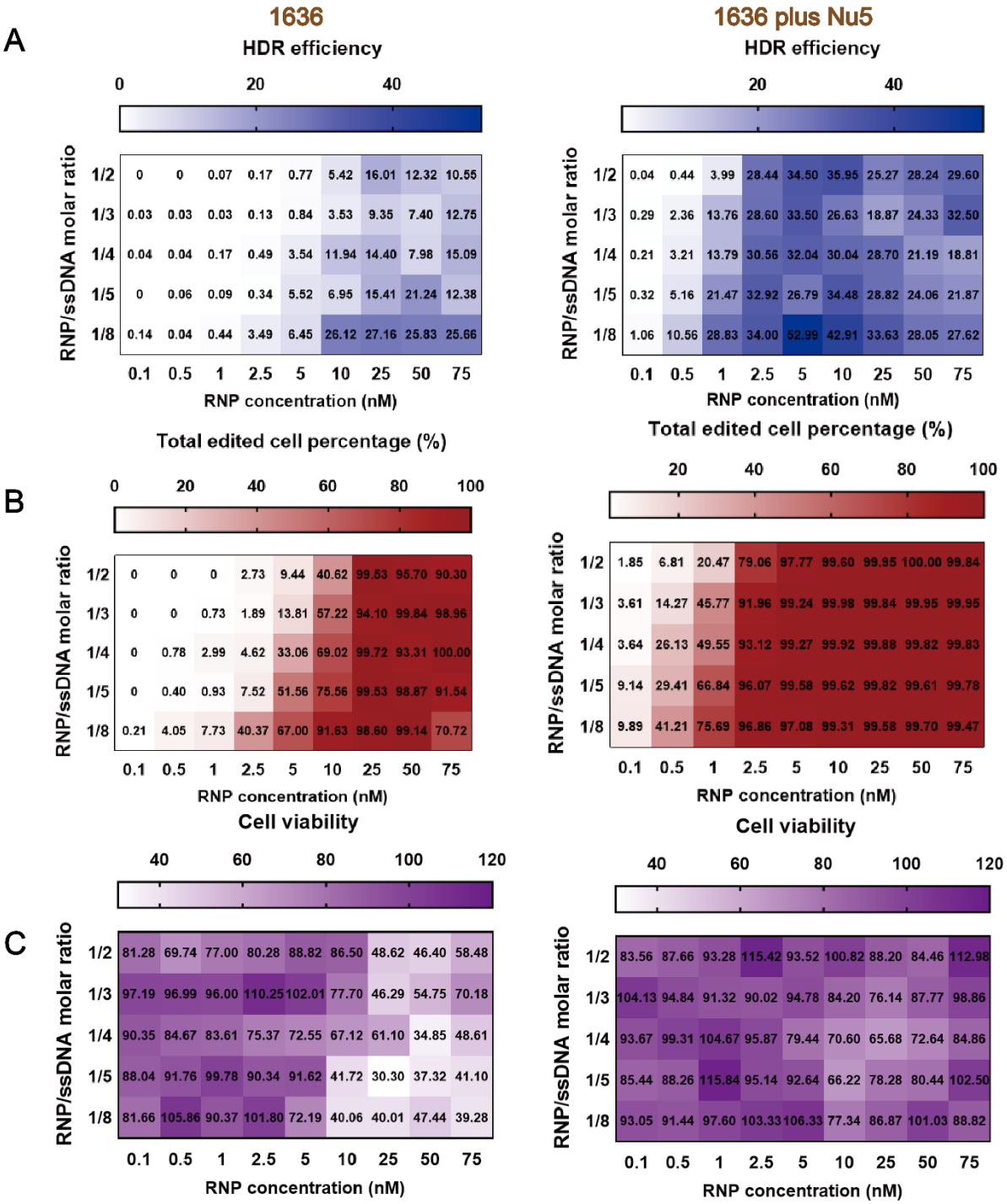

Figure 14. Enhanced HDR-mediated genome editing of HeLa-eGFPd2 applying the optimized HDR T-shape XP (*1636*)-based Cas9 RNP/ssDNA complexes with Nu7441. (**A**) HDR efficiency, (**B**) total gene editing performance, and (**C**) cellular viability were evaluated in HeLa-eGFPd2 cells following treatment with *1636*-based Cas9 RNP/ssDNA complexes at varying sgRNA/ssDNA

ratios (1:2, 1:3, 1:4, 1:5, 1:8) and RNP concentrations ranging from 0.1 nM to 75 nM. Figures were labeled with specific values. Figures were labeled with specific values. Cytotoxicity was assessed using the MTT assay. All formulations maintained an N/P ratio of 12. Data are presented as mean (*n = 3*).

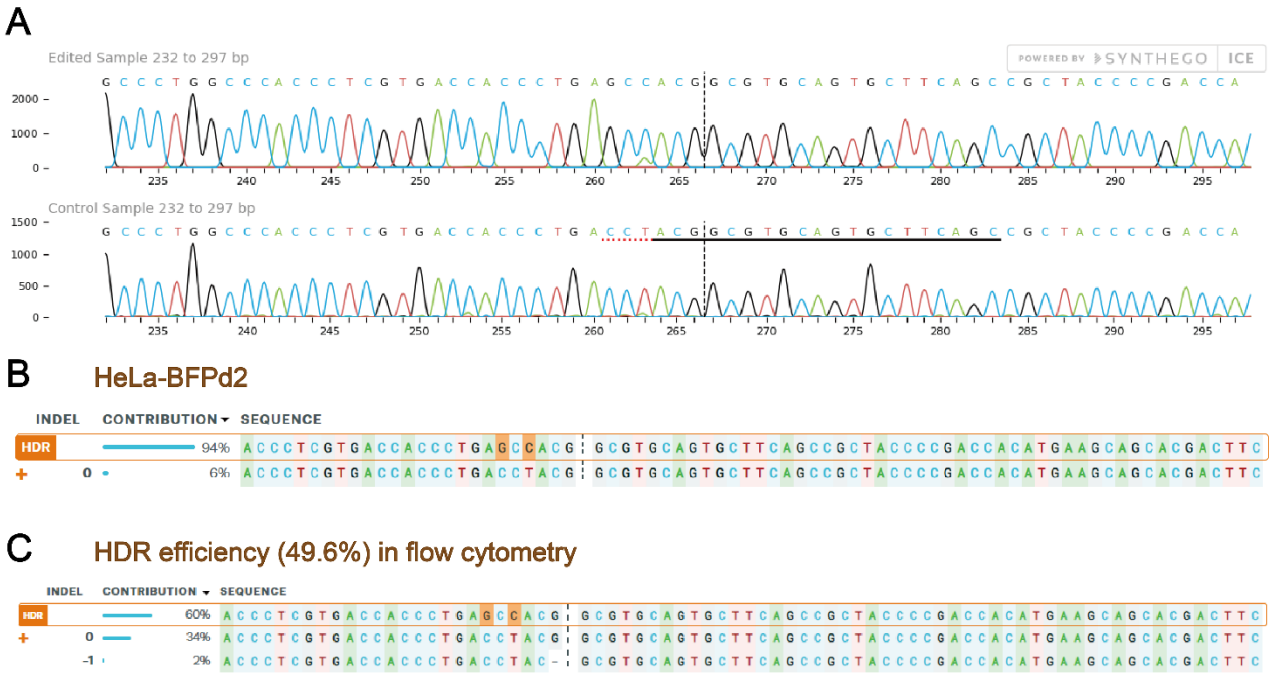

Figure 15. Gene sequence analysis of edited HeLa cells. (**A**) Gene sequence comparison between the edited sample and the untreated control sample. (**B**) Gene sequence analysis of HeLa-BFPd2 cells after single-clone selection. (**C**) Gene sequence analysis of a sample with 49.6% HDR efficiency, as determined by flow cytometry, in the HeLa-eGFPd2 cell model.

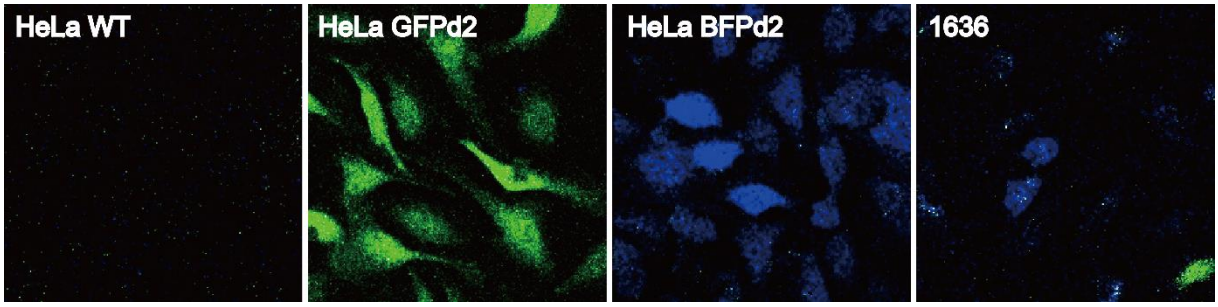

Figure 16. CLSM images of various HeLa cell samples. The CLSM images depicted from standard HeLa cells ('wild-type = WT), HeLa-eGFPd2, and HeLa-BFPd2 cells obtained through single-clone selection, as well as HeLa-eGFPd2 cells following *1636 (1445-Gtt)* treatment.

4.Summary

In the first part of this thesis, dual pH-responsive xenopeptide (XP) carriers were optimized for efficient CRISPR/Cas9 ribonucleoprotein (RNP) delivery. A library of amphiphilic XPs, incorporating lipophilic cationizable lipoamino fatty acids (LAFs) and hydrophilic oligoaminoethylene acid units (e.g., Stp, dGtp, GEIPA) was screened for their ability to form uniform, serum-compatible Cas9 RNP complexes with high encapsulation efficiency. The lead candidates, *1611* (LAF_2-Stp) and *1719* (LAF_4-Stp_2), exhibited robust gene-editing performance in multiple reporter cell lines, including HeLa-eGFPd2, CT26-eGFPd2, and a Duchenne muscular dystrophy (DMD) exon-skipping reporter cell model. Their strong cellular uptake, and efficient endosomal escape (confirmed via Gal8-mRuby3 reporter assays) enabled robust cytosolic delivery of RNP, resulting in gene knockout efficiencies of up to 90% at sub-nanomolar concentrations. Importantly, these systems maintained high activity even after pre-incubation in over 95% fetal bovine serum, highlighting their exceptional serum stability.

Further structural optimization, specifically by replacing Stp with more hydrophobic analogues such as dGtp and GEIPA, led to enhanced editing potency, with the most effective variant (EC_{50} = 0.51 nM) observed in DMD reporter cells. Beyond gene knockout, these carriers also supported HDR-mediated gene correction. For instance, the carrier LAF_4-$GEIPA_2$ (*1863*) enabled up to 43% eGFP-to-BFP conversion in HeLa cells when co-delivering Cas9 RNP with single-stranded DNA templates.

In the second part of this thesis, the role of small-molecule-mediated DNA repair modulation was investigated as a strategy to further enhance gene correction efficiency. The DNA-PKcs inhibitor Nu7441, which suppresses the NHEJ pathway, was identified as a potent enhancer of HDR. When used in combination with the T-shaped XP carrier *1636* (Gtt), Nu7441 increased HDR efficiency, achieving up to 53% correction in HeLa-eGFPd2 cells. This result was further supported by Sanger sequencing, which confirmed HDR efficiencies as high as 61%. Interestingly, Nu7441 also significantly enhanced overall gene-editing outcomes, including those mediated by NHEJ. In a DMD reporter model, Nu7441 led to a 30-fold increase in exon skipping efficiency by promoting splice-site disruption via the NHEJ pathway.

Mechanistic investigations revealed that Nu7441 does not affect the initial uptake or endosomal escape of the RNP complexes. Instead, its impact is attributed to modulation of the cell cycle—specifically, reducing the proportion of cells in the G1 phase while prolonging the S and G2/M phases. To further explore this mechanism, a co-transfection assay using plasmid DNA (which requires nuclear entry for transcription) and mRNA (which is translated in the cytoplasm) showed that Nu7441 enhanced plasmid-based gene

expression but reduced mRNA translation, indirectly suggesting that its action promotes nuclear access while limiting cytosolic translation. Based on these findings, it is hypothesized that Nu7441 enhances HDR efficiency by arresting cells in the S and G2/M phases, where DNA repair activity is heightened and nuclear access of Cas9 RNP/ssDNA complexes is more favorable. This mechanistic effect was consistently validated across multiple cell lines, including HeLa, even C2C12, and 16HBE14o-, and was also observed in the context of Cas9 mRNA/sgRNA polyplexes, demonstrating the broad applicability of this approach to HDR- or NHEJ-mediated gene editing.

To sum up, this thesis establishes a versatile CRISPR/Cas9 delivery platform that integrates optimized XP carriers with HDR modulators, achieving highly efficient gene editing and correction *in vitro*. The findings underscore the potential of synthetic peptide-based delivery systems and small-molecule enhancers to overcome key challenges in therapeutic genome editing, paving the way for future applications in genetic disorders and precision medicine.

5 Appendix

5.1 Abbreviations

Cas9	CRISPR-associated protein 9
chGtp	Cyclohexyl-glutaryl-tetraethylene pentamine
CLSM	Confocal laser scanning microscopy
CRISPR	Clustered regularly interspaced short palindromic repeats
DAPI	4′,6-Diamidino-2-phenylindole
DSBs	Double-strand breaks
DNA-PKcs	DNA-dependent protein kinase
dGtp	Diglycoloyl tetraethylene pentamine
dmGtp	Dimethyl-glutaryl-tetraethylene pentamine
DLS	Dynamic light scattering
DMD	Duchenne muscular dystrophy
DMEM	Dulbecco’s modified eagle’s medium
DMSO	Dimethyl sulfoxide
FACS	Flow cytometry staining

FBS	Fetal bovine serum
LAF	Lipo-amino fatty acid
GEIPA	Glutaryl-ethylenediImine-dipropylamine.
Gtp	(Glutaryl-tetraethylene pentamine)
Gtt	Glutaryl-triethylene tetramine
HBG	HEPES-buffered glucose solution
HEPES	4-(2-Hydroxyethyl)-1-piperazineethanesulfonic acid
HDR	Homology-directed repair
Htp	Cyclohexaryl-tetraethylene pentamine
N/P	Nitrogen-to-phosphate
NHEJ	Non-homologous end joining
NLRP3	NOD-like receptor family pyrin domain containing 3
MEM	Minimum essential medium
MFI	Median fluorescence intensity
MTT	3-(4,5-Dimethylthiazol-2-yl)-2,5-diphenyltetrazolium bromide
sgRNA	Single guide RNA
ssDNA	Single-stranded DNA

PD-L1	Programmed cell death- ligand 1
PI	Propidium Iodide
RNP	Ribonucleoprotein
Stp	Succinyl-tetraethylene pentamine
Stt	Succinyl-triethylene tetramine
TEM	Transmission Electron Microscopy
TFE	Trifluoroethyl-iminodiacetyl-tetraethylene pentamine
XP	Xenopeptide

6 References

[1] M. Jasin, Genetic manipulation of genomes with rare-cutting endonucleases, Trends Genet., 12 (1996) 224-228.
[2] J.K. Joung, J.D. Sander, TALENs: a widely applicable technology for targeted genome editing, Nat. Rev. Mol. Cell Biol., 14 (2013) 49-55.
[3] A.J. Wood, T.-W. Lo, B. Zeitler, C.S. Pickle, E.J. Ralston, A.H. Lee, R. Amora, J.C. Miller, E. Leung, X. Meng, Targeted genome editing across species using ZFNs and TALENs, Science, 333 (2011) 307-307.
[4] R. Barrangou, C. Fremaux, H. Deveau, M. Richards, P. Boyaval, S. Moineau, D.A. Romero, P. Horvath, CRISPR provides acquired resistance against viruses in prokaryotes, Science, 315 (2007) 1709-1712.
[5] P.M. Nussenzweig, L.A. Marraffini, Molecular mechanisms of CRISPR-Cas immunity in bacteria, Annu. Rev. Genet., 54 (2020) 93-120.
[6] E. Deltcheva, K. Chylinski, C.M. Sharma, K. Gonzales, Y. Chao, Z.A. Pirzada, M.R. Eckert, J. Vogel, E. Charpentier, CRISPR RNA maturation by trans-encoded small RNA and host factor RNase III, Nature, 471 (2011) 602-607.
[7] Z. Kozovska, S. Rajcaniova, P. Munteanu, S. Dzacovska, L. Demkova, CRISPR: History and perspectives to the future, Biomed. Pharmacother., 141 (2021) 111917.
[8] P. Mali, L. Yang, K.M. Esvelt, J. Aach, M. Guell, J.E. DiCarlo, J.E. Norville, G.M. Church, RNA-guided human genome engineering via Cas9, Science, 339 (2013) 823-826.
[9] L. Cong, F.A. Ran, D. Cox, S. Lin, R. Barretto, N. Habib, P.D. Hsu, X. Wu, W. Jiang, L.A. Marraffini, Multiplex genome engineering using CRISPR/Cas systems, Science, 339 (2013) 819-823.
[10] S. Chen, S.P. Carneiro, O.M. Merkel, Anionic polymer coating for enhanced delivery of Cas9 mRNA and sgRNA nanoplexes, Biomater. Sci., 13 (2025) 659–676.
[11] C.D. Richardson, G.J. Ray, M.A. DeWitt, G.L. Curie, J.E. Corn, Enhancing homology-directed genome editing by catalytically active and inactive CRISPR-Cas9 using asymmetric donor DNA, Nat. Biotechnol., 34 (2016) 339-344.
[12] C. Liang, F. Li, L. Wang, Z.-K. Zhang, C. Wang, B. He, J. Li, Z. Chen, A.B. Shaikh, J. Liu, Tumor cell-targeted delivery of CRISPR/Cas9 by aptamer-functionalized lipopolymer for therapeutic genome editing of VEGFA in osteosarcoma, Biomaterials, 147 (2017) 68-85.
[13] H. Deng, S. Tan, X. Gao, C. Zou, C. Xu, K. Tu, Q. Song, F. Fan, W. Huang, Z. Zhang, Cdk5 knocking out mediated by CRISPR-Cas9 genome editing for PD-L1 attenuation and enhanced antitumor immunity, Acta Pharm. Sin. B, 10 (2020) 358-373.
[14] S. Abbasi, S. Uchida, K. Toh, T.A. Tockary, A. Dirisala, K. Hayashi, S. Fukushima, K. Kataoka, Co-encapsulation of Cas9 mRNA and guide RNA in polyplex micelles enables genome editing in mouse brain, J. Control. Release., 332 (2021) 260-268.

[15] J.D. Finn, A.R. Smith, M.C. Patel, L. Shaw, M.R. Youniss, J. van Heteren, T. Dirstine, C. Ciullo, R. Lescarbeau, J. Seitzer, A single administration of CRISPR/Cas9 lipid nanoparticles achieves robust and persistent in vivo genome editing, Cell reports, 22 (2018) 2227-2235.
[16] T. Wei, Q. Cheng, Y.-L. Min, E.N. Olson, D.J. Siegwart, Systemic nanoparticle delivery of CRISPR-Cas9 ribonucleoproteins for effective tissue specific genome editing, Nat. Commun., 11 (2020) 3232.
[17] S. Krishnamurthy, C. Wohlford-Lenane, S. Kandimalla, G. Sartre, D.K. Meyerholz, V. Théberge, S. Hallée, A.-M. Duperré, T. Del'Guidice, J.-P. Lepetit-Stoffaes, Engineered amphiphilic peptides enable delivery of proteins and CRISPR-associated nucleases to airway epithelia, Nat. Commun., 10 (2019) 4906.
[18] E. Haapaniemi, S. Botla, J. Persson, B. Schmierer, J. Taipale, CRISPR–Cas9 genome editing induces a p53-mediated DNA damage response, Nat. Med., 24 (2018) 927-930.
[19] O. Pelea, T.A. Fulga, T. Sauka-Spengler, RNA-responsive gRNAs for controlling CRISPR activity: current advances, future directions, and potential applications, CRISPR J., 5 (2022) 642-659.
[20] H. Shivram, B.F. Cress, G.J. Knott, J.A. Doudna, Controlling and enhancing CRISPR systems, Nat. Chem. Biol., 17 (2021) 10-19.
[21] T. Wiegand, S. Karambelkar, J. Bondy-Denomy, B. Wiedenheft, Structures and strategies of anti-CRISPR-mediated immune suppression, Annu. Rev. Microbiol., 74 (2020) 21-37.
[22] N.M. Gaudelli, A.C. Komor, H.A. Rees, M.S. Packer, A.H. Badran, D.I. Bryson, D.R. Liu, Programmable base editing of A• T to G• C in genomic DNA without DNA cleavage, Nature, 551 (2017) 464-471.
[23] A.V. Anzalone, L.W. Koblan, D.R. Liu, Genome editing with CRISPR–Cas nucleases, base editors, transposases and prime editors, Nat. Biotechnol., 38 (2020) 824-844.
[24] A.C. Komor, Y.B. Kim, M.S. Packer, J.A. Zuris, D.R. Liu, Programmable editing of a target base in genomic DNA without double-stranded DNA cleavage, Nature, 533 (2016) 420-424.
[25] J.L. Doman, A. Raguram, G.A. Newby, D.R. Liu, Evaluation and minimization of Cas9-independent off-target DNA editing by cytosine base editors, Nat. Biotechnol., 38 (2020) 620-628.
[26] M.F. Richter, K.T. Zhao, E. Eton, A. Lapinaite, G.A. Newby, B.W. Thuronyi, C. Wilson, L.W. Koblan, J. Zeng, D.E. Bauer, Phage-assisted evolution of an adenine base editor with improved Cas domain compatibility and activity, Nat. Biotechnol., 38 (2020) 883-891.
[27] D.K. Lam, P.R. Feliciano, A. Arif, T. Bohnuud, T.P. Fernandez, J.M. Gehrke, P. Grayson, K.D. Lee, M.A. Ortega, C. Sawyer, Improved cytosine base editors generated from TadA variants, Nat. Biotechnol., 41 (2023) 686-697.
[28] T.R. Damase, J.P. Cooke, RNA therapeutics in cardiovascular medicine, Curr. Opin. Cardiol., (2025) 10.1097.

[29] L.N. Kasiewicz, S. Biswas, A. Beach, H. Ren, C. Dutta, A.M. Mazzola, E. Rohde, A. Chadwick, C. Cheng, S.P. Garcia, GalNAc-Lipid nanoparticles enable non-LDLR dependent hepatic delivery of a CRISPR base editing therapy, Nat. Commun., 14 (2023) 2776.
[30] Y. Sun, S. Chatterjee, X. Lian, Z. Traylor, S.R. Sattiraju, Y. Xiao, S.A. Dilliard, Y.-C. Sung, M. Kim, S.M. Lee, In vivo editing of lung stem cells for durable gene correction in mice, Science, 384 (2024) 1196-1202.
[31] P.J. Chen, D.R. Liu, Prime editing for precise and highly versatile genome manipulation, Nat. Rev. Genet., 24 (2023) 161-177.
[32] R. Masarwy, L. Stotsky-Oterin, A. Elisha, I. Hazan-Halevy, D. Peer, Delivery of nucleic acid based genome editing platforms via lipid nanoparticles: clinical applications, Adv. Drug Deliv. Rev., (2024) 115359.
[33] J.R. Davis, S. Banskota, J.M. Levy, G.A. Newby, X. Wang, A.V. Anzalone, A.T. Nelson, P.J. Chen, A.D. Hennes, M. An, Efficient prime editing in mouse brain, liver and heart with dual AAVs, Nat. Biotechnol., 42 (2024) 253-264.
[34] Y. Lin, E. Wagner, U. Lächelt, Non-viral delivery of the CRISPR/Cas system: DNA versus RNA versus RNP, Biomater. Sci., 10 (2022) 1166-1192.
[35] Z. Chen, K. Kelly, H. Cheng, X. Dong, A.K. Hedger, L. Li, E.J. Sontheimer, J.K. Watts, In vivo prime editing by lipid nanoparticle co-delivery of chemically modified pegRNA and prime editor mRNA, GEN Biotechnol., 2 (2023) 490-502.
[36] M. Li, Y. Lin, Q. Cheng, T. Wei, Prime Editing: A Revolutionary Technology for Precise Treatment of Genetic Disorders, Cell Prolif., (2025) e13808.
[37] E.A. Saunderson, P. Stepper, J.J. Gomm, L. Hoa, A. Morgan, M.D. Allen, J.L. Jones, J.G. Gribben, T.P. Jurkowski, G. Ficz, Hit-and-run epigenetic editing prevents senescence entry in primary breast cells from healthy donors, Nat. Commun., 8 (2017) 1450.
[38] J.K. Nuñez, J. Chen, G.C. Pommier, J.Z. Cogan, J.M. Replogle, C. Adriaens, G.N. Ramadoss, Q. Shi, K.L. Hung, A.J. Samelson, Genome-wide programmable transcriptional memory by CRISPR-based epigenome editing, Cell, 184 (2021) 2503-2519. e2517.
[39] I.B. Hilton, A.M. D'ippolito, C.M. Vockley, P.I. Thakore, G.E. Crawford, T.E. Reddy, C.A. Gersbach, Epigenome editing by a CRISPR-Cas9-based acetyltransferase activates genes from promoters and enhancers, Nat. Biotechnol., 33 (2015) 510-517.
[40] D.Y. Kwon, Y.-T. Zhao, J.M. Lamonica, Z. Zhou, Locus-specific histone deacetylation using a synthetic CRISPR-Cas9-based HDAC, Nat. Commun., 8 (2017) 15315.
[41] C. Kuscu, S. Arslan, R. Singh, J. Thorpe, M. Adli, Genome-wide analysis reveals characteristics of off-target sites bound by the Cas9 endonuclease, Nat. Biotechnol., 32 (2014) 677-683.
[42] H. O'Geen, I.M. Henry, M.S. Bhakta, J.F. Meckler, D.J. Segal, A genome-wide analysis of Cas9 binding specificity using ChIP-seq and targeted sequence capture, Nucleic Acids Res., 43 (2015) 3389-3404.

[43] L. Dölken, Z. Ruzsics, B. Rädle, C.C. Friedel, R. Zimmer, J. Mages, R. Hoffmann, P. Dickinson, T. Forster, P. Ghazal, High-resolution gene expression profiling for simultaneous kinetic parameter analysis of RNA synthesis and decay, RNA, 14 (2008) 1959-1972.
[44] A. Özcan, R. Krajeski, E. Ioannidi, B. Lee, A. Gardner, K.S. Makarova, E.V. Koonin, O.O. Abudayyeh, J.S. Gootenberg, Programmable RNA targeting with the single-protein CRISPR effector Cas7-11, Nature, 597 (2021) 720-725.
[45] K. Kato, W. Zhou, S. Okazaki, Y. Isayama, T. Nishizawa, J.S. Gootenberg, O.O. Abudayyeh, H. Nishimasu, Structure and engineering of the type III-E CRISPR-Cas7-11 effector complex, Cell, 185 (2022) 2324-2337. e2316.
[46] M. Pacesa, O. Pelea, M. Jinek, Past, present, and future of CRISPR genome editing technologies, Cell, 187 (2024) 1076-1100.
[47] X. Ou, Q. Ma, W. Yin, X. Ma, Z. He, CRISPR/Cas9 gene-editing in cancer immunotherapy: Promoting the present revolution in cancer therapy and exploring more, Front. Cell. Infect. Microbiol., 9 (2021) 674467.
[48] S. Valletta, H. Dolatshad, M. Bartenstein, B.H. Yip, E. Bello, S. Gordon, Y. Yu, J. Shaw, S. Roy, L. Scifo, ASXL1 mutation correction by CRISPR/Cas9 restores gene function in leukemia cells and increases survival in mouse xenografts, Oncotarget, 6 (2015) 44061.
[49] R. Craig, MCL1 provides a window on the role of the BCL2 family in cell proliferation, differentiation and tumorigenesis, Leukemia, 16 (2002) 444-454.
[50] F. Baylis, M. McLeod, First-in-human phase 1 CRISPR gene editing cancer trials: are we ready?, Curr. Gene Ther., 17 (2017) 309-319.
[51] S. He, The first human trial of CRISPR-based cell therapy clears safety concerns as new treatment for late-stage lung cancer, Signal Transduct. Target. Ther., 5 (2020) 168.
[52] F. Morshedzadeh, M. Ghanei, M. Lotfi, M. Ghasemi, M. Ahmadi, P. Najari-Hanjani, S. Sharif, S. Mozaffari-Jovin, M. Peymani, M.R. Abbaszadegan, An update on the application of CRISPR technology in clinical practice, Mol. Biotechnol., 66 (2024) 179-197.
[53] T. Liu, Z. Li, Q. Zhang, K.D.A. Bernstein, S. Lozano-Calderon, E. Choy, F.J. Hornicek, Z. Duan, Targeting ABCB1 (MDR1) in multi-drug resistant osteosarcoma cells using the CRISPR-Cas9 system to reverse drug resistance, Oncotarget, 7 (2016) 83502.
[54] H. Tang, J.B. Shrager, CRISPR/Cas-mediated genome editing to treat EGFR-mutant lung cancer: a personalized molecular surgical therapy, EMBO Mol. Med., 8 (2016) 83-85.
[55] W. Dampier, N.T. Sullivan, J.C. Mell, V. Pirrone, G.D. Ehrlich, C.-H. Chung, A.G. Allen, M. DeSimone, W. Zhong, K. Kercher, Broad-spectrum and personalized guide RNAs for CRISPR/Cas9 HIV-1 therapeutics, AIDS Res. Hum. Retroviruses, 34 (2018) 950-960.
[56] T.I. Cornu, C. Mussolino, M.C. Müller, C. Wehr, W.V. Kern, T. Cathomen, HIV gene therapy: an update, Hum. Gene Ther., 32 (2021) 52-65.
[57] L. Xu, J. Wang, Y. Liu, L. Xie, B. Su, D. Mou, L. Wang, T. Liu, X. Wang, B. Zhang, CRISPR-edited stem cells in a patient with HIV and acute lymphocytic leukemia, N. Engl. J. Med., 381 (2019) 1240-1247.

[58] H. Lin, G. Li, X. Peng, A. Deng, L. Ye, L. Shi, T. Wang, J. He, The use of CRISPR/Cas9 as a tool to study human infectious viruses, Front. Cell. Infect. Microbiol., 11 (2021) 590989.
[59] L. Yu, X. Wang, D. Zhu, W. Ding, L. Wang, C. Zhang, X. Jiang, H. Shen, S. Liao, D. Ma, Disruption of human papillomavirus 16 E6 gene by clustered regularly interspaced short palindromic repeat/Cas system in human cervical cancer cells, OncoTargets Ther., (2014) 37-44.
[60] J.L. Schultze, A.C. Aschenbrenner, COVID-19 and the human innate immune system, Cell, 184 (2021) 1671-1692.
[61] B. Zhang, D. Yue, Y. Wang, F. Wang, S. Wu, H. Hou, The dynamics of immune response in COVID-19 patients with different illness severity, J. Med. Virol., 93 (2021) 1070-1077.
[62] X. He, X.X. Zeng, Immunotherapy and CRISPR cas systems: potential cure of COVID-19?, Drug Des. Dev. Ther., (2023) 951-972.
[63] S.L. Saraf, R.E. Molokie, M. Nouraie, C.A. Sable, L. Luchtman-Jones, G.J. Ensing, A.D. Campbell, S.R. Rana, X.M. Niu, R.F. Machado, Differences in the clinical and genotypic presentation of sickle cell disease around the world, Paediatr. Respir. Rev., 15 (2014) 4-12.
[64] H. Frangoul, D. Altshuler, M.D. Cappellini, Y.-S. Chen, J. Domm, B.K. Eustace, J. Foell, J. de la Fuente, S. Grupp, R. Handgretinger, CRISPR-Cas9 gene editing for sickle cell disease and β-thalassemia, N. Engl. J. Med., 384 (2021) 252-260.
[65] H. Tariq, F. Khurshid, M.H. Khan, A. Dilshad, A. Zain, W. Rasool, A. Jawaid, D. Kunwar, S. Khanduja, A. Akbar, CRISPR/Cas9 in the treatment of sickle cell disease (SCD) and its comparison with traditional treatment approaches: a review, Ann. Med. Surg., 86 (2024) 5938-5946.
[66] H. Zhao, Y. Li, L. He, W. Pu, W. Yu, Y. Li, Y.-T. Wu, C. Xu, Y. Wei, Q. Ding, In vivo AAV-CRISPR/Cas9–mediated gene editing ameliorates atherosclerosis in familial hypercholesterolemia, Circulation, 141 (2020) 67-79.
[67] D.Y. Richards, S.R. Winn, S. Dudley, S. Nygaard, T.L. Mighell, M. Grompe, C.O. Harding, AAV-mediated CRISPR/Cas9 gene editing in murine phenylketonuria, Mol. Ther. Methods Clin. Dev., 17 (2020) 234-245.
[68] D.G. Ousterout, A.M. Kabadi, P.I. Thakore, W.H. Majoros, T.E. Reddy, C.A. Gersbach, Multiplex CRISPR/Cas9-based genome editing for correction of dystrophin mutations that cause Duchenne muscular dystrophy, Nat. Commun., 6 (2015) 6244.
[69] N.E. Bengtsson, J.K. Hall, G.L. Odom, M.P. Phelps, C.R. Andrus, R.D. Hawkins, S.D. Hauschka, J.R. Chamberlain, J.S. Chamberlain, Muscle-specific CRISPR/Cas9 dystrophin gene editing ameliorates pathophysiology in a mouse model for Duchenne muscular dystrophy, Nat. Commun., 8 (2017) 14454.
[70] Y. Zhang, H. Li, Y.-L. Min, E. Sanchez-Ortiz, J. Huang, A.A. Mireault, J.M. Shelton, J. Kim, P.P. Mammen, R. Bassel-Duby, Enhanced CRISPR-Cas9 correction of Duchenne

muscular dystrophy in mice by a self-complementary AAV delivery system, Sci. Adv., 6 (2020) eaay6812.
[71] R. Farooq, K. Hussain, M. Tariq, A. Farooq, M. Mustafa, CRISPR/Cas9: targeted genome editing for the treatment of hereditary hearing loss, J. Appl. Genet., 61 (2020) 51-65.
[72] N. Bischoff, S. Wimberger, M. Maresca, C. Brakebusch, Improving precise CRISPR genome editing by small molecules: is there a magic potion?, Cells, 9 (2020) 1318.
[73] J. Mianné, L. Chessum, S. Kumar, C. Aguilar, G. Codner, M. Hutchison, A. Parker, A.-M. Mallon, S. Wells, M.M. Simon, Correction of the auditory phenotype in C57BL/6N mice via CRISPR/Cas9-mediated homology directed repair, Genome Med., 8 (2016) 1-12.
[74] J. Kuhn, Y. Lin, A. Krhac Levacic, N. Al Danaf, L. Peng, M. Höhn, D.C. Lamb, E. Wagner, U. Lächelt, Delivery of Cas9/sgRNA ribonucleoprotein complexes via hydroxystearyl oligoamino amides, Bioconjug. Chem., 31 (2020) 729-742.
[75] Y. Lin, U. Wilk, J. Pöhmerer, E. Hörterer, M. Höhn, X. Luo, H. Mai, E. Wagner, U. Lächelt, Folate receptor-mediated delivery of Cas9 RNP for enhanced immune checkpoint disruption in cancer cells, Small, 19 (2023) 2205318.
[76] Y. Lin, X. Luo, T. Burghardt, S. Dorrer, M. Höhn, E. Wagner, U. Lächelt, Chemical evolution of amphiphilic xenopeptides for potentiated Cas9 ribonucleoprotein delivery, J. Am. Chem. Soc., 145 (2023) 15171-15179.
[77] A.-L. Lessl, J. Pöhmerer, Y. Lin, U. Wilk, M. Höhn, E. Hörterer, E. Wagner, U. Lächelt, mCherry on Top: A Positive Read-Out Cellular Platform for Screening DMD Exon Skipping Xenopeptide–PMO Conjugates, Bioconjug. Chem., 34 (2023) 2263-2274.
[78] S. Thalmayr, M. Grau, L. Peng, J. Pöhmerer, U. Wilk, P. Folda, M. Yazdi, E. Weidinger, T. Burghardt, M. Höhn, Molecular chameleon carriers for nucleic acid delivery: the sweet spot between lipoplexes and polyplexes, Adv. Mater., 35 (2023) 2211105.
[79] J. Germer, A.-L. Lessl, J. Pöhmerer, M. Grau, E. Weidinger, M. Höhn, M. Yazdi, M.A. Cappelluti, A. Lombardo, U. Lächelt, Lipo-Xenopeptide polyplexes for CRISPR/Cas9 based gene editing at ultra-low dose, J. Control. Release., 370 (2024) 239-255.
[80] C. Wong, UK first to approve CRISPR treatment for diseases: what you need to know, Nature, 623 (2023) 676-677.
[81] A. Papapetropoulos, S. Topouzis, S.P. Alexander, M. Cortese-Krott, D.A. Kendall, K.A. Martemyanov, C. Mauro, N. Nagercoil, R.A. Panettieri Jr, H.H. Patel, Novel drugs approved by the EMA, the FDA, and the MHRA in 2023: A year in review, Br J Pharmacol, 181 (2024) 1553-1575.
[82] D. Ja, E. Charpentier, Genome editing. The new frontier of genome engineering with CRISPR-Cas9, Science, 346 (2014) 1258096.
[83] J. Walther, D. Porenta, D. Wilbie, C. Seinen, N. Benne, Q. Yang, O.G. de Jong, Z. Lei, E. Mastrobattista, Comparative analysis of lipid Nanoparticle-Mediated delivery of CRISPR-Cas9 RNP versus mRNA/sgRNA for gene editing in vitro and in vivo, Eur. J. Pharm. Biopharm., 196 (2024) 114207.

[84] B. Tafech, M.R. Rokhforouz, J. Leung, M.M. Sung, P.J. Lin, D.D. Sin, D. Lauster, S. Block, B.S. Quon, Y. Tam, Exploring Mechanisms of Lipid Nanoparticle-Mucus Interactions in Healthy and Cystic Fibrosis Conditions, Adv. Healthc. Mater., 13 (2024) 2304525.
[85] Y. Chen, Y. Ping, Development of CRISPR/Cas delivery systems for in vivo precision genome editing, Acc. Chem. Res., 56 (2023) 2185-2196.
[86] J.A. Zuris, D.B. Thompson, Y. Shu, J.P. Guilinger, J.L. Bessen, J.H. Hu, M.L. Maeder, J.K. Joung, Z.-Y. Chen, D.R. Liu, Cationic lipid-mediated delivery of proteins enables efficient protein-based genome editing in vitro and in vivo, Nat. Biotechnol., 33 (2015) 73-80.
[87] Folate Receptor-Mediated Delivery of Cas9 RNP for Enhanced Immune Checkpoint Disruption in Cancer Cells, Small, (2022).
[88] M. Öktem, E. Mastrobattista, O.G. de Jong, Amphipathic cell-penetrating peptide-aided delivery of Cas9 RNP for in vitro gene editing and correction, Pharmaceutics, 15 (2023) 2500.
[89] E. Kenjo, H. Hozumi, Y. Makita, K.A. Iwabuchi, N. Fujimoto, S. Matsumoto, M. Kimura, Y. Amano, M. Ifuku, Y. Naoe, Low immunogenicity of LNP allows repeated administrations of CRISPR-Cas9 mRNA into skeletal muscle in mice, Nat. Commun., 12 (2021) 7101.
[90] C.A. Tsuchida, K.M. Wasko, J.R. Hamilton, J.A. Doudna, Targeted nonviral delivery of genome editors in vivo, Proc. Natl. Acad. Sci. U.S.A., 121 (2024) e2307796121.
[91] L. Farbiak, Q. Cheng, T. Wei, E. Álvarez-Benedicto, L.T. Johnson, S. Lee, D.J. Siegwart, All-in-one dendrimer-based lipid nanoparticles enable precise HDR-mediated gene editing in vivo, Adv. Mater., 33 (2021) 2006619.
[92] K. Chen, E.C. Stahl, M.H. Kang, B. Xu, R. Allen, M. Trinidad, J.A. Doudna, Engineering self-deliverable ribonucleoproteins for genome editing in the brain, Nat. Commun., 15 (2024) 1727.
[93] J.D. Gillmore, E. Gane, J. Taubel, J. Kao, M. Fontana, M.L. Maitland, J. Seitzer, D. O'Connell, K.R. Walsh, K. Wood, CRISPR-Cas9 in vivo gene editing for transthyretin amyloidosis, N. Engl. J. Med., 385 (2021) 493-502.
[94] Y. Sato, K. Hashiba, K. Sasaki, M. Maeki, M. Tokeshi, H. Harashima, Understanding structure-activity relationships of pH-sensitive cationic lipids facilitates the rational identification of promising lipid nanoparticles for delivering siRNAs in vivo, J. Control. Release., 295 (2019) 140-152.
[95] U. Lächelt, E. Wagner, Nucleic acid therapeutics using polyplexes: a journey of 50 years (and beyond), Chem. Rev., 115 (2015) 11043-11078.
[96] M. Noga, D. Edinger, R. Kläger, S.V. Wegner, J.P. Spatz, E. Wagner, G. Winter, A. Besheer, The effect of molar mass and degree of hydroxyethylation on the controlled shielding and deshielding of hydroxyethyl starch-coated polyplexes, Biomaterials, 34 (2013) 2530-2538.

[97] R. Kumar, C.F. Santa Chalarca, M.R. Bockman, C.V. Bruggen, C.J. Grimme, R.J. Dalal, M.G. Hanson, J.K. Hexum, T.M. Reineke, Polymeric delivery of therapeutic nucleic acids, Chem. Rev., 121 (2021) 11527-11652.
[98] B. Winkeljann, D.C. Keul, O.M. Merkel, Engineering poly-and micelleplexes for nucleic acid delivery–A reflection on their endosomal escape, J. Control. Release., 353 (2023) 518-534.
[99] P. Cullis, P. Felgner, The 60-year evolution of lipid nanoparticles for nucleic acid delivery, Nat. Rev. Drug Discov., 23 (2024) 709-722.
[100] P. Zhang, E. Wagner, History of polymeric gene delivery systems, Top Curr Chem (Cham), (2017) 1-39.
[101] M. Noga, D. Edinger, W. Rödl, E. Wagner, G. Winter, A. Besheer, Controlled shielding and deshielding of gene delivery polyplexes using hydroxyethyl starch (HES) and alpha-amylase, J. Control. Release., 159 (2012) 92-103.
[102] L. Peng, E. Wagner, Polymeric carriers for nucleic acid delivery: current designs and future directions, Biomacromolecules, 20 (2019) 3613-3626.
[103] Q. Leng, S.T. Chou, P.V. Scaria, M.C. Woodle, A.J. Mixson, Increased tumor distribution and expression of histidine-rich plasmid polyplexes, J. Gene Med., 16 (2014) 317-328.
[104] L. Hartmann, Polymers for Control Freaks: Sequence-Defined Poly (amidoamine) s and Their Biomedical Applications, Macromol. Chem. Phys., 212 (2011) 8-13.
[105] S. El Andaloussi, T. Lehto, I. Mäger, K. Rosenthal-Aizman, I.I. Oprea, O.E. Simonson, H. Sork, K. Ezzat, D.M. Copolovici, K. Kurrikoff, Design of a peptide-based vector, PepFect6, for efficient delivery of siRNA in cell culture and systemically in vivo, Nucleic Acids Res., 39 (2011) 3972-3987.
[106] P. Heller, A. Birke, D. Huesmann, B. Weber, K. Fischer, A. Reske-Kunz, M. Bros, M. Barz, Introducing peptoplexes: Polylysine-block-polysarcosine based polyplexes for transfection of HEK 293T Cells, Macromol. Biosci., 14 (2014) 1380-1395.
[107] F. Freitag, E. Wagner, Optimizing synthetic nucleic acid and protein nanocarriers: The chemical evolution approach, Adv. Drug Deliv. Rev., 168 (2021) 30-54.
[108] D. Schaffert, C. Troiber, E.E. Salcher, T. Fröhlich, I. Martin, N. Badgujar, C. Dohmen, D. Edinger, R. Kläger, G. Maiwald, Solid-phase synthesis of sequence-defined T-, i-, and U-shape polymers for pDNA and siRNA delivery, Angew. Chem. Int. Ed., 50 (2011) 8986.
[109] U. Lächelt, P. Kos, F.M. Mickler, A. Herrmann, E.E. Salcher, W. Rödl, N. Badgujar, C. Bräuchle, E. Wagner, Fine-tuning of proton sponges by precise diaminoethanes and histidines in pDNA polyplexes, Nanomedicine (Lond.), 10 (2014) 35-44.
[110] A.K. Levačić, S. Berger, J. Müller, A. Wegner, U. Lächelt, C. Dohmen, C. Rudolph, E. Wagner, Dynamic mRNA polyplexes benefit from bioreducible cleavage sites for in vitro and in vivo transfer, J. Control. Release., 339 (2021) 27-40.
[111] S. Berger, U. Lächelt, E. Wagner, Dynamic carriers for therapeutic RNA delivery, Proc. Natl. Acad. Sci. U.S.A., 121 (2024) e2307799120.

[112] E.E. Salcher, P. Kos, T. Fröhlich, N. Badgujar, M. Scheible, E. Wagner, Sequence-defined four-arm oligo (ethanamino) amides for pDNA and siRNA delivery: Impact of building blocks on efficacy, J. Control. Release., 164 (2012) 380-386.
[113] M. Grau, E. Wagner, Strategies and mechanisms for endosomal escape of therapeutic nucleic acids, Curr. Opin. Chem. Biol., 81 (2024) 102506.
[114] F. Haase, J. Pöhmerer, M. Yazdi, M. Grau, Y. Zeyn, U. Wilk, T. Burghardt, M. Höhn, C. Hieber, M. Bros, Lipoamino bundle LNPs for efficient mRNA transfection of dendritic cells and macrophages show high spleen selectivity, Eur. J. Pharm. Biopharm., 194 (2024) 95-109.
[115] M. Yazdi, J. Pöhmerer, M. Hasanzadeh Kafshgari, J. Seidl, M. Grau, M. Höhn, V. Vetter, C.C. Hoch, B. Wollenberg, G. Multhoff, In vivo endothelial cell gene silencing by siRNA-LNPs tuned with lipoamino bundle chemical and ligand targeting, Small, 20 (2024) 2400643.
[116] M. Lyu, M. Yazdi, Y. Lin, M. Höhn, U. Lächelt, E. Wagner, Receptor-targeted dual pH-triggered intracellular protein transfer, ACS Biomater. Sci. Eng., 10 (2022) 99-114.
[117] Y. Rui, D.R. Wilson, S.Y. Tzeng, H.M. Yamagata, D. Sudhakar, M. Conge, C.A. Berlinicke, D.J. Zack, A. Tuesca, J.J. Green, High-throughput and high-content bioassay enables tuning of polyester nanoparticles for cellular uptake, endosomal escape, and systemic in vivo delivery of mRNA, Sci. Adv., 8 (2022) eabk2855.
[118] Y.-L. Min, H. Li, C. Rodriguez-Caycedo, A.A. Mireault, J. Huang, J.M. Shelton, J.R. McAnally, L. Amoasii, P.P. Mammen, R. Bassel-Duby, CRISPR-Cas9 corrects Duchenne muscular dystrophy exon 44 deletion mutations in mice and human cells, Sci. Adv., 5 (2019) eaav4324.
[119] C. Long, L. Amoasii, A.A. Mireault, J.R. McAnally, H. Li, E. Sanchez-Ortiz, S. Bhattacharyya, J.M. Shelton, R. Bassel-Duby, E.N. Olson, Postnatal genome editing partially restores dystrophin expression in a mouse model of muscular dystrophy, Science, 351 (2016) 400-403.
[120] P. Gee, M.S. Lung, Y. Okuzaki, N. Sasakawa, T. Iguchi, Y. Makita, H. Hozumi, Y. Miura, L.F. Yang, M. Iwasaki, Extracellular nanovesicles for packaging of CRISPR-Cas9 protein and sgRNA to induce therapeutic exon skipping, Nat. Commun., 11 (2020) 1334.
[121] S. Berger, A. Krhač Levačić, E. Hörterer, U. Wilk, T. Benli-Hoppe, Y. Wang, O.z.r. Öztürk, J. Luo, E. Wagner, Optimizing pDNA lipo-polyplexes: a balancing act between stability and cargo release, Biomacromolecules, 22 (2021) 1282-1296.
[122] S. Berger, M. Berger, C. Bantz, M. Maskos, E. Wagner, Performance of nanoparticles for biomedical applications: The in vitro/in vivo discrepancy, Biophys. Rev., 3 (2022).
[123] E.M. Porto, A.C. Komor, I.M. Slaymaker, G.W. Yeo, Base editing: advances and therapeutic opportunities, Nat. Rev. Drug Discov., 19 (2020) 839-859.

[124] M.A. Cappelluti, V. Mollica Poeta, S. Valsoni, P. Quarato, S. Merlin, I. Merelli, A. Lombardo, Durable and efficient gene silencing in vivo by hit-and-run epigenome editing, Nature, 627 (2024) 416-423.
[125] B.J. Booth, S. Nourreddine, D. Katrekar, Y. Savva, D. Bose, T.J. Long, D.J. Huss, P. Mali, RNA editing: Expanding the potential of RNA therapeutics, Mol. Ther., 31 (2023) 1533-1549.
[126] M. Jinek, K. Chylinski, I. Fonfara, M. Hauer, J.A. Doudna, E. Charpentier, A programmable dual-RNA–guided DNA endonuclease in adaptive bacterial immunity, science, 337 (2012) 816-821.
[127] J.R. Chapman, M.R. Taylor, S.J. Boulton, Playing the end game: DNA double-strand break repair pathway choice, Mol. Cell., 47 (2012) 497-510.
[128] K.K. Chiruvella, Z. Liang, T.E. Wilson, Repair of double-strand breaks by end joining, Cold Spring Harb. Perspect. Biol., 5 (2013) a012757.
[129] J. Scholefield, P.T. Harrison, Prime editing–an update on the field, Gene Ther., 28 (2021) 396-401.
[130] T.S. Nambiar, L. Baudrier, P. Billon, A. Ciccia, CRISPR-based genome editing through the lens of DNA repair, Mol. Cell., 82 (2022) 348-388.
[131] K. Schumann, S. Lin, E. Boyer, D.R. Simeonov, M. Subramaniam, R.E. Gate, G.E. Haliburton, C.J. Ye, J.A. Bluestone, J.A. Doudna, Generation of knock-in primary human T cells using Cas9 ribonucleoproteins, Proc. Natl. Acad. Sci. U.S.A., 112 (2015) 10437-10442.
[132] K. Kim, S.-M. Ryu, S.-T. Kim, G. Baek, D. Kim, K. Lim, E. Chung, S. Kim, J.-S. Kim, Highly efficient RNA-guided base editing in mouse embryos, Nat. Biotechnol., 35 (2017) 435-437.
[133] N. Merienne, G. Vachey, L. de Longprez, C. Meunier, V. Zimmer, G. Perriard, M. Canales, A. Mathias, L. Herrgott, T. Beltraminelli, The self-inactivating KamiCas9 system for the editing of CNS disease genes, Cell Rep., 20 (2017) 2980-2991.
[134] L. Xu, K.H. Park, L. Zhao, J. Xu, M. El Refaey, Y. Gao, H. Zhu, J. Ma, R. Han, CRISPR-mediated genome editing restores dystrophin expression and function in mdx mice, Mol. Ther., 24 (2016) 564-569.
[135] R. Ibraheim, P.W. Tai, A. Mir, N. Javeed, J. Wang, T.C. Rodríguez, S. Namkung, S. Nelson, E.S. Khokhar, E. Mintzer, Self-inactivating, all-in-one AAV vectors for precision Cas9 genome editing via homology-directed repair in vivo, Nat. Commun., 12 (2021) 6267.
[136] H. Cheng, F. Zhang, Y. Ding, CRISPR/Cas9 delivery system engineering for genome editing in therapeutic applications, Pharmaceutics, 13 (2021) 1649.
[137] K. Paunovska, C.D. Sago, C.M. Monaco, W.H. Hudson, M.G. Castro, T.G. Rudoltz, S. Kalathoor, D.A. Vanover, P.J. Santangelo, R. Ahmed, A direct comparison of in vitro and in vivo nucleic acid delivery mediated by hundreds of nanoparticles reveals a weak correlation, Nano Lett., 18 (2018) 2148-2157.

[138] H. Cabral, K. Miyata, K. Osada, K. Kataoka, Block copolymer micelles in nanomedicine applications, Chem. Rev., 118 (2018) 6844-6892.
[139] H. Onuma, R. Shimizu, Y. Suzuki, M. Sato, H. Harashima, Y. Sato, Engineering branched ionizable lipid for hepatic delivery of clustered regularly interspaced short palindromic repeat-Cas9 ribonucleoproteins, iScience, 27 (2024) 110928.
[140] H. Onuma, Y. Sato, H. Harashima, Lipid nanoparticle-based ribonucleoprotein delivery for in vivo genome editing, J. Control. Release., 355 (2023) 406-416.
[141] D. Zhang, G. Wang, X. Yu, T. Wei, L. Farbiak, L.T. Johnson, A.M. Taylor, J. Xu, Y. Hong, H. Zhu, Enhancing CRISPR/Cas gene editing through modulating cellular mechanical properties for cancer therapy, Nat. Nanotechnol., 17 (2022) 777-787.
[142] F. Shams, H. Bayat, O. Mohammadian, S. Mahboudi, H. Vahidnezhad, M. Soosanabadi, A. Rahimpour, Advance trends in targeting homology-directed repair for accurate gene editing: An inclusive review of small molecules and modified CRISPR-Cas9 systems, BioImpacts, 12 (2022) 371.
[143] C.A. Waters, N.T. Strande, D.W. Wyatt, J.M. Pryor, D.A. Ramsden, Nonhomologous end joining: a good solution for bad ends, DNA Repair 17 (2014) 39-51.
[144] S.K. Radhakrishnan, S.P. Lees-Miller, DNA requirements for interaction of the C-terminal region of Ku80 with the DNA-dependent protein kinase catalytic subunit (DNA-PKcs), DNA Repair, 57 (2017) 17-28.
[145] E. Weterings, A.C. Gallegos, L.N. Dominick, L.S. Cooke, T.N. Bartels, J. Vagner, T.O. Matsunaga, D. Mahadevan, A novel small molecule inhibitor of the DNA repair protein Ku70/80, DNA Repair, 43 (2016) 98-106.
[146] D. Kostyushev, A. Kostyusheva, S. Brezgin, D. Zarifyan, A. Utkina, I. Goptar, V. Chulanov, Suppressing the NHEJ pathway by DNA-PKcs inhibitor NU7026 prevents degradation of HBV cccDNA cleaved by CRISPR/Cas9, Sci. Rep., 9 (2019) 1847.
[147] T. Maruyama, S.K. Dougan, M.C. Truttmann, A.M. Bilate, J.R. Ingram, H.L. Ploegh, Increasing the efficiency of precise genome editing with CRISPR-Cas9 by inhibition of nonhomologous end joining, Nat. Biotechnol., 33 (2015) 538-542.
[148] F. Robert, M. Barbeau, S. Éthier, J. Dostie, J. Pelletier, Pharmacological inhibition of DNA-PK stimulates Cas9-mediated genome editing, Genome Med., 7 (2015) 93.
[149] B. Budke, W. Lv, A.P. Kozikowski, P.P. Connell, Recent developments using small molecules to target RAD51: how to best modulate RAD51 for anticancer therapy?, ChemMedChem, 11 (2016) 2468-2473.
[150] X. Luo, J. Germer, T. Burghardt, M. Grau, Y. Lin, M. Höhn, U. Lächelt, E. Wagner, Dual pH-responsive CRISPR/Cas9 ribonucleoprotein xenopeptide complexes for genome editing, Eur. J. Pharm. Sci., 205 (2025) 106983.
[151] S. Riesenberg, T. Maricic, Targeting repair pathways with small molecules increases precise genome editing in pluripotent stem cells, Nat. Commun., 9 (2018) 2164.

[152] R. Jayavaradhan, D.M. Pillis, P. Malik, A versatile tool for the quantification of CRISPR/Cas9-induced genome editing events in human hematopoietic cell lines and hematopoietic stem/progenitor cells, J. Mol. Biol., 431 (2019) 102-110.
[153] J. Song, D. Yang, J. Xu, T. Zhu, Y.E. Chen, J. Zhang, RS-1 enhances CRISPR/Cas9- and TALEN-mediated knock-in efficiency, Nat. Commun., 7 (2016) 10548.
[154] Z. Hu, Z. Shi, X. Guo, B. Jiang, G. Wang, D. Luo, Y. Chen, Y.-S. Zhu, Ligase IV inhibitor SCR7 enhances gene editing directed by CRISPR–Cas9 and ssODN in human cancer cells, Cell Biosci., 8 (2018) 12.
[155] G.E. Greco, Y. Matsumoto, R.C. Brooks, Z. Lu, M.R. Lieber, A.E. Tomkinson, SCR7 is neither a selective nor a potent inhibitor of human DNA ligase IV, DNA repair, 43 (2016) 18-23.
[156] T. Gutschner, M. Haemmerle, G. Genovese, G.F. Draetta, L. Chin, Post-translational regulation of Cas9 during G1 enhances homology-directed repair, Cell Rep., 14 (2016) 1555-1566.
[157] S. Riesenberg, M. Chintalapati, D. Macak, P. Kanis, T. Maricic, S. Pääbo, Simultaneous precise editing of multiple genes in human cells, Nucleic Acids Res., 47 (2019) e116-e116.
[158] Y.-W. Fu, X.-Y. Dai, W.-T. Wang, Z.-X. Yang, J.-J. Zhao, J.-P. Zhang, W. Wen, F. Zhang, K.C. Oberg, L. Zhang, Dynamics and competition of CRISPR–Cas9 ribonucleoproteins and AAV donor-mediated NHEJ, MMEJ and HDR editing, Nucleic Acids Res., 49 (2021) 969-985.
[159] H.C. Bermudez-Cabrera, S. Culbertson, S. Barkal, B. Holmes, M.W. Shen, S. Zhang, D.K. Gifford, R.I. Sherwood, Small molecule inhibition of ATM kinase increases CRISPR-Cas9 1-bp insertion frequency, Nat. Commun., 12 (2021) 5111.
[160] J.-P. Zhang, X.-L. Li, G.-H. Li, W. Chen, C. Arakaki, G.D. Botimer, D. Baylink, L. Zhang, W. Wen, Y.-W. Fu, Efficient precise knockin with a double cut HDR donor after CRISPR/Cas9-mediated double-stranded DNA cleavage, Genome Biol., 18 (2017) 35.
[161] Y. Zhao, X. Li, C. Liu, C. Jiang, X. Guo, Q. Xu, Z. Yin, Z. Liu, Y. Mu, Improving the Efficiency of CRISPR Ribonucleoprotein-Mediated Precise Gene Editing by Small Molecules in Porcine Fibroblasts, Animals, 14 (2024) 719.
[162] B.R. Shy, V.S. Vykunta, A. Ha, A. Talbot, T.L. Roth, D.N. Nguyen, W.G. Pfeifer, Y.Y. Chen, F. Blaeschke, E. Shifrut, High-yield genome engineering in primary cells using a hybrid ssDNA repair template and small-molecule cocktails, Nat. Biotechnol., 41 (2023) 521-531.
[163] T.L. Maurissen, K. Woltjen, Synergistic gene editing in human iPS cells via cell cycle and DNA repair modulation, Nat. Commun., 11 (2020) 2876.
[164] A. Wittrup, A. Ai, X. Liu, P. Hamar, R. Trifonova, K. Charisse, M. Manoharan, T. Kirchhausen, J. Lieberman, Visualizing lipid-formulated siRNA release from endosomes and target gene knockdown, Nat. Biotechnol., 33 (2015) 870-876.

[165] W.-D. Heyer, K.T. Ehmsen, J. Liu, Regulation of homologous recombination in eukaryotes, Annu. Rev. Genet., 44 (2010) 113-139.
[166] N. Hustedt, D. Durocher, The control of DNA repair by the cell cycle, Nat. Cell Biol., 19 (2017) 1-9.
[167] S. Brunner, T. Sauer, S. Carotta, M. Cotten, M. Saltik, E. Wagner, Cell cycle dependence of gene transfer by lipoplex, polyplex and recombinant adenovirus, Gene Ther., 7 (2000) 401-407.
[168] N. Symens, S.J. Soenen, J. Rejman, K. Braeckmans, S.C. De Smedt, K. Remaut, Intracellular partitioning of cell organelles and extraneous nanoparticles during mitosis, Adv. Drug Deliv. Rev., 64 (2012) 78-94.
[169] K. Remaut, N. Symens, B. Lucas, J. Demeester, S. De Smedt, Cell division responsive peptides for optimized plasmid DNA delivery: the mitotic window of opportunity?, J. Control. Release., 179 (2014) 1-9.
[170] S. Lin, B.T. Staahl, R.K. Alla, J.A. Doudna, Enhanced homology-directed human genome engineering by controlled timing of CRISPR/Cas9 delivery, Elife, 3 (2014) e04766.
[171] S. Selvaraj, W.N. Feist, S. Viel, S. Vaidyanathan, A.M. Dudek, M. Gastou, S.J. Rockwood, F.K. Ekman, A.R. Oseghale, L. Xu, High-efficiency transgene integration by homology-directed repair in human primary cells using DNA-PKcs inhibition, Nat. Biotechnol., 42 (2024) 731-744.
[172] Advance trends in targeting homology-directed repair for accurate gene editing: An inclusive review of small molecules and modified CRISPR-Cas9 systems, BioImpacts, (2023).
[173] Y.A. Aksoy, D.T. Nguyen, S. Chow, R.S. Chung, G.J. Guillemin, N.J. Cole, D. Hesselson, Chemical reprogramming enhances homology-directed genome editing in zebrafish embryos, Commun. Biol., 2 (2019) 198.
[174] H. Babačić, A. Mehta, O. Merkel, B. Schoser, CRISPR-cas gene-editing as plausible treatment of neuromuscular and nucleotide-repeat-expansion diseases: A systematic review, PLOS ONE, 14 (2019) e0212198.
[175] D. Conant, T. Hsiau, N. Rossi, J. Oki, T. Maures, K. Waite, J. Yang, S. Joshi, R. Kelso, K. Holden, Inference of CRISPR edits from Sanger trace data, CRISPR J., 5 (2022) 123-130.
[176] E.K. Brinkman, T. Chen, M. Amendola, B. Van Steensel, Easy quantitative assessment of genome editing by sequence trace decomposition, Nucleic Acids Res., 42 (2014) e168-e168.
[177] Y. Fu, J.A. Foden, C. Khayter, M.L. Maeder, D. Reyon, J.K. Joung, J.D. Sander, High-frequency off-target mutagenesis induced by CRISPR-Cas nucleases in human cells, Nat. Biotechnol., 31 (2013) 822-826.
[178] M. Pacesa, C.-H. Lin, A. Cléry, A. Saha, P.R. Arantes, K. Bargsten, M.J. Irby, F.H.-T. Allain, G. Palermo, P. Cameron, Structural basis for Cas9 off-target activity, Cell, 185 (2022) 4067-4081. e4021.

[179] M. Naeem, S. Majeed, M.Z. Hoque, I. Ahmad, Latest developed strategies to minimize the off-target effects in CRISPR-Cas-mediated genome editing, Cells, 9 (2020) 1608.
[180] Y. Zhao, H.D. Thomas, M.A. Batey, I.G. Cowell, C.J. Richardson, R.J. Griffin, A.H. Calvert, D.R. Newell, G.C. Smith, N.J. Curtin, Preclinical evaluation of a potent novel DNA-dependent protein kinase inhibitor NU7441, Cancer research, 66 (2006) 5354-5362.
[181] Z.J. Waldrip, B. Acharya, D. Armstrong, M. Hanafi, R.R. Rainwater, S. Amole, M. Fulmer, A.C. Azevedo-Pouly, A. Burns, L. Burdine, Discovery of the DNA-PKcs inhibitor DA-143 which exhibits enhanced solubility relative to NU7441, Sci. Rep., 14 (2024) 19999.
[182] Y. Matsumoto, Development and evolution of DNA-dependent protein kinase inhibitors toward cancer therapy, Int. J. Mol. Sci., 23 (2022) 4264.
[183] A. Tichy, K. Durisova, B. Salovska, J. Pejchal, L. Zarybnicka, J. Vavrova, N.A. Dye, Z. Sinkorova, Radio-sensitization of human leukaemic MOLT-4 cells by DNA-dependent protein kinase inhibitor, NU7441, Radiat. Environ. Biophys., 53 (2014) 83-92.
[184] S.Q. Tsai, Z. Zheng, N.T. Nguyen, M. Liebers, V.V. Topkar, V. Thapar, N. Wyvekens, C. Khayter, A.J. Iafrate, L.P. Le, GUIDE-seq enables genome-wide profiling of off-target cleavage by CRISPR-Cas nucleases, Nat. Biotechnol., 33 (2015) 187-197.
[185] B. Wienert, S.K. Wyman, C.D. Richardson, C.D. Yeh, P. Akcakaya, M.J. Porritt, M. Morlock, J.T. Vu, K.R. Kazane, H.L. Watry, Unbiased detection of CRISPR off-targets in vivo using DISCOVER-Seq, Science, 364 (2019) 286-289.

7 Publications

Original article

Luo, X., Weidinger, E., Burghardt, T., Höhn, M. and Wagner, E., 2025. CRISPR/Cas9 Ribonucleoprotein Delivery Enhanced by Lipo-Xenopeptide Carriers and Homology-Directed Repair Modulators: Insights from Reporter Cell Lines. *International Journal of Molecular Sciences*, 26(9), p.4361.

Luo, X., Germer, J., Burghardt, T., Grau, M., Lin, Y., Höhn, M., Lächelt, U. and Wagner, E., 2025. Dual pH-responsive CRISPR/Cas9 ribonucleoprotein xenopeptide complexes for genome editing. *European Journal of Pharmaceutical Sciences*, *205*, p.106983.

Shen, F., Lin, Y., Höhn, M., **Luo, X.**, Döblinger, M., Wagner, E. and Lächelt, U., 2023. Iron-gallic acid peptide nanoparticles as a versatile platform for cellular delivery with synergistic ROS enhancement effect. *Pharmaceutics*, *15*(7), p.1789.

Lin, Y., **Luo, X**., Burghardt, T., Dorrer, S., Höhn, M., Wagner, E. and Lächelt, U., 2023. Chemical evolution of amphiphilic xenopeptides for potentiated Cas9 ribonucleoprotein delivery. *Journal of the American Chemical Society*, *145*(28), pp.15171-15179.

Lin, Y., Wilk, U., Pöhmerer, J., Hörterer, E., Höhn, M., **Luo, X**., Mai, H., Wagner, E., and Lächelt, U., 2023. Folate receptor-mediated delivery of Cas9 RNP for enhanced immune checkpoint disruption in cancer cells. *Small*, *19*(2), 2205318.

8 Acknowledgements

My journey in Germany has been one of the most wonderful experiences of my life, and I believe it will have a profound impact on my future. As I reach the conclusion of my PhD studies, I would like to sincerely express my gratitude to everyone who has supported me over the past several years.

First and foremost, I would like to extend my heartfelt thanks to Prof. Dr. Ernst Wagner for giving me the opportunity to pursue my PhD in such an outstanding research group. I deeply appreciate his support, patience, and professional guidance. Under his mentorship, I have learned invaluable skills, including experimental design, in-depth analysis of experimental phenomena, and manuscript preparation. His passion for science and relentless pursuit of knowledge have been a great source of motivation for me throughout the past four years. Beyond research, I also enjoyed our philosophical discussions, during which he generously shared his life experiences with me.

I am also immensely grateful to Dr. Yi Lin for supervising and supporting me. His patience in teaching me everything in the lab—from synthesis to literature review—has been invaluable. I truly enjoyed our discussions on research topics, which broadened my vision and deepened my curiosity for science. I still remember his perspective on scientific research: he once told me that he would rather choose science over money, reputation, or status. His dedication and integrity in scientific pursuits have left a profound impact on me.

I would like to express my sincere gratitude to Prof. Ulrich Lächelt, Dr. Janin Germer, Eric Weidinger, and Tobias Burghardt for their discussions and collaboration on the Cas9 RNP delivery system project. My thanks also go to Dr. Lun and Dr. Faqian for teaching me synthesis, and to Dr. Fengrong and Dr. Meng for their generous support in my research. I am particularly grateful to Miriam Höhn for her help with CLSM experiments and the production of high-quality Cas9 proteins, as well as to Hongcheng Mai and Yirong Zhou for their assistance with CLSM experiments. Many thanks to Sophie Thalmayr, Melina Grau, Paul Folda, Alexandra Mony, Johanna Seidl, Victoria Vetter, and Mina Yazdi for insightful discussions. I also appreciate Melina Grau, Tobias Burghardt, Teoman Benli-Hoppe, and Simone Berger for their support with MALDI-TOF MS measurements, and Dr. Fengrong for TEM measurements. Special thanks to Prof. Christian Kupatt-Jeremias, Allessandra Moretti, Julian Grünewald, and Sofia Ottonello for their collaboration on the LNP/Cas9 project.

My sincere appreciation also goes to Wolfgang for his assistance in the lab, as well as to Melinda, Markus, Lorina, and Olga for ensuring the smooth operation of the laboratory. I am grateful to Dr. Andreas Roidl for safety instructions and our discussions on European culture.

Additionally, I would like to express my gratitude to several groups:

"UPGRADE Meeting Group" (Yi, Janin, Franzi, Şurhan, and Eric) for our monthly discussions on the Cas9 projects—it has been exciting to witness our lab's progress together.

"Lunch Group" (Yi, Lun, Meng, Faqian, Fengrong) and the "Second Generation" (Min, Jiayi, Jinke) for making lunchtime the most relaxing and enjoyable part of my day.

"3C Group" (Jinke, Siyu, Yifan, Xiaohu, Shizhe, Tianhao, and Jiancheng) for the fun times cooking and playing games together.

"Basketball Group" (Faqian, Li, Jie Zhu, Yuan Gu, De Gu, Fengsen, Shaoke, etc.) for the great moments we shared on the court.

"Night Snack Group" (Li, Jin, Qiubo, Bo, and Xiangyu) for all the fun and memorable late-night gatherings.

"Ski Supervisor Group" (Johanna, Victoria, Sophie, Andi, and Lisa) for teaching me new skills and how to truly enjoy skiing.

I would also like to extend my gratitude to my dear friends Jintian, Yijun, KuiJu, Honglei, Shuhe, Weijia, Pei Xu, Qiurui, and many others for their companionship and support.

Many thanks to all the AK Wagner members for creating a wonderful atmosphere and for the unforgettable moments we shared. I am also deeply grateful to the China Scholarship Council for financially supporting my PhD studies and life in Munich.

Finally, I want to express my deepest gratitude to my parents for their unwavering support and for giving me the confidence to pursue my dreams.